RESOURCE ARTICLE

SELECTIVE PERSULFIDE DETECTION REVEALS EVOLUTIONARILY CONSERVED ANTI-AGING EFFECTS OF *S*-SULFHYDRATION

Jasmina Zivanovic,[1,2,14] Emilia Kouroussis,[1,2,14] Biljana Bursac,[1,2] Joshua B. Kohl,[3] Bikash Adhikari,[1,2] Sonia Schott-Roux,[1,2] Dunja Petrovic,[1,2] Jan Lj. Miljkovic,[1,2] Daniel Thomas Lopez,[4] Youngeun Jung,[5] Marko Miler,[6] Sarah Mitchell,[7] Verica Milosevic,[6] Jose Eduardo Gomes,[1,2] Moran Benhar,[8] Bruno Gonzales-Zorn,[4] Ivana Ivanovic-Burmazovic,[9] Roberta Torregrossa,[10] James R. Mitchell,[7] Matthew Whiteman,[10] Guenter Schwarz,[3] Solomon H. Snyder,[11,12,13] Bindu D. Paul,[11] Kate Carroll,[5] Milos R. Filipovic[1,2,*]

[1]CNRS, Institut de Biochimie et Génétique Cellulaires UMR5095, Université de Bordeaux, France

[2]Université de Bordeaux, France, CNRS, IBGC, UMR5095

[3]Department of Biochemistry, Center for Molecular Medicine, Institute of Biochemistry, University of Cologne, Cologne, Germany

[4]Departamento de Sanidad Animal, Facultad de Veterinaria and VISAVET, Universidad Complutense de Madrid, Spain

[5]Department of Chemistry, The Scripps Research Institute, 130 Scripps Way, Jupiter, FL 33458, USA

[6]Department of Cytology, Institute for Biological Research "Sinisa Stankovic", University of Belgrade, Belgrade, Serbia

[7]Department of Genetics and Complex Diseases, Harvard School of Public Health, Boston, MA 02115, USA

[8]Department of Biochemistry, Rappaport Institute for Research in the Medical Sciences, Faculty of Medicine, Technion-Israel Institute of Technology, Haifa 31096, Israel

[9]Department of Chemistry and Pharmacy, Friedrich-Alexander University of Erlangen-Nuremberg, Germany

[10]University of Exeter Medical School, St. Luke's Campus, Exeter, UK

[11]The Solomon H. Snyder Department of Neuroscience, Johns Hopkins University School of Medicine, Baltimore, MD 21205, USA

[12]Department of Pharmacology and Molecular Sciences, Johns Hopkins University School of Medicine, Baltimore, MD 21205, USA

[13]Department of Psychiatry, Johns Hopkins University School of Medicine, Baltimore, MD 21205, USA

[14]co-first author

[*]correspondence: milos.filipovic@ibgc.cnrs.fr

ABSTRACT

Life on Earth emerged in a hydrogen sulfide (H_2S)-rich environment eons ago and with it protein persulfidation mediated by H_2S evolved as a signaling mechanism. Protein persulfidation or *S*-sulfhydration is a posttranslational modification of reactive cysteine residues, which modulate protein structure and/or function. Persulfides are difficult to label and study due to their reactivity and similarity with cysteine. Here, we report a facile strategy for chemoselective persulfide bioconjugation using dimedone-based probes, to achieve highly selective, rapid, and robust persulfide labeling in biological samples with broad utility. Using this method, we show that persulfidation is an evolutionarily conserved modification and that waves of persulfidation are employed by cells to resolve sulfenylation and prevent irreversible cysteine overoxidation to preserve protein function. We report an age-associated decline in persulfidation which is conserved across evolutionary boundaries. Accordingly, dietary or pharmacological interventions to increase persulfidation associate with increased longevity and improved capacity to cope with stress stimuli.

One Sentence Summary: A new method for chemoselective persulfide labeling reveals the role of protein persulfidation in signal transduction, oxidative stress resistance and lifespan extension.

INTRODUCTION

Although considered a toxic gas for more than a century, hydrogen sulfide (H_2S) was one of the essential ingredients required for life to emerge on Earth (Patel et al., 2015). Early anaerobic bacteria flourished in H_2S-rich environments and even used H_2S instead of water for the first photosynthetic process (Filipovic et al., 2018a; Wang, 2012). Two decades ago H_2S reemerged as an important signaling molecule produced by cells (Filipovic et al., 2018a; Paul and Snyder, 2012; Szabó, 2007; Wang, 2012). Genetic deletion of the H_2S producing enzyme cystathionine γ-lyase (CSE) can lead to hypertension (Yang et al., 2008). Animals exposed to H_2S enter a suspended animation-like state (Blackstone, 2005), while dietary restriction-induced stress resistance and lifespan extension depends on intracellular H_2S production (Hine et al., 2015). Despite beneficial effects of H_2S, observed in a plethora of pathological states (Filipovic et al., 2018a; Paul and Snyder, 2012; Szabó, 2007; Wallace and Wang, 2015), the mechanism or mechanisms underlying these effects remain poorly characterized. However, its role in the oxidative posttranslational modification (oxPTM) of cysteine residues, known either as protein *S*-sulfhydration or persulfidation, is thought to be one of its main beneficial mechanisms of action (Filipovic et al., 2018b; Paul and Snyder, 2015).

Cysteine is a rare amino acid residue that often occurs in functional sites of proteins and represents a site for redox control of protein function (Marino and Gladyshev, 2010; Paulsen and Carroll, 2013). For example, hydrogen peroxide (H_2O_2) signals via the oxidation of cysteine residues to sulfenic acids (P-SOH), while part of nitric oxide signaling could be explained by cysteine *S*-nitrosation (Foster et al., 2009; Paulsen and Carroll, 2013). A variety of chemical approaches have been used to label and study cysteine modifications, leading to a broad range of fundamental and applied advances (Furdui and Poole, 2014; Paulsen and Carroll, 2013). However, protein persulfides (P-SSH) and their role in cell signaling managed to remain understudied, due to the fact that P-SSH are very reactive and their reactivity is similar to that of cysteine residues (Cuevasanta et al., 2015; Filipovic et al., 2018a; Pan and Carroll, 2013), has made it difficult to design tools for selective labeling, hampering a better understanding of the function of this specific oxPTM. Current methods rely on blocking both thiols and persulfides with electrophiles and then releasing the latter with a reducing agent, but this approach is linked to many caveats (Dóka et al., 2016; Filipovic et al., 2018a; Reisz et al., 2013).

On the other hand, due to their enhanced nucleophilicity persulfides react readily with reactive oxygen species (ROS), while H_2S itself is a poor ROS scavenger (Cuevasanta et al., 2015; Filipovic et al., 2018a; Ono et al., 2014). Given the fact that ROS play an important role in signaling (D'Autréaux and Toledano, 2007; Finkel, 2011) and aging (Finkel and Holbrook, 2000) it is tempting to speculate that the general beneficial effects of H_2S are evolutionary conserved and conveyed through protein persulfidation.

To better understand persulfidation *in vivo,* we explored the phenomenon that, if first transformed to mixed aromatic disulfides, protein persulfides could be selectively labeled by certain nucleophiles. Here we report the development of a new, dimedone-based method that enables chemoselective persulfide bioconjugation of proteins from a wide range of source materials in vitro and in vivo. Using this new method, we report that persulfidation plays an integral role in hydrogen peroxide-based signal transduction. We also found that protein persulfidation decreases with age and is maintained by interventions that increase lifespan across evolutionary boundaries, and may thus play a previously unrecognized protective role against aging.

RESULTS

Development of dimedone switch method

To be able to use nucleophilic substitution to tag persulfides, P-SSH need to be transformed into a mixed disulfide (Wedmann et al., 2016; Zhang et al., 2014) in such way that one of the sulfurs in the S-S bond possesses much more enhanced electrophilicity (Figure S1A). Despite their selectivity in sulfenic acid labeling (Klomsiri et al., 2010; Paulsen and Carroll, 2013; Yang et al., 2014), dimedone-based probes (**Figure 1A**) could be an excellent candidate for the nucleophile. They are additionally attractive candidates since a plethora of those probes with different reporting moieties are already available and thoroughly tested (Furdui and Poole, 2014; Paulsen and Carroll, 2013). However, for dimedone-based probes to be used in P-SSH labeling, the initial thiol blocking reagent must block sulfenic acids as well. 4-chloro-7-nitrobenzofurazan (NBF-Cl) fulfills this criterion, since it is used as a tool for detection of thiols, amines and sulfenic acids (Bernal-Perez et al., 2012; Ellis and Poole, 1997) (**Figure 1B**). We initiated our study by monitoring the labeling of the low molecular weight persulfide, *N*-methoxycarbonyl penicillamine persulfide (nmc-PSSH, (Artaud and Galardon, 2014)) (**Figure 1C**). Nmc-PSSH reacted readily with NBF-Cl resulting in a characteristic absorbance maximum at 412 nm (**Figure 1D**). The addition of an equimolar

amount of dimedone led to a fast disappearance of the 412 nm peak, suggesting that switching did occur (**Figure 1E**). ESI-TOF MS/MS analysis of the reaction mixture confirmed that the two main products are the NBF-SH and dimedone labeled nmc-PSSH (**Figure 1C**, Figure S1B-F).

We then evaluated the selectivity of the dimedone switch method by using human serum albumin (HSA) as a model (Cuevasanta et al., 2015). HSA has 17 disulfides and 1 free thiolate and is therefore both a good control and an example of a protein with an oxPTM of cysteine. Human serum albumin (HSA-SH), its sulfenylated (HSA-SOH) and persulfidated (HSA-SSH) forms reacted with NBF-Cl to generate products with distinct absorbance maxima that fit well to those reported in the literature (Ellis and Poole, 1997) (Figure S1G, I, K). The addition of dimedone caused tag-switching only in the HSA-SSH sample (**Figure 1F**, **G,** Figure S1H, J) resulting in the loss of HSA-SS-NBF absorbance and formation of the HSA-S-dimedone and NBF-SH products. Separation of treated samples by electrophoresis and subsequent immunoblotting with anti-dimedone antibody (Seo and Carroll, 2009) gave a positive signal for HSA-SSH only (**Figure 2A**). To confirm the labeling of naturally occurring persulfides, we used thiosulfate sulfur transferase (TST, also known as rhodanese), an enzyme that forms a persulfide during its catalytic cycle, as a model (Filipovic et al., 2018b). Both immunoblotting with anti-dimedone antibody (**Figure 2B**) and ESI-TOF-MS (**Figure 2C**) revealed TST labeled with dimedone.

Dimedone switch method for MS analysis

With these data in hand, we envisioned that the dimedone switch method could enable the installation of various payloads onto a protein of interest that would allow specific identification/visualization. We first used DCP-Bio1, a biotinylated form of dimedone (**Figure 1A)**. Persulfides of HSA and GAPDH showed positive staining (Figure S2A, B), as detected by Cy5-streptavidin. Separation of samples by streptavidin magnetic beads and subsequent in-gel detection of green fluorescence originating from amino groups labeled with NBF-Cl (**Figure 1B**), showed the selective labeling of P-SSH but not other oxPTM (Figure S2A, B).

Next, we tested if the method can be used for proteomic analysis. TST persulfide was tag-switched with DCP-Bio1 and subjected to either trypsin or chymotrypsin digestion. Combined they covered 95% of the structure (Figure S2C, Supporting Data S1, S2) and only C248, present as a persulfide in the active site of the enzyme, was found to be labeled (Figure S2C). Other cysteine residues and several lysine residues were labeled with NBF alone (Supporting Data S1, S2), according to the reaction scheme in **Figure 1B.**

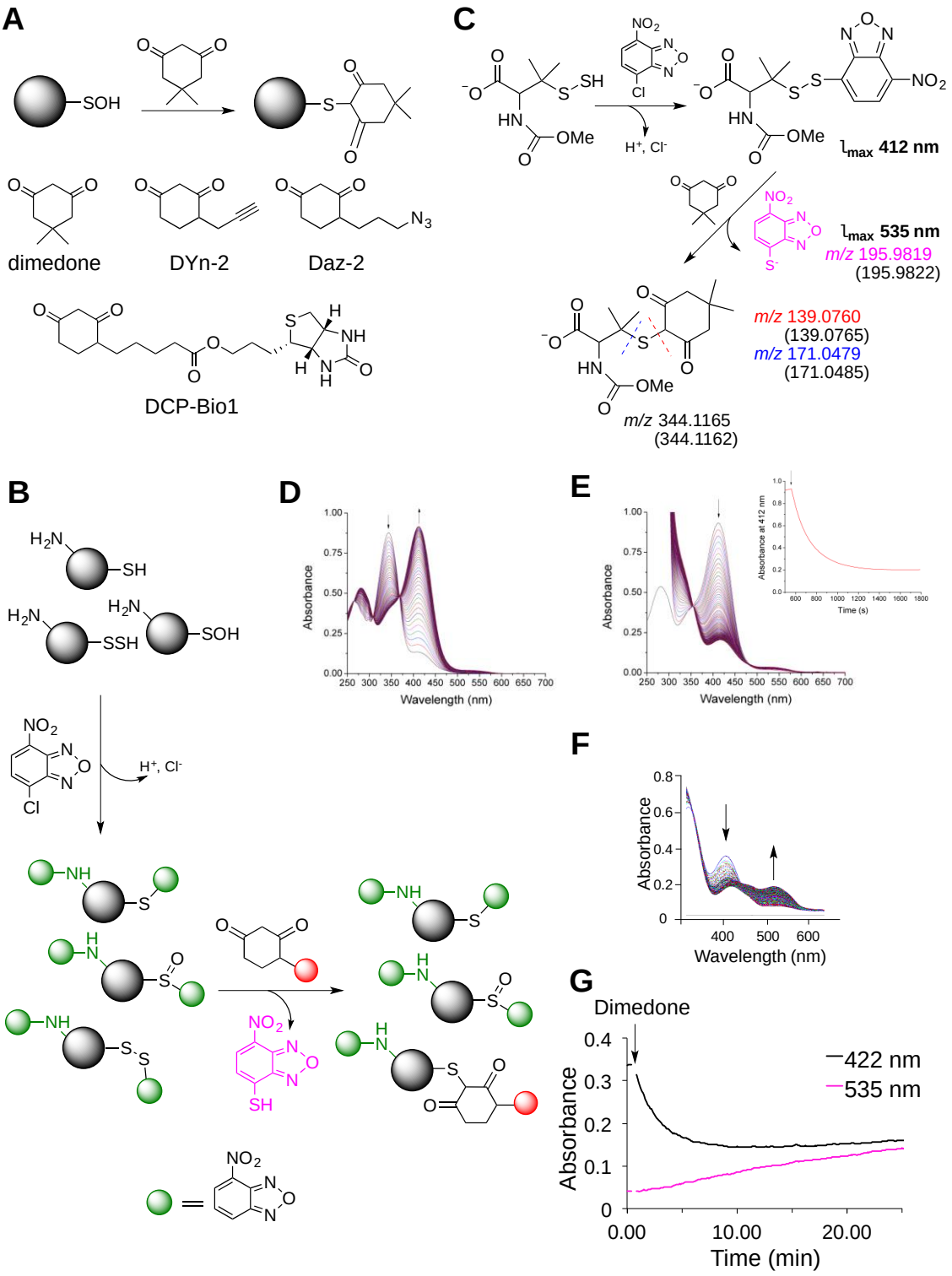

Fig. 1. Probing dimedone switch strategy for persulfide labeling.

(**A**) (Upper) Labeling of sulfenic acids with dimedone. (Lower) Structures of dimedone-based probes.
(**B**) Proposed dimedone switch strategy for persulfide labeling. In the first step proteins react with 4-chloro-7-nitrobenzofurazan (NBF-Cl) to label persulfides, thiols, sulfenic acids, and amino groups. Reaction with amino groups gives characteristic green fluorescence. In the second step, NBF tag is switched by a dimedone-based probe, selectively labeling persulfides.

(**C**) Model switch reaction with 100 µM N-methoxycarbonyl penicillamine persulfide (nmc-PSSH), 100 µM NBF-Cl and 500 µM dimedone. MS analysis reveals formation of 4-thio-7-nitrobenzofurazan (535 nm) and dimedone labeled nmc-penicillamine, which under MS/MS conditions decomposes along the blue or red dash line. Numbers given in the brackets represent calculated *m/z* for the observed ions.
(**D**) Time-resolved spectra for the reaction of 100 µM nmc-PSSH with 100 µM NBF-Cl (pH 7.4, 23 °C). Arrows indicated disappearance of NBF-Cl and appearance of nmc-PSS-NBF adduct at 412 nm.
(**E**) Time-resolved spectral changes upon addition of 200 µM dimedone to a reaction mixture shown in (**D**) (pH 7.4, 23 °C). Inset: Kinetics of decay of 412 nm absorbance maximum after addition of dimedone.
(F-G) 23 µM HSA-SH was left to react with 100 µM NBF-Cl over 30 min in phosphate buffer (50 mM, pH 7.4) with 1% SDS, at 37 °C and then 200 µM dimedone was added. UV-Vis spectral changes (**F**) and kinetic traces (**G**) show the decay of the 422 nm absorbance and the appearance of a 535 nm peak.

Furthermore, we used DCP-Bio1 labeling to identify the endogenously persulfidated proteins in human erythrocytes (**Figure 2D,** Table S1). Out of 56 identified proteins more than half were previously reported to contain reactive cysteine residues. These proteins were either found to be prone to cysteine oxidation in red blood cells (RBC) depleted of haemoglobin (Delobel et al., 2016) or treated with diamide (Zaccarin et al., 2014), in RBC from peroxiredoxin II deficient mice (Yang et al., 2012) or are found to be directly persulfidated (Valentine et al., 1987). More importantly, both enzymes involved in H_2S production in erythrocytes were also found to be persulfidated: 3-mercaptopyruvate sulfur transferase (MPST) and methanethiol oxidase. The former is known to form a persulfide during the catalytic cycle (Yadav et al., 2013) while the latter produces both H_2O_2 and H_2S (Pol et al., 2018), facilitating the oxidation of a cysteine residue to a sulfenic acid first and then to form a persulfide. In addition, peroxiredoxins, known to form sulfenic acid during the catalytic cycle (Wood et al., 2003), were found to be persulfidated as well. It is also worth noting that all identified peptides, even those not falling within selection criteria (at least 2 reliable peptides and -10logP>50) originated from cysteine containing proteins, indicative of the very high selectivity of this approach.

In-gel detection of intracellular protein persulfidation

We next tested the possibility of detecting P-SSH directly in gel, by installing a Cy5-fluorescence moiety through Copper(I)-catalyzed Azide-Alkyne Cycloaddition (CuAAC, click chemistry). In addition to labeling cysteines, NBF-Cl also reacts with amino groups giving a characteristic fluorescence with λ_{ex} at 488 nm (Bernal-Perez et al., 2012). Low NBF-Cl/protein ratio showed that NBF-persulfide adduct contributed to the overall green fluorescence detected in the gel, resulting in the loss of green fluorescence upon switching (Figure S2D). Commercially available TST (already partially present as a persulfide) was incubated with either thiosulfate or dithiothreitol (DTT) to form a fully persulfidated or fully reduced form, respectively. 20 µM

enzyme was mixed with 50 μM NBF-Cl and the persulfide was visualized using Daz-2/Cy5 CuAAC. While both untreated and thiosulfate treated showed Cy5 signal, the green fluorescence signal was significantly reduced in the fully persulfidated enzyme, despite the same load. On the other hand, the green fluorescence signal was much stronger in the fully reduced enzyme, suggesting that at low NBF-Cl/protein ratio, switching caused by the dimedone-based probe could affect the intensity of green fluorescence (Figure 2SD), so we opted for using at least 10-fold excess of NBF-Cl (Figure S2E). This use of NBF-Cl in excess additionally offered the opportunity to use the green fluorescence as a measure of the total protein load and to therefore quantify the persulfidation levels by measuring the Cy5/488 fluorescence signal ratio. Different components of click chemistry did not show any interference with the labeling in the presence of NBF-Cl (Figure S2F). Together these data presage the utility of the dimedone switch approach in biological environments.

Cell lysis with NBF-Cl, switching with DAz-2 (that bears a biorthogonal azide group) and then the subsequent coupling to Cy5-alkyne via a CuAAC reaction resulted in the labeling and in-gel detection of a red fluorescence signal only when all three reagents were used (**Figure 2E**). We found that lysis with 5 mM NBF-Cl is already sufficient to give maximal persulfide signal (Figure S2G). Treatment of cell lysates with TCEP to reduce the disulfide bond formed in the reaction of NBF-Cl and protein persulfidation, diminished the detected Cy5 fluorescence (**Figure 2F**), confirming the chemical basis for the dimedone switch approach proposed in **Figure 1B**. Additionally, treatment of HeLa cells with different sources of H_2S increased the intracellular persulfidation levels several-fold (**Figure 2G, H**). 200 nM mitochondria-targeted H_2S donor, AP39, induced comparable increase as 200 μM Na_2S, confirming the strong pharmacological potential of this compound (**Figure 2G, H**).

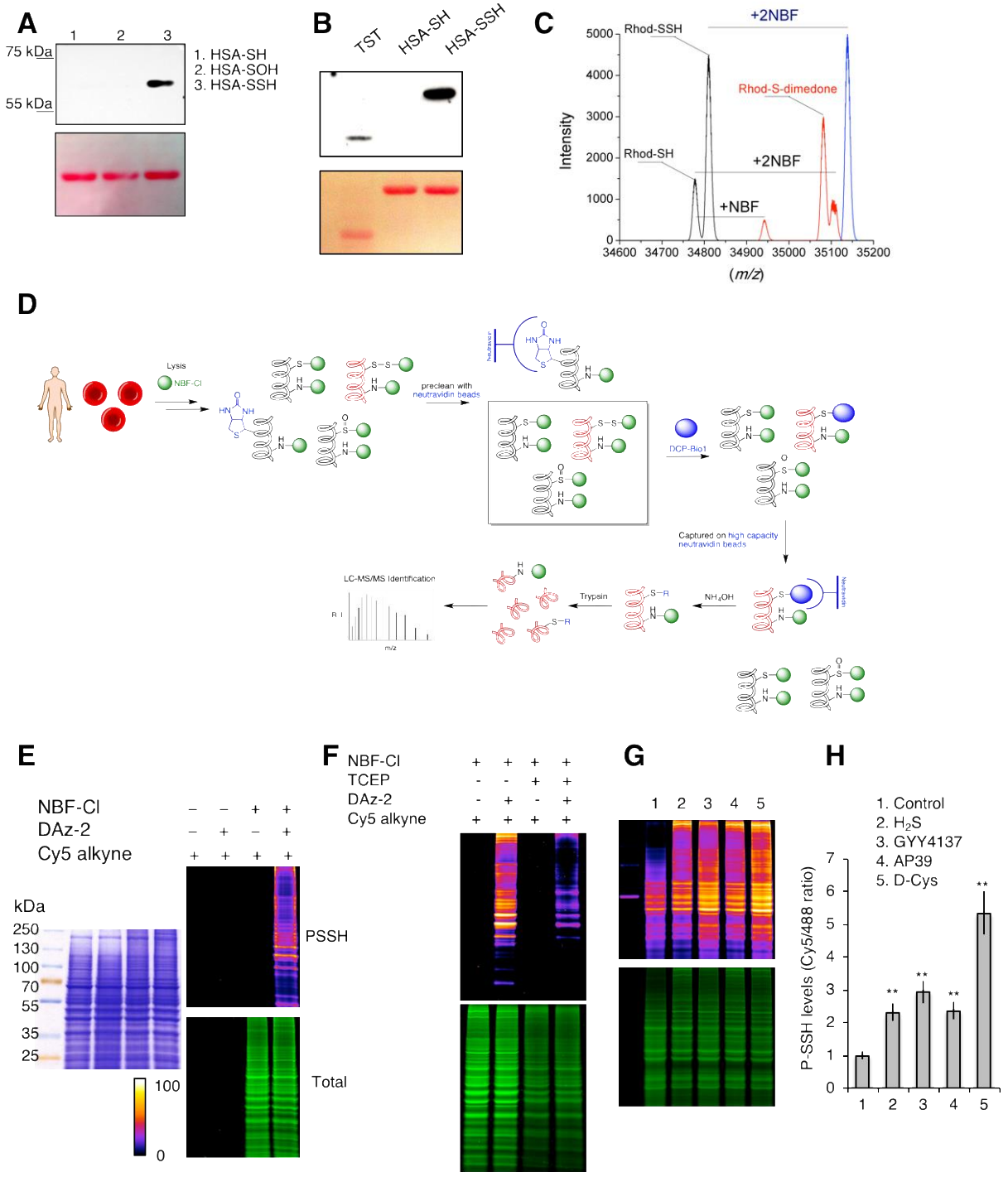

Figure 2. Protein persulfide labeling and identification.

(**A-B**) Selectivity of dimedone-switch method for protein persulfides. Human serum albumin (A) and TST (B) were used as a model. Dimedone labeling was visualized by rabbit polyclonal anti-dimedone antibody. Ponceau S staining was used for the protein load.

(**C**) Deconvoluted mass spectra 20 μM rhodanese (black), rhodanese treated with 100 μM NBF-Cl (blue) and rhodanese treated first with 100 μM NBF-Cl then with 500 μM dimedone (red).

(**D**) Schematic depiction of the protocol used for the proteomic analysis of endogenous persulfidation in RBC.

(**E**) In-gel detection of P-SSH levels in cells using CuAAC. HeLa cells were lysed either with or without 5 mM NBF-Cl and probed for persulfide labeling with DAz-2 and Cy5-alkyne by CuAAC. Gels were also stained with Coomassie

Brilliant Blue. Fire pseudo-colouring was used to visually enhance the signal. Green fluorescence corresponds to the total protein load (NBF-protein adducts).
(**F**) After lysis with 5 mM NBF-Cl samples were treated with or without 5 mM TCEP and labeled with Daz-2/Cy5-alkyne CuAAC.
(**G-H**) Protein persulfidation levels in HeLa cells treated with different H_2S donors: 200 μM Na_2S (H_2S) for 45 min, 200 μM GYY4137 for 2 h, 200 nM AP39 for 2 hr and 2 mM D-cysteine for 1 hr. Ratio of Cy5/488 signals is used for the quantification (**G**). Data shown as mean ± SD of 3 individual experiments.

Persulfidation is evolutionarily conserved and controlled by H_2S generation from cysteine metabolism

Although initial studies suggested that the main source of intracellular persulfides is H_2S, produced predominantly by CSE (**Figure 3A**) (Filipovic et al., 2018b; Mustafa et al., 2009; Paul and Snyder, 2012), recent findings questioned this by claiming that persulfides are synthesized during protein translation and are not related to the reverse transsulfuration pathway or cysteine catabolism (**Figure 3A**) (Akaike et al., 2017). Persulfidation levels were significantly reduced in mouse embryonic fibroblasts (MEFs) originating from $CSE^{-/-}$ animals (**Figure 3B**). Interestingly, repeated cell splitting of the same cell line leads to less pronounced differences in these levels due to compensatory overexpression of cystathionine-β-synthase (CBS, Figure S3A, B). CSE is profoundly diminished in Huntington's Disease (HD), a neurodegenerative disease triggered by the expansion of polyglutamine repeats in the huntingtin protein (Paul et al., 2014). In striatal cell-line models of HD (ST$Hdh^{Q7/Q7}$ and ST$Hdh^{Q111/Q111}$) harboring 7 and 111 polyglutamine repeats, we now show that the lack of CSE results in the barely detectable P-SSH levels in the ST$Hdh^{Q111/Q111}$ cells (**Figure 3C**). CSE is known to be the predominant source of H_2S in this cell type (Paul et al., 2014; Sbodio et al., 2016). Furthermore, inhibition of cystine transporter, system x_c^- with erastin also resulted in the loss of protein persulfidation (**Figure 3D**). Additionally, pharmacologically induced overexpression of CSE by Golgi stressor, monensin (Sbodio et al., 2018), on the other hand, resulted in an increase of intracellular persulfidation (**Figure 3E**).

We expanded the screening to different phyla and regna, and in all of them endogenous persulfidation was found to be controlled by H_2S produced via the transsulfuration pathway or cysteine catabolism (**Figure 3A**). We used an *E. coli* strain that is transformed with the phsABC operon (pSB74 plasmid) encoding for thiosulfate reductase, causing increased H_2S production. Treatment of these bacteria with thiosulfate resulted in a two-fold increase of bacterial protein persulfidation when compared to control (**Figure 3F**). On the other hand, *cth-1* and *mpst-3* mutants of *C. elegans* (lacking CSE and MPST, respectively, **Figure 3G**) also showed lower P-SSH levels. *Drosophila melanogaster* flies overexpressing CSE (Snijder et al., 2015) showed increased P-SSH

levels (**Figure 3H**) while kidneys from $CSE^{-/-}$ mice showed reduced persulfidation levels (**Figure 3I**). Finally, endogenous persulfidation could be observed in human RBC, in both membrane and cytoplasm, confirming the proteomic data (**Figure 3J, Table 1**).

The dimedone switch method was also successfully applied for the visualization of intracellular persulfides by confocal microscopy (**Figure 3K,** Figure S3C). MEFs lacking CSE showed barely any detectable intracellular levels of P-SSH, while both H_2S and D-cysteine treatments increased those levels several-fold. Independent of CSE, both sources of H_2S increased the P-SSH levels highlighting the essential role of H_2S in protein persulfide formation (**Figure 3K,** Figure S3C). Furthermore, wide-field fluorescence deconvolution microscopy provided the first high-resolution images of intracellular persulfidation (Figure S3D-F). The P-SSH signal is dispersed throughout the cell, with some of it being detected even in the nucleus. The P-SSH signal in D-cysteine treated cells seems to be predominantly localized in mitochondria, in accordance with the fact that D-cysteine is a substrate for cysteine catabolism path via MPST (Shibuya et al., 2013) (Figure S3F).

Broad applicability of dimedone switch method: antibody microarray

To further showcase the applicability of the dimedone switch method, we used an antibody microarray-like approach, where antibodies for specific proteins were immobilized on an NHS-activated surface (**Figure 3L**). As the samples carry both green and red fluorescence, reflecting the total load and P-SSH levels respectively, proteins of interest could be analyzed by this approach and their P-SSH levels assessed. We selected antibodies against a series of proteins (**Figure 3L**) for which persulfidation has been shown, or which form persulfides in their catalytic cycles. In general, the lack of CSE reduced P-SSH levels of target proteins while D-cysteine treatment increased it, albeit with different efficiencies. The selectivity of the method is once more demonstrated, as enzymes reported to form persulfides at their active sites during the H_2S oxidation, sulfide:quinone oxidoreductase (SQOR) and TST, showed high endogenous P-SSH levels with minimal changes upon further D-cysteine treatment. However, a significant decrease of steady-state persulfide levels of those enzymes was observed in cells lacking CSE. Aside from the proteins whose persulfidation has already been demonstrated (GAPDH, HSP70, Keap 1, ß-actin, Parkin) (Mustafa et al., 2009; Vandiver et al., 2013; Yang et al., 2013; Zhang et al., 2014), this approach led to the observation that manganese superoxide dismutase (MnSOD) could be persulfidated as well (**Figure 3L**). Unlike prokaryotes, most eukaryotic MnSOD have at least one cysteine residue (**Figure 3M**, Figure S3G) and exhibit strong product inhibition by H_2O_2 (Hearn

et al., 2001). Our experiments with human recombinant MnSOD showed that a 15 min exposure to a 3-fold excess of H_2O_2, inhibited MnSOD activity (0.15 ± 0.06 x 10^3 U/mg vs. 2.91 ± 0.07 x 10^3 U/mg in the control) while the co-treatment with 5-fold excess of H_2S rescued the enzymatic activity (1.92 ± 0.07 x 10^3 U/mg) (**Figure 3N**). MS/MS analysis of human recombinant MnSOD treated with H_2O_2 and H_2S and labeled by the dimedone switch method (using DCP-Bio1) confirmed that C193 was indeed persulfidated (Figure S3H, I, Data S3, S4). Other studies have pointed out that the same cysteine residue is redox sensitive (Matsuda et al., 1990). Furthermore, persulfidated MnSOD was more resilient to tyrosine nitration by peroxynitrite (yield of nitration per subunit 3±2%) when compared to the control (15±4%/subunit), suggesting that persulfidation of MnSOD might serve as a protective mechanism against detrimental enzyme nitration found in many disease states (Szabó et al., 2007).

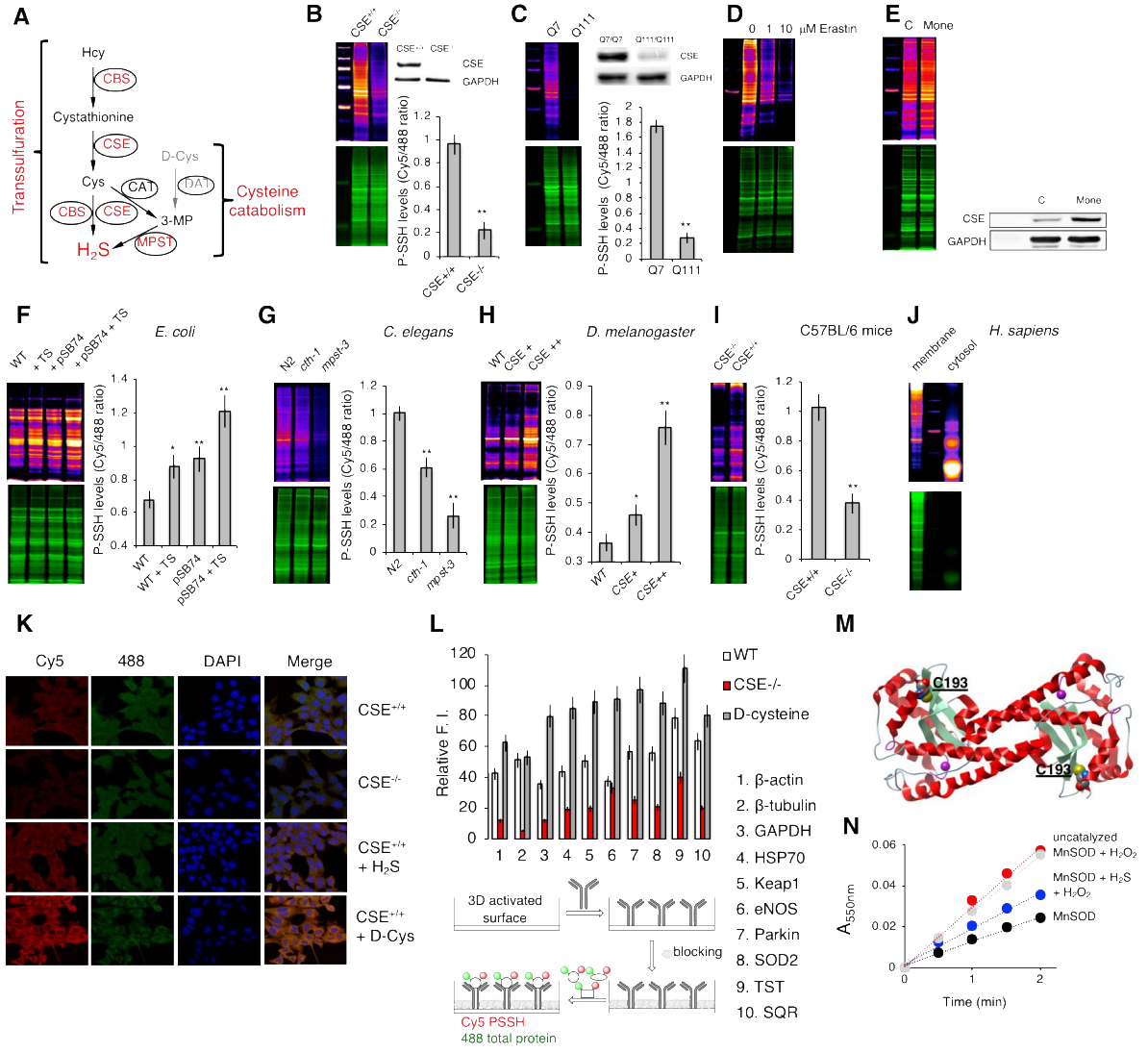

Figure 3. Intracellular persulfidation is evolutionarily conserved and controlled by H_2S producing enzymes.

(**A**) Intracellular H_2S production is catalyzed by cystathionine gamma lyase (CSE) and cystathionine beta synthase (CBS), *via* the reverse transsulfuration pathway, and by 3-mercaptopyruvate sulfur transferase (MPST) in cysteine catabolism pathway. Hcy: homocysteine; Cys: cysteine; 3MP: 3-mercaptopyruvate; CAT: cysteine aminotransferase; DAT: D-amino acid aminotransferase.
(**B**) P-SSH levels in MEFs from wild type and $CSE^{-/-}$ mice. Inset: Western blot analysis of CSE levels. n = 3.
(**C**) P-SSH levels in ST$Hdh^{Q7/Q7}$ and ST$Hdh^{Q111/Q111}$ cells. Inset: Western blot analysis of CSE levels. n = 3.
(**D**) The effect of 1 and 10 μM Erastin on P-SSH levels in WT MEF cells. n = 3.
(**E**) P-SSH levels in WT MEF cells for control, C, and treated with 1 μM Monensin, Mone. Inset: Western blot analysis of CSE levels. n = 3.
(**F**) P-SSH levels in *E. coli* without or with phsABC operon (pSB74 plasmid) that encodes thiosulfate reductase and results in H_2S production. TS- thiosulfate. n = 3.
(**G**) P-SSH levels in wild type (N2), *cth-1* (CSE) and *mpst-1* (MST) *Caenorhabditis elegans* mutants. ~ 4000 worms per sample. n = 3.
(**H**) P-SSH levels in wild type (y^1w^{118}) *Drosophila melanogaster* and flies with different levels of CSE overexpression. 3-4 flies per samples. n = 3.
(**I**) P-SSH levels in kidney extracts form wild type (C57BL/6J) and $CSE^{-/-}$ mice. n = 5 animals.
(**J**) Protein persulfidation in RBC membrane and cytosol from a healthy human donor.
(**K**) Confocal microscopy images of intracellular protein persulfide levels of WT and $CSE^{-/-}$ MEFs treated or not with 200 μM Na_2S or 2 mM D-cysteine for 1 hr. Cy5 signal corresponds to protein persulfides, 488 nm signal corresponds to NBF-adduct with amino groups of proteins. Nuclei are stained with DAPI. Scale bar 20 μm.
(**L**) Antibody microarray-like approach to study persulfidation status of specific proteins. Schematic depiction of the method (lower part) and the actual readout (upper part) for the ten listed proteins. Cell lysates from WT, $CSE^{-/-}$ and WT MEFs treated with D-cysteine (2 mM, 1 hr) were compared. Results are presented as mean ± SD from 3 independent experiments.
(**M**) Ribbon structure of two subunits from human MnSOD (PDB: 1pl4), highlighting the cysteine residues and manganese containing active site.
(**N**) SOD activity of 13 μM MnSOD, MnSOD pretreated with 3-fold excess of H_2O_2 (15 min, 37 °C) and MnSOD pretreated with both 3-fold excess of H_2O_2 and 5-fold excess of H_2S. SOD activity was measured using cytochrome c as a reporting molecule and xanthine/xanthine oxidase system as a source of superoxide. Results are presented as mean ± SD from 3 independent experiments.

Persulfidation is intrinsically linked to H_2O_2

For H_2S to be able to modify cysteine residues, an oxidant is required - a role that could be played by H_2O_2. Protein sulfenylation, as a consequence of H_2O_2 production, represents an important signaling event (Paulsen and Carroll, 2013; Poole et al., 2004). However, P-SOH formation should be controlled in order to prevent overoxidation of cysteine residues to sulfinic (P-SO_2H) and sulfonic acids (P-SO_3H) that results in a loss of protein function (**Figure 4A**). Previous studies showed that protein P-SOH react two orders of magnitude faster with H_2S, than with glutathione (Cuevasanta et al., 2015) and our proteomic analysis of persulfidated proteins in RBC showed a significant overlap with proteins known to be sulfenylated (Table S1). We hypothesized that the reaction of H_2S with P-SOH could represent an integral part of H_2O_2-induced redox signaling and the main way for resolving P-SOH back to thiols. To test this, we first exposed $CSE^{+/+}$ and $CSE^{-/-}$ MEFs to H_2O_2. While 100 μM H_2O_2 induced no detectable increase in P-SOH levels in $CSE^{+/+}$

cells, a massive increase in sulfenylation was detected in $CSE^{-/-}$ that decreased as exposure time increased (**Figure 4B**). 500 μM H_2O_2 was required to cause the same magnitude of P-SOH formation in $CSE^{+/+}$ cells (**Figure 4B**). This effect that could be completely abolished by pre-incubating the cells with 100 μM H_2S donor GYY4137 (Figure S4A). Conversely, the P-SSH levels in $CSE^{+/+}$ cells increased time-dependently when treated with 100 and 500 μM H_2O_2 but remained very low in $CSE^{-/-}$ cells (**Figure 4C**). Recent development of selective probes for sulfinic acids (P-SO_2H) (Akter et al., 2018) allowed us to test how sulfinylation changes in cells lacking endogenous H_2S. A strong overall increase of sulfinylation was observed in $CSE^{-/-}$ cells treated with 100 μM H_2O_2 for 15 min, but this P-SO_2H dropped back to normal after 30 min suggesting that those cysteines either became hyperoxidized or reduced back by sulfiredoxin (Akter et al., 2018) (**Figure 4D**). 500 μM H_2O_2 caused increase of sulfinylation only on a selected group of proteins in $CSE^{+/+}$ cells.

To address how endogenous H_2S controls H_2O_2-induced cysteine oxidation on a molecular level we opted for monitoring the cysteine oxidation status in a redox sensitive protein, DJ-1. C106 is known to undergo oxidation to a sulfinic (Akter et al., 2018) and even sulfonic acid (Fernandez-Caggiano et al., 2016), while our proteomic analysis indentified DJ-1 as a target for persulfidation as well (Suppoting Table S1). $CSE^{+/+}$ and $CSE^{-/-}$ cells were treated with 100 μM H_2O_2 for 15 and 30 min, labeled for P-SOH (using DCP-Bio1), P-SSH (using DCP-Bio1 as a switching reagent) and P-SO_2H (using BioDiaAlk) and immunoprecipitated. In parallel, using an antibody selective for C106 sulfonic acid we assessed the DJ-1-SO_3H levels in those samples (**Figure 4E**, Figure S4B). H_2O_2 treatment of $CSE^{+/+}$ cells resulted in increased persulfidation of DJ-1 (in 15 and 30 min) and increased sulfonylation after 30 min. However, in $CSE^{-/-}$ cells a further decrease of DJ1-SSH levels was observed in cells treated with H_2O_2 but a pronounced increase of DJ1-SOH, DJ1-SO_2H and DJ1-SO_3H levels. Furthermore, the basal levels of these modifications were much higher in untreated $CSE^{-/-}$ cells when compared to $CSE^{+/+}$ (**Figure 4E**, Figure S4B). Taken together these data confirmed that persulfidation, controlled by endogenous H_2S production, is an integral part of H_2O_2-induced redox changes in proteins.

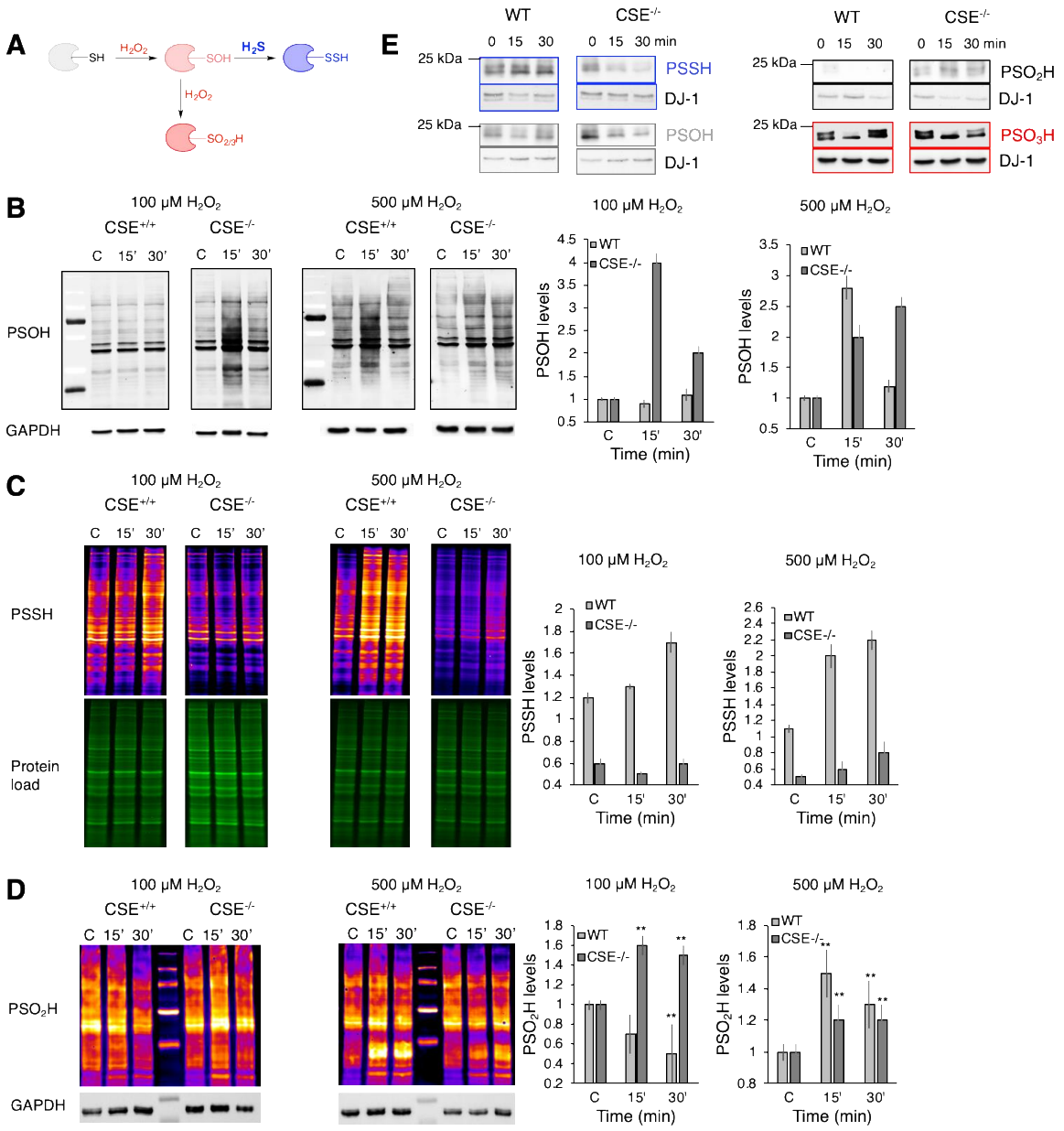

Figure 4. Endogenous H_2S controls cysteine oxidation caused by H_2O_2.

(**A**) The proposed mechanism for the redox switching between H2O2-induced thiol oxidation and persulfidation.
(B) Protein sulfenylation in $CSE^{+/+}$ and $CSE^{-/-}$ MEF cells treated with 100 or 500 μM H_2O_2 for 15 or 30 min. Blots were visualized with streptavidin-488 on a Typhoon FLA 9500. GAPDH was used as a loading control. Representative blots of n=4.
(**C**) Protein persulfidation in $CSE^{+/+}$. Fire pseudo-colouring was used to visually enhance the PSSH signal. Green fluorescence corresponds to the total protein load (NBF-protein adducts). Ratio of Cy5/488 signals is used for the quantification. n = 3.
(**D**) Protein sulfinylation in $CSE^{+/+}$ and $CSE^{-/-}$ MEF cells treated with 100 or 500 μM H_2O_2 for 15 or 30 min. Blots were visualized with streptavidin-Cy3. GAPDH was used as a loading control. Representative blots of n = 5.
(**E**) Persulfidation, sulfenylation, sulfinylation and sulfonylation of DJ-1. $CSE^{+/+}$ and $CSE^{-/-}$ MEF cells were treated with 100 μM H_2O_2 for 15 or 30 min, labelled for P-SSH, P-SOH and P-SO_2H using biotnylated reagents, immunoprecipitated with anti DJ-1 antibody immobilized to agarose beads and bloted with anti-biotin antibody. For sulfonylated DJ-1, antibody selective for C106 sulfonic acid of DJ-1 was used. n = 4.

P-SSH waves follow P-SOH formation: implications for RTK-H_2O_2 signaling

The importance of P-SOH signaling is best exemplified by the receptor tyrosine kinase (RTK) activation (Finkel, 2011; Paulsen et al., 2011; Sundaresan et al., 1995), thus we looked for the temporal correlation between P-SOH and P-SSH (**Figure 5A**). HeLa cells treated with 100 ng/ml of epithelial growth factor (EGF) responded by a sharp rise in P-SOH within the first 5-15 min that dropped back to basal values by 30 min (**Figure 5B**). P-SSH levels however, followed a phase shifted curve, with the levels initially dropping at 5 min and then reaching a maximum at 30 min. This correlated well with the overexpression of all three H_2S producing enzymes (Figure S4C).

To confirm the interplay between of P-SOH and P-SSH, we pretreated cells with GYY4137 (**Figure 5C**, Figure S5D) or with a mix of CSE and CBS inhibitors (propargylglycine and aminooxyacetic acid, **Figure 5D**, Figure S5E) for 30 min to either increase or decrease, respectively, the intracellular H_2S and P-SSH levels. Pretreatment with GYY4137 indeed induced an increase of P-SSH, and upon EGF stimulation these levels continued to rise over 30 min, while P-SOH dropped, remaining low and unchanged (**Figure 5C**, Figure S5D). In contrast, the pharmacological inhibition of endogenous H_2S production resulted in a sharp rise of P-SOH levels, peaking at 5 min, and being fully resolved at 15 min, presumably due to cysteine overoxidation, as P-SSH levels remained very low and unchanged (**Figure 5D**, Figure S5E). These results strongly suggested that persulfidation represents the innate mechanism that cells use to resolve signaling by sulfenylation. At the same time, as both labeling approaches use dimedone-based probes, these data confirmed once more that the dimedone switch method can distinguish P-SSH from P-SOH.

We then tested other RTK pathways. The treatment of human umbilical endothelial vein cells (HUVEC) with 40 ng/ml of vascular endothelial growth factor (VEGF) showed similar phase-shift curves for P-SOH and P-SSH, with P-SOH peaking at 5 min and reverting back to basal levels already after 15 min, while P-SSH levels peaked at 15 min and stayed high even after 30 min (**Figure 5E**, Figure S4F). P-SSH increased ~ 9 times in cells exposed to VEGF for 15 min, in accordance with very high H_2S production rate that these cells possess (Filipovic et al., 2018b; Lin et al., 2013). The treatment of neuroblastoma cells (SH-SY5Y) with insulin, produced again a distinct peak of P-SSH levels, with the peaking time and the intensity of change correlating directly with the dose of insulin (**Figure 5F,** Figure S4G). The kinetics of sulfenylation preceded the P-SSH wave in a phase shifted manner (Figure S4H). Finally, we used WT and $CSE^{-/-}$ MEFs and

treated them with 100 ng/ml EGF. The temporal profile of P-SSH in WT was quite similar to that observed for HeLa cells and was inhibited in $CSE^{-/-}$ cells (Figure S4I,J). On the other hand, sulfenylation was much stronger in $CSE^{-/-}$ cells (Figure S4I,J).

Next, we turned our attention to understanding the biological relevance of these ostensible waves of persulfidation. EGF receptor activation is regulated by sulfenylation (Paulsen et al., 2011) so we focused on understanding if and how persulfidation could control the duration of EGF signaling. We first looked for the persulfidation of EGFR using commercially available antibody microarray plates for the EGFR pathway. Pentaplicates of two different antibodies for EGFR showed a strong increase in EGFR persulfidation in HeLa cells treated with EGF for 30 min (**Figure 5G**). Persulfidation of EGFR had a functional effect on the downstream signaling. Phosphorylation of Y1068, activated by cysteine sulfenylation, was strongly impaired in GYY4137 pretreated HeLa cells (**Figure 5H**). Correspondingly, the activation of the EGF receptor monitored in live cells also revealed a stronger receptor activation in cells pretreated with CSE and CBS inhibitors (PG and AOAA), an effect that could be reduced by GYY4137 pretreatment (**Figure 5I**). Furthermore, the inhibition of H_2S production to increase the half-life of EGFR sulfenylation caused a significant increase of extracellular signal-regulated kinase (ERK) phosphorylation even without EGF stimulation (Figure S4K).

Many of the cysteine containing phosphatases important for EGFR signaling have been already shown to be sulfenylated (Paulsen et al., 2011). This is particularly true for PTEN, PTP1B and SHPTP2, which we now find to be persulfidated as well (Figure S4L). In addition, using the EGFR pathway antibody microarray, we also assessed the persulfidation status of kinases downstream of EGFR (**Figure 5J**, Supporting Data set 5). Numerous protein targets were identified with an increased persulfidation status upon exposure to EGF. It is interesting that besides actin, kinases involved in the regulation of cystoskeleton rearrangements and cell motility are particularly affected (**Figure 5K**, Figures S4M-R). Taken together these data suggest that the formation of protein persulfides represents a redox switch for controlling cellular signaling initiated by H_2O_2 and P-SOH formation.

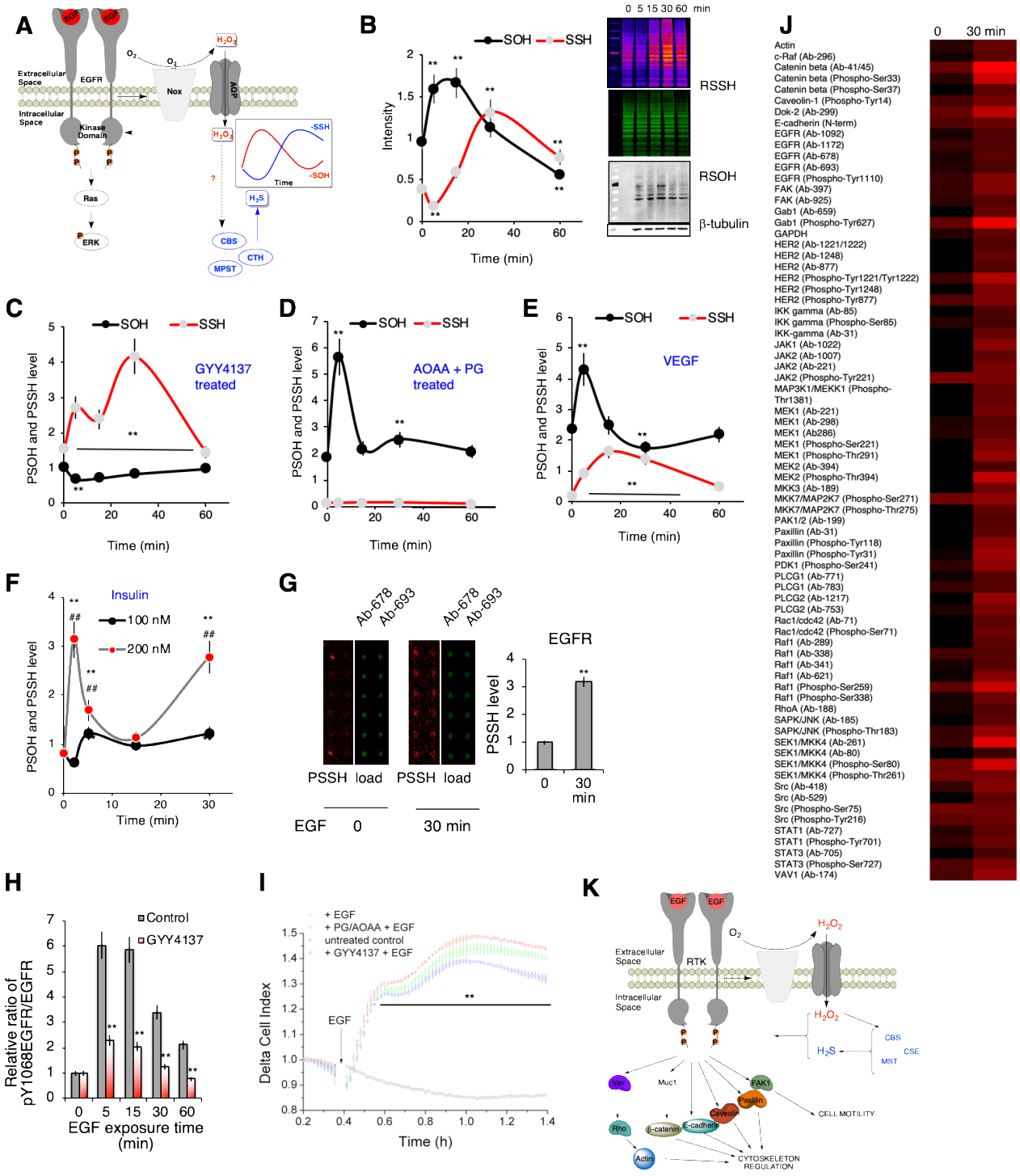

Figure 5. Waves of protein persulfidation in RTK signaling.

(**A**) Schematic representation of the signaling events triggered by the epidermal growth factor receptor (EGFR) activation. Nox: NADPH oxidase; AQP: aquaporin.
(**B**) HeLa cells treated with 100 ng/mL EGF for 5, 15, 30 or 60 min were analyzed for protein sulfenylation (using dimedone biotin and then streptavidin-488) and protein persulfidation (using dimedone switch method with Cy5 as a reporting molecule). (Right) In-gel fluorescence of P-SSH levels and Western blots for P-SOH levels. (Left) Quantification of P-SSH and P-SOH changed as a function of time of EGF exposure. n≥3. Values are presented as mean ± SD.

(**C**) Quantification of P-SSH and P-SOH changes as a function of time of EGF exposure in HeLa cells pretreated with 100 μM GYY4137 for 30 min prior the EGF treatment. n≥3. Values are presented as mean ± SD.
(**D**) Quantification of P-SSH and P-SOH changes as a function of time of EGF exposure in HeLa cells pretreated with 2 mM mixture of aminooxyacetic acid (AOAA) and propargylglycine (PG) (1:1) for 30 min prior the EGF treatment. n≥3. Values are presented as mean ± SD.
(**E**) Quantification of P-SSH and P-SOH changes in human umbilical vein endothelial cells as a function of time of VEGF (40 ng/mL) exposure. n≥3. Values are presented as mean ± SD.
(**F**) The effect of different insulin concentrations on P-SSH levels in neuroblastoma SHSY5Y cells as a function of time of insulin exposure.
(**G**) Persulfidation of EGF receptor of HeLa cells treated with 100 ng/mL EGF for 30 min, detected by two different antibodies using antibody microarray slides. n = 2.
(**H**) Time dependent phosphorylation of EGF receptor tyrosine 1068 (Y1068) as a response to 100 ng/mL EGF. HeLa cells were pretreated or not with 100 μM GYY4137 for 2 h prior to exposure to EGF. n = 3.
(**I**) Real-time measurement of EGF receptor activation in living cells recorded with xCELLigence RTCA DP system. HeLa cells were also pretreated with GYY4137 (100 μM, 30 min) or with 2 mM mixture of AOAA and PG (1:1, 30 min). EGF receptor activation was initiated by the addition of 150 ng/mL EGF.
(**J**) Antibody microarray analysis of persulfidation of different kinases involved in the EGF signaling. HeLa cells were treated with 100 ng/mL EGF for 30 min. n = 2
(**K**) Schematic presentation of protein targets involved in actin remodeling, cytoskeleton regulation and cell motility, found to be persulfidated in cells treated with 100 ng/mL EGF for 30 min.

Protein persulfidation as a rescuing path from cysteine hyperoxidation

While protein sulfenylation (and even sulfinylation for some proteins) represents a signaling event, uncontrollable production of H_2O_2 or any of the reactive oxygen species would results in the cysteine hyperoxidation and loss of function (**Figure 6A**). Our initial hypothesis was that due to its small size, diffusibility and high production flux (Cuevasanta et al., 2012; Filipovic et al., 2018b; Vitvitsky et al., 2012), H_2S could react as the first line of cellular defense against cysteine hyperoxidation (**Figure 6A**). Formed persulfides would be much better nucleophiles than cysteines alone, and could scavenge (Cuevasanta et al., 2015) more of the damaging oxidants. Owing to their reducible S-S bond, the ensuing S-sulfocysteine should be readily reduced by disulfide reductases, such as thioredoxin (Trx) (**Figure 6A**) creating a rescue loop. This is indeed the case for one of the known substrates for Trx, 3′-phosphoadenosine-5′-phosphosulfate reductase (Palde and Carroll, 2015).

To address the reversibility of persulfide oxidation, we used S-sulfocysteine (SSC) as a model system (**Figure 6B**). Incubation of human recombinant Trx with SSC at an equimolar ratio resulted in the complete oxidation of Trx, as observed by the leftward mass shift ($\Delta m/z$ = -2), corresponding to the formation of a disulfide bond (**Figure 6C**). When the C32S mutant, which is catalytically inactive, was incubated with the same amount of SSC, no spectral change could be observed (Figure S5A); whilst incubation with the C35S mutant, which initially reacts with the substrate but cannot complete the catalytic cycle, resulted in the characterization of the disulfide

adduct of Trx with cysteine (**Figure 6D**, Figure S5B). Spectrofluorometric kinetic analysis of the reaction (**Figure 6E,** S5C) derived an estimated rate constant of 6.1 ± 0.2 x 10^4 M^{-1} s^{-1}, one order of magnitude faster than the reaction with cysteine persulfide and two orders of magnitude faster than the reaction with cystine (Wedmann et al., 2016). Coupled with thioredoxin reductase (TrxR), the reaction was also faster than with cystine (Figure S5D). Thioredoxin-related protein (TRP14) however, was not as efficient in cleaving SSC as human Trx (Figure S5E).

We then assessed how persulfidation levels of different living systems correlate with their ability to resist stress. $CSE^{-/-}$ MEFs showed slower growth when compared to the wildtype cells and were much more sensitive to H_2O_2 (**Figure 6F**). *Saccharomyces cerevisiae* proved to be no exception either. Despite a slightly different cysteine and H_2S metabolism (Figure S5F), the *Δcys3* (CSE) *Saccharomyces cerevisiae* mutant showed growth retardation (Figure S5G), had lower P-SSH levels (Figure S5H), lower H_2S levels (Figure S5I) and was more sensitive to H_2O_2 than the wild type (**Figure 6G,H,** Figure S5J). *Δcys4* (CBS), on the other hand, exhibited somewhat higher H_2S and P-SSH levels and therefore was more resistant to H_2O_2.

We also tested the sensitivity of *C. elegans* to different ROS-inducing stressors. *cth-1* and *mpst-3 C. elegans* mutants showed enhanced sensitivity to paraquat (**Figure 6I**) with ~50% of *cth-1* animals dead within 4 hr of exposure (compared to ~80% alive for N2). Another ROS stressor, sodium arsenite, also proved to be more toxic to *cth-1* mutants compared to N2 (**Figure 6J**). Enhanced sensitivity of *cth-1* to paraquat and arsenite could be rescued by pretreatment with H_2S donors to increase the intracellular P-SSH levels (**Figure 6K,** Figure S5K, L). Even the N2 showed better survival after exposure to paraquat or arsenite, just by a 3 hr pretreatment with either GYY4137 or AP39 (Figure S5K, L).

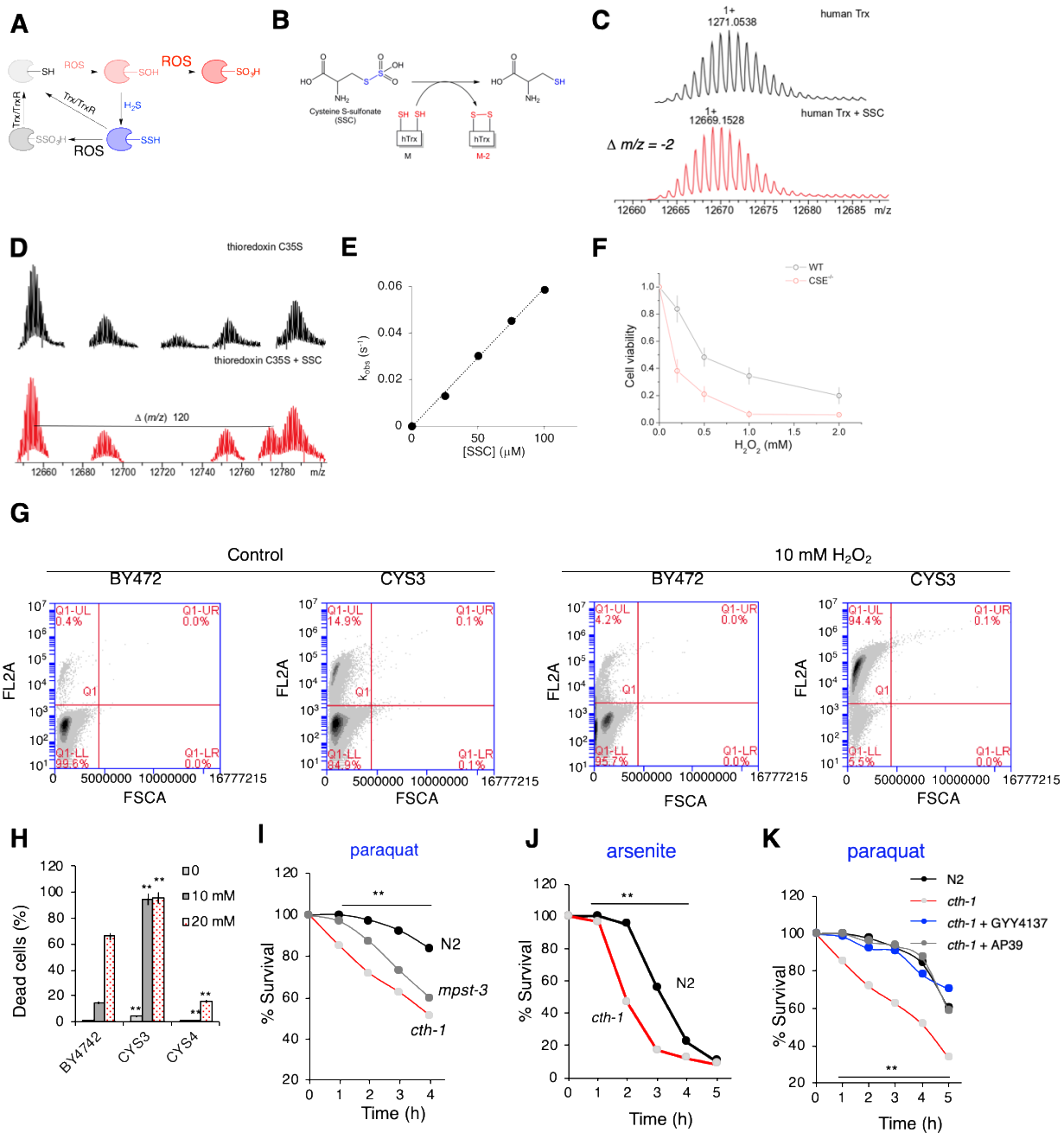

Figure 6. Cytoprotective effects of protein persulfidation.

(**A**) The proposed mechanism for the protective effects of protein persulfidation. Trx-thioredoxin, TrxR-thioredoxin reductase.
(**B**) Model reaction of S-sulfocysteine (SSC) with human thioredoxin (hTrx).
(**C**) Deconvoluted MS spectrum of 10 μM human recombinant Trx (black) and Trx treated with 10 μM S-sulfocysteine (SSC).
(**D**) Deconvolution of mass spectra of 10 μM C35S Trx before (black) and after (red) the reaction with 10 μM SSC showing appearance of TrxS-S-Cys adduct in sample treated with SSC.
(**E**) Plot of k_{obs} *vs.* concentration of SSC for the reaction with human recombinant Trx. Reaction was followed fluorometrically by measuring conformational changes induced in Trx due to the cysteine oxidation.
(**F**) Toxicity of H_2O_2 in WT and $CSE^{-/-}$ MEFs. Values presented as mean± S.D. n = 3.

(**G-H**) Flow cytometry analysis of cell death using propidium iodide (FL2A channel). Different yeast strains were grown to reach the stationary phase and then exposed to H_2O_2. Upper left quadrant was used as a measure of dead cells. 150000 cells were analysed per measurement. n=3.
(**I-J**) Survival curves of N2, *cth-1* and *mpst-3 C. elegans* strains exposed to 60 mM paraquat (**I**) and 5 mM sodium arsenite (**J**). N>80 worms. Experiments were performed in triplicate.
(**K**) The effect of short-term (3h) pre-exposure to GYY4137 (500 µM) or AP39 (100 nM) on survival rate of *cth-1 C. elegans* mutants treated with 60 mM paraquat. N>80 worms. Experiments were performed in triplicate.

Protein persulfidation decreases with aging

With aging there is an imbalance between ROS production and removal, resulting in an increase in oxidative damage (Balaban et al., 2005; Finkel and Holbrook, 2000; Liochev, 2013; Redman et al., 2018). Moreover, two independent quantitative proteomics studies found that in *C. elegans*, CSE is decreased during aging (Aging et al., 2015; Narayan et al., 2016). Here we tested the hypothesis that protective pools of intracellular P-SSH decline with age and correlate with the lifespan of individuals within a given species. While the *cth-1 C. elegans* mutants did not display an overall significantly shorter median/maximal life span, they initially exhibited a much higher death rate (Figure S6A). *Mpst-3* mutants, which had an even lower P-SSH pool (**Figure 3G**), lived significantly shorter (Figure S6A). Additionally, the persulfidation levels in wild type N2 worms gradually decreased from day 1 to day 7 of adulthood (Figure S6B). To confirm the evolutionary conservation of this phenomenon, we looked at Wistar rats of 1, 3, 6, 12, and 24 months of age. In brain extracts, reduced protein persulfidation levels were observed beginning at 6 months of age, with an approximately 50% lower persulfidation in 24-month-old rats relative to 1-month-old rats (**Figure 7A**). The reduction of P-SSH correlated with the loss of protein expression of all three H_2S producing enzymes (**Figure 7B**, Figure S6C). We also observed a profound decrease in protein persulfidation and H_2S-generating enzyme levels (CSE, 3MST) in rat hearts as a function of age (**Figure 7C**), while in liver P-SSH and CSE and CBS levels trended lower but were not significantly different between 12 and 24 month old mice, (Figure S6D).

Finally, as a proof-of-concept experiment we analyzed the persulfidation and sulfinylation levels in human fibroblasts originating from the same individual but collected at different ages (31 and 48 years of age). The results displayed a decrease in P-SSH levels and an increase in P-SO_2H (**Figure 7D**) in accordance with our hypothesis (Figure 6A).

Life-span extension by dietary restriction is caused by increased protein persulfidation

Recent studies suggest that dietary restriction (DR) increases endogenous H_2S production (Hine et al., 2015; Mitchell et al., 2016) and that this increase is associated with multiple DR benefits

including extended longevity in different species. However, the mechanism by which H_2S contributes to DR benefits remains poorly characterized. We tested the hypothesis that DR increases longevity in part by increasing protein persulfidation. We started with *C. elegans* by using the *eat-2* genetic model of DR which eat less and live longer than N2 controls. Additional deletion of either *cth-1* or *mpst-3* reduced the lifespan of *eat-2* mutant back to control levels (**Figure 7E**). Interestingly, this was in excellent concordance with the total P-SSH pool in these worms; *eat-2* mutants had approximately 3 times higher P-SSH levels than N2, while double mutants had P-SSH levels close to or even lower than N2 (**Figure 7F**). Furthermore, lifespan extension induced by 2-deoxy-D-glucose (DOG) treatment in wildtype N2 worms was completely reversed in *cth-1* and *mpst-3* mutants (**Figure 7G**).

We next looked at 7 and 20 month old C57BL/6J mice fed *ad libitum* (AL) or subject to daily 30% calorie restricted (CR) from the age of 2 months. Liver persulfidation levels declined with age, but were higher in both CR groups compared to AL (**Figure 7H**).

Furthermore, we monitored changes in persulfidation of young and old mice (2 vs 12 month-old) challenged with i.p. glucose injection. The wave of persulfidation was observed in the muscle tissue of the young mice that was blunted in the 12 month-old animals (**Figure 7I**), confirming the waves observed in cells treated with insulin (**Figure 5F**). Lower persulfidation in old mice as well as the decrease of the H_2S producing enzymes could be confirmed on yet another model system (Figure S6E).

Finally, we tested whether pharmacological interventions to increase persulfidation levels could extend lifespan. While many H_2S donors have shown considerable pre-clinical efficacy and are currently undergoing clinical evaluation (Wallace and Wang, 2015), we opted for testing an established FDA approved therapeutic drug, sodium thiosulfate, which does not release H_2S itself but exhibits beneficial effects mimicking those of H_2S (Snijder et al., 2015). We observed that treatment of cell lysates with either thiosulfate, TST or both increased the persulfidation levels several fold (Figure S6F). *C. elegans* grown on medium supplemented with 1 mM thiosulfate showed higher persulfidation levels (**Figure 7J**) as such, we opted for testing its effect on lifespan. Indeed, worms grown on medium supplemented with 1 mM thiosulfate had a significant increase (~ 15%) in median longevity (**Figure 7K**).

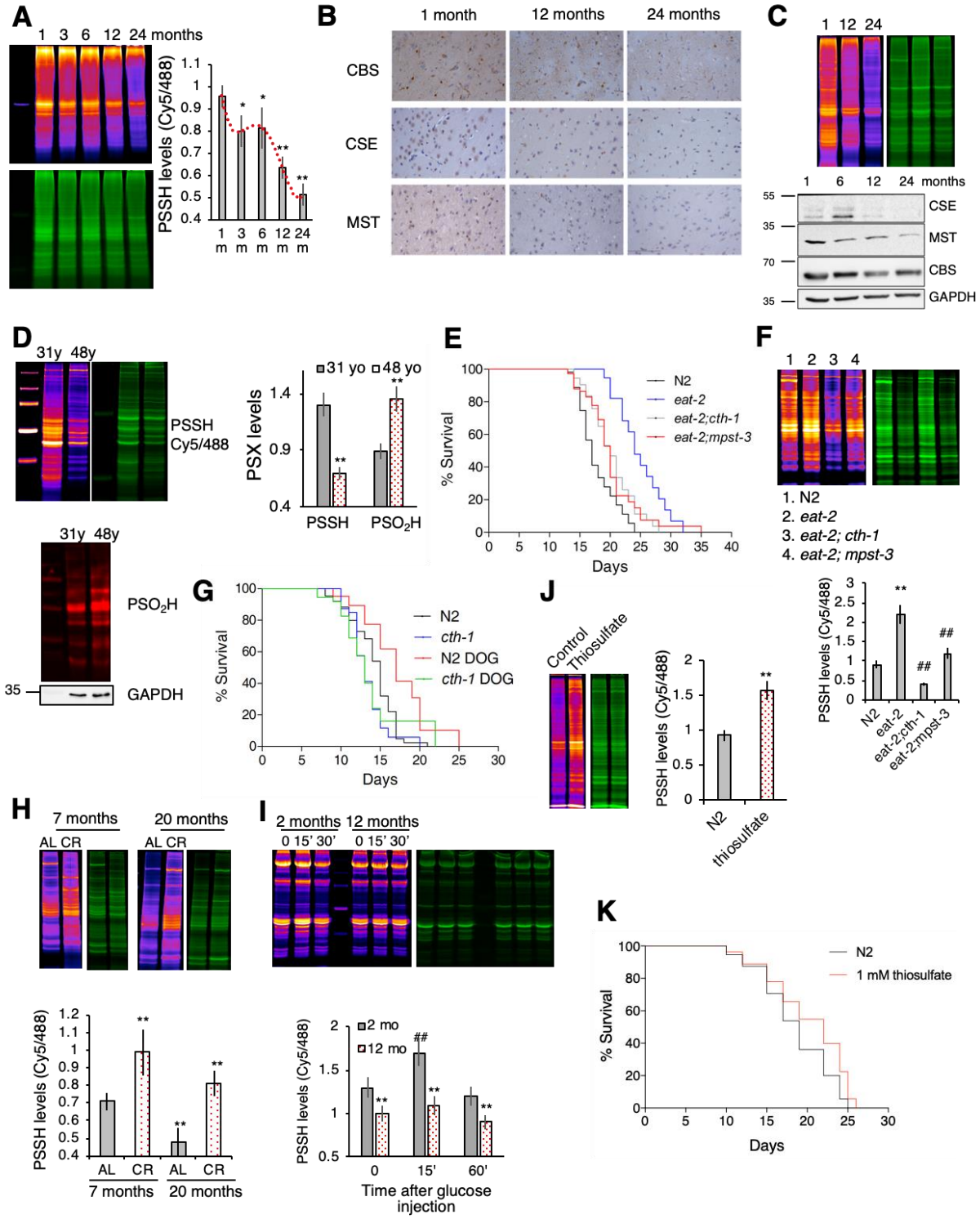

Figure 7. Anti-aging properties of protein persulfidation.

(**A**) Changes in the persulfidation levels in brain extracts from Wistar rats 1, 3, 6, 12 and 24 months of age. Values are presented as mean ± S.D. n = 3/age group.

(**B**) Immunohistochemical analysis of CSE, CBS and MST expression levels in the cortex of 1, 12 and 24 month old male Wistar rats. Images are representative of 3 animals per experimental group, magnification 20x.

(**C**) Protein persulfidation levels of 1, 12 and 24 month old hearts of male Wistar rats (top). Expression levels of CSE, CBS and MPST in hearts of 1,6, 12 and 24 month old male Wistar rats (bottom). Images are representative of 3 animals per experimental group.

(**D**) PSSH and PSO_2H levels (marked on y axis as PSX) in human fibroblasts originating from the same donor but collected at the age of 31 and 48.
(**E**) Survival curves for N2, *eat-2*, *eat-2;cth-1* and *eat-2; mpst-3* double mutants. n > 100 per each line.
(**F**) Persulfidation levels in N2, *eat-2*, *eat-2;cth-1* and *eat-2; mpst-3 C. elegans* mutants. For the fluorescence in-gel detection, P-SSH levels were calculated as a ratio of Cy5/488 fluorescence readouts. Values are presented as average ± S.D. Protein extracts from ~16000 worms were used for each lane. Experiments were performed in triplicates.
(**G**) Survival curves for N2 and *cth-1* mutants grown in the absence or presence of 5 mM 2-deoxy-D-glucose (DOG). n = 100 per each line.
(**H**) Age-induced persulfidation changes in mice fed *ad libitum* and mice fed with calorie restriction diet. Values are presented as mean ± S.D. n=5
(**I**) Time-dependent PSSH changes in the muscle tissue of mice injected i.p. with D-glucose (2 g/kg body weight). Values are presented as mean ± S.D. n ≥ 3.
(**J**) Persulfidation levels in N2 worms before and after the treatment with 1 mM thiosulfate. Values are presented as mean ± S.D.
(**K**) Survival curves for N2 *C. elegans*, and N2 treated with 1 mM thiosulfate. n > 160 per group.

DISCUSSION

Versatility and selectivity of dimedone switch method

By combining commercially available and well-characterized chemicals, our novel dimedone switch method is a simple and robust approach for selectively labeling protein persulfides, that enables the installation of various groups to proteins and the use of a wide range of detection methods. Moreover, our chemical method allows for a wide scale analysis of metabolic pathways that could be controlled by persulfidation and the identification of new redox switches. The constant green fluorescence introduced by the NBF-Cl probe provides not only the information about total load but could also be explored for high-throughput screening. It is easy to envision a setup where by measuring only the green fluorescence in microplates with immobilized neutravidin, total persulfidation labeled with DCP-Bio1 could be screened. The versatility of dimedone based probes also permits site-centric identification and quantitation of persulfides by MS, as done for protein sulfenylation (Yang et al., 2014). The installation of different fluorophores through CuAAC and almost undetectable unselective background in microscopic analysis also carries a potential for further exploration of protein persulfidation in tissue sections. Finally, the use of simple in-gel detection prevents all the problems associated with column separation and Western blot transfer, commonly used in other persulfide detection methods (Dóka et al., 2016).

Protein persulfidation is controlled by transsulfuration pathway and cysteine catabolism

From the data presented here, we conclude that protein persulfidation is almost exclusively controlled by the three H_2S producing enzymes involved in the transsulfuration pathway and cysteine catabolism (**Figure 3A**). This is evident in all tested life forms. However, in mammalian cells and under basal substrate availability (assuming that all 3 enzymes are present in the cell),

CSE is expected to be the major source of H_2S (Filipovic et al., 2018b). CBS would predominantly be involved in cystathionine production while the activity of MPST would depend on thioredoxin availability and CAT activity (**Figure 3A**). MPST could nonetheless play a significant role in controlling protein persulfidation given that D-cysteine causes a dramatic increase in protein persulfidation representing an interesting venue for drug development.

Persulfidation as integral part of H_2O_2 signaling or/and as evolutionary conserved route to rescue cysteines

As life emerged in an H_2S-enriched environment (Olson and Straub, 2016) and in under conditions of extensive radiation where ROS were formed by photolysis of water (Liang et al., 2006), protection of cysteine residues was necessitated. The formation of persulfides poses as the simplest answer. In persulfides, sulfur atoms are oxidized, however concurrently sulfur is deprotonated and highly nucleophilic, reducing ROS at least one order of magnitude faster than its corresponding thiolate (Cuevasanta et al., 2015; Filipovic et al., 2018b). In other words, while a cysteine gets oxidized to form a persulfide, it forms a strong reducing agent at the same time.

H_2O_2 as main ROS player is now widely accepted as a signaling molecule (D'Autréaux and Toledano, 2007; Holmström and Finkel, 2014; Yang et al., 2014). This is best exemplified in the case of growth factor receptor signaling (Paulsen and Carroll, 2013; Sundaresan et al., 1995). Approximately 1000 cysteine sites have been found to be sulfenylated, raising the question of, how are these sites rescued? In our study, waves of persulfidation are observed following sulfenylation, as a response to RTK activation, confirming that persulfidation is an integral part of RTK signaling. A recent study demonstrated that a large number of proteins undergo further oxidation to sulfinic acid as well (Akter et al., 2018). Our results demonstrate that without H_2S/persulfidation proteins undergo a substantial thiol oxidation (sulfenylation, sulfinylation and sulfonylation) even with H_2O_2 concentrations that cause no change in normal cells. This overlooked phenomenon questions whether and in which concentration range H_2O_2 acts as a signaling molecule without H_2S.

We demonstrate that as cells age their persulfidation levels decrease due to the loss of H_2S producing enzymes. Reacting with ROS, a persulfide will form a *S*-sulfonate which we show could be readily reduced back to a thiolate by thioredoxin. This rescue loop for preserving cysteine residues in proteins and preventing their loss of function is probably an evolutionary remnant used as a general protective mechanism in all life forms. This is best documented by the enhanced

sensitivity of different life forms with low P-SSH levels to oxidant stressors and their increased resistance once the intracellular P-SSH pool is increased even by a short-term pretreatment with H_2S donors. This unifying mechanism explains the beneficial effects of dietary restriction, already known to result in H_2S overproduction (Hine et al., 2015), as well as lifespan extension caused by pharmacological increase of protein persulfidation. Thus, our results further strengthen the ROS theory of aging (Redman et al., 2018).

It is worth mentioning that beside a general protection, persulfidation of specific proteins could result in alteration of their function (Filipovic et al., 2018b; Paul and Snyder, 2015; Vandiver et al., 2013), as we observe in the case of MnSOD, whose activity is preserved after persulfidation. It is possible that DR-induced decrease of ROS (Redman et al., 2018) could also be partially related to better activity of ROS removing enzymes.

Beside aging, general protective effects of protein persulfidation could be translated to many other disease states. HD and neurodegeneration are strongly linked to CSE expression and pharmacological interventions to increase CSE levels, such as monensin treatment, show promising therapeutic effects (Paul et al., 2014; Sbodio et al., 2016, 2018). Decreased persulfidation in HD cells and increased P-SSH levels by upregulating CSE expression reported in our study could provide a general explanation for this. Taken together, our data represent a good starting point for the fine tuning of targeted therapeutic approaches to increase health and lifespan.

REFERENCES

Aging, C., Walther, D.M., Kasturi, P., Mann, M., Hartl, F.U., Walther, D.M., Kasturi, P., Zheng, M., Pinkert, S., Vecchi, G., et al. (2015). Article Widespread Proteome Remodeling and Aggregation in Aging C . elegans. Cell *161*, 919–932.

Akaike, T., Ida, T., Wei, F.Y., Nishida, M., Kumagai, Y., Alam, M.M., Ihara, H., Sawa, T., Matsunaga, T., Kasamatsu, S., et al. (2017). Cysteinyl-tRNA synthetase governs cysteine polysulfidation and mitochondrial bioenergetics. Nat. Commun. *8*, 1177.

Akter, S., Fu, L., Jung, Y., Conte, M. Lo, Lawson, J.R., Lowther, W.T., Sun, R., Liu, K., Yang, J., and Carroll, K.S. (2018). Chemical proteomics reveals new targets of cysteine sulfinic acid reductase. Nat. Chem. Biol. *14*, 995–1004.

Alexander, B.E., Coles, S.J., Fox, B.C., Khan, T.F., Maliszewski, J., Perry, A., Pitak, M.B.,

Whiteman, M., Wood, M.E., Nakashima, I., et al. (2015). Investigating the generation of hydrogen sulfide from the phosphonamidodithioate slow-release donor GYY4137. Med. Chem. Commun. *6*, 1649–1655.

Artaud, I., and Galardon, E. (2014). A persulfide analogue of the nitrosothiol SNAP: formation, characterization and reactivity. Chembiochem *15*, 2361–2364.

Balaban, R.S., Nemoto, S., and Finkel, T. (2005). Mitochondria, Oxidants, and Aging. Cell *120*, 483–495.

Bernal-Perez, L.F., Prokai, L., and Ryu, Y. (2012). Selective N-terminal fluorescent labeling of proteins using 4-chloro-7-nitrobenzofurazan: A method to distinguish protein N-terminal acetylation. Anal. Biochem. *428*, 13–15.

Blackstone, E. (2005). H2S Induces a Suspended Animation-Like State in Mice. Science (80-.). *308*, 518–518.

Brenner, S. (1974). The genetics of Caenorhabditis elegans. Genetics *77*, 71–94.

Crouzet, M., Claverol, S., Lomenech, A.M., Le Sénéchal, C., Costaglioli, P., Barthe, C., Garbay, B., Bonneu, M., and Vilain, S. (2017). Pseudomonas aeruginosa cells attached to a surface display a typical proteome early as 20 minutes of incubation. PLoS One *12*, e0180341.

Cuevasanta, E., Denicola, A., Alvarez, B., and Möller, M.N. (2012). Solubility and Permeation of Hydrogen Sulfide in Lipid Membranes. PLoS One *7*, e34562.

Cuevasanta, E., Lange, M., Bonanata, J., Coitiño, E.L., Ferrer-Sueta, G., Filipovic, M.R., and Alvarez, B. (2015). Reaction of Hydrogen Sulfide with Disulfide and Sulfenic Acid to Form the Strongly Nucleophilic Persulfide. J. Biol. Chem. *290*, 26866–26880.

D'Autréaux, B., and Toledano, M.B. (2007). ROS as signalling molecules: Mechanisms that generate specificity in ROS homeostasis. Nat. Rev. Mol. Cell Biol. *8*, 813–824.

Delobel, J., Prudent, M., Crettaz, D., ElHajj, Z., Riederer, B.M., Tissot, J.D., and Lion, N. (2016). Cysteine redox proteomics of the hemoglobin-depleted cytosolic fraction of stored red blood cells. Proteomics - Clin. Appl. *10*, 883–893.

Dóka, É., Pader, I., Bíró, A., Johansson, K., Cheng, Q., Ballagó, K., Prigge, J.R., Pastor-Flores, D., Dick, T.P., Schmidt, E.E., et al. (2016). A novel persulfide detection method reveals protein persulfide- and polysulfide-reducing functions of thioredoxin and glutathione systems. Sci. Adv.

2, e1500968.

Ellis, H.R., and Poole, L.B. (1997). Novel application of 7-chloro-4-nitrobenzo-2-oxa-1,3-diazole to identify cysteine sulfenic acid in the AhpC component of alkyl hydroperoxide reductase. Biochemistry *36*, 15013–15018.

Fernandez-Caggiano, M., Schröder, E., Cho, H.J., Burgoyne, J., Barallobre-Barreiro, J., Mayr, M., and Eaton, P. (2016). Oxidant-induced interprotein disulfide formation in cardiac protein DJ-1 occurs via an interaction with peroxiredoxin 2. J. Biol. Chem. *291*, 10399–10410.

Filipovic, M.R., Miljkovic, J., Allgäuer, A., Chaurio, R., Shubina, T., Herrmann, M., and Ivanovic-Burmazovic, I. (2012). Biochemical insight into physiological effects of H_2 S: reaction with peroxynitrite and formation of a new nitric oxide donor, sulfinyl nitrite. Biochem. J. *441*, 609–621.

Filipovic, M.R., Zivanovic, J., Alvarez, B., and Banerjee, R. (2018a). Chemical Biology of H 2 S Signaling through Persulfidation. Chem. Rev. *118*, 1253–1337.

Filipovic, M.R., Zivanovic, J., Alvarez, B., and Banerjee, R. (2018b). Chemical Biology of H2S Signaling through Persulfidation. Chem. Rev. *118*, 1253–1337.

Finkel, T. (2011). Signal transduction by reactive oxygen species. J. Cell Biol. *194*, 7–15.

Finkel, T., and Holbrook, N.J. (2000). Oxidants, oxidative stress and the biology of ageing. Nature *408*, 239–247.

Foster, M.W., Hess, D.T., and Stamler, J.S. (2009). Protein S-nitrosylation in health and disease: a current perspective. Trends Mol. Med. *15*, 391–404.

Furdui, C.M., and Poole, L.B. (2014). Chemical approaches to detect and analyze protein sulfenic acids. Mass Spectrom. Rev. *33*, 126–146.

Hearn, A.S., Stroupe, M.E., Cabelli, D.E., Lepock, J.R., Tainer, J.A., Nick, H.S., and Silverman, D.N. (2001). Kinetic analysis of product inhibition in human manganese superoxide dismutase. Biochemistry *40*, 12051–12058.

Hine, C., Harputlugil, E., Zhang, Y., Ruckenstuhl, C., Lee, B.C., Brace, L., Longchamp, A., Treviño-Villarreal, J.H., Mejia, P., Ozaki, C.K., et al. (2015). Endogenous Hydrogen Sulfide Production Is Essential for Dietary Restriction Benefits. Cell *160*, 132–144.

Holmström, K.M., and Finkel, T. (2014). Cellular mechanisms and physiological consequences

of redox-dependent signalling. Nat. Rev. Mol. Cell Biol. *15*, 411–421.

Klomsiri, C., Nelson, K.J., Bechtold, E., Soito, L., Johnson, L.C., Lowther, W.T., Ryu, S.-E., King, S.B., Furdui, C.M., and Poole, L.B. (2010). Use of dimedone-based chemical probes for sulfenic acid detection evaluation of conditions affecting probe incorporation into redox-sensitive proteins. Methods Enzymol. *473*, 77–94.

Liang, M.-C., Hartman, H., Kopp, R.E., Kirschvink, J.L., and Yung, Y.L. (2006). Production of hydrogen peroxide in the atmosphere of a Snowball Earth and the origin of oxygenic photosynthesis. Proc. Natl. Acad. Sci. 18896–18899.

Lin, V.S., Lippert, A.R., and Chang, C.J. (2013). Cell-trappable fluorescent probes for endogenous hydrogen sulfide signaling and imaging H2O2-dependent H2S production. Proc. Natl. Acad. Sci. *110*, 7131–7135.

Liochev, S.I. (2013). Reactive oxygen species and the free radical theory of aging. Free Radic. Biol. Med. *60*, 1–4.

Liu, H.C., Chen, W.S., Chiang, C.M., Shia, B.C., and Ju, J.M. (2015). Extending Liu???s ordering theory for cognitive diagnosis and remedial instruction. ICIC Express Lett. Part B Appl. *6*, 491–496.

Marino, S.M., and Gladyshev, V.N. (2010). Cysteine Function Governs Its Conservation and Degeneration and Restricts Its Utilization on Protein Surfaces. J. Mol. Biol. *404*, 902–916.

Markó, L., Szijártó, I.A., Filipovic, M.R., Kaßmann, M., Balogh, A., Park, J.-K., Przybyl, L., N'diaye, G., Krämer, S., Anders, J., et al. (2016). Role of Cystathionine Gamma-Lyase in Immediate Renal Impairment and Inflammatory Response in Acute Ischemic Kidney Injury. Sci. Rep. *6*, 27517.

Matsuda, Y., Higashiyama, S., Kijima, Y., Suzuki, K., Kawano, K., Akiyama, M., Kawata, S., Tarui, S., Deutsch, H.F., and Taniguchi, N. (1990). Human liver manganese superoxide dismutase: Purification and crystallization, subunit association and sulfhydryl reactivity. Eur. J. Biochem. *194*, 713–720.

Mitchell, S.J., Madrigal-Matute, J., Scheibye-Knudsen, M., Fang, E., Aon, M., González-Reyes, J.A., Cortassa, S., Kaushik, S., Gonzalez-Freire, M., Patel, B., et al. (2016). Effects of Sex, Strain, and Energy Intake on Hallmarks of Aging in Mice. Cell Metab. *23*, 1093–1112.

Mustafa, A.K., Gadalla, M.M., Sen, N., Kim, S., Mu, W., Gazi, S.K., Barrow, R.K., Yang, G.,

Wang, R., and Snyder, S.H. (2009). H2S Signals Through Protein S-Sulfhydration. Sci. Signal. *2*, ra72–ra72.

Narayan, V., Ly, T., Pourkarimi, E., Murillo, A.B., Gartner, A., Lamond, A.I., and Kenyon, C. (2016). Deep Proteome Analysis Identifies Age-Related Processes in C. elegans. Cell Syst. *3*, 144–159.

Olson, K.R., and Straub, K.D. (2016). The Role of Hydrogen Sulfide in Evolution and the Evolution of Hydrogen Sulfide in Metabolism and Signaling. Physiology *31*, 60–72.

Ono, K., Akaike, T., Sawa, T., Kumagai, Y., Wink, D.A., Tantillo, D.J., Hobbs, A.J., Nagy, P., Xian, M., Lin, J., et al. (2014). Redox chemistry and chemical biology of H2S, hydropersulfides, and derived species: implications of their possible biological activity and utility. Free Radic. Biol. Med. *77*, 82–94.

Palde, P.B., and Carroll, K.S. (2015). A universal entropy-driven mechanism for thioredoxin–target recognition. Proc. Natl. Acad. Sci. *112*, 7960–7965.

Pan, J., and Carroll, K.S. (2013). Persulfide reactivity in the detection of protein S-sulfhydration. ACS Chem. Biol. *8*, 1110–1116.

Pasini, E.M., Kirkegaard, M., Mortensen, P., Lutz, H.U., Thomas, A.W., and Mann, M. (2006). In-depth analysis of the membrane and cytosolic proteome of red blood cells. Blood *108*, 791–801.

Patel, B.H., Percivalle, C., Ritson, D.J., Duffy, C.D., and Sutherland, J.D. (2015). Common origins of RNA, protein and lipid precursors in a cyanosulfidic protometabolism. Nat. Chem. *7*, 301–307.

Paul, B.D., and Snyder, S.H. (2012). H2S signalling through protein sulfhydration and beyond. Nat. Rev. Mol. Cell Biol. *13*, 499–507.

Paul, B.D., and Snyder, S.H. (2015). H2S: A Novel Gasotransmitter that Signals by Sulfhydration. Trends Biochem. Sci. *40*, 687–700.

Paul, B.D., Sbodio, J.I., Xu, R., Vandiver, M.S., Cha, J.Y., Snowman, A.M., and Snyder, S.H. (2014). Cystathionine γ-lyase deficiency mediates neurodegeneration in Huntington's disease. Nature *509*, 96–100.

Paulsen, C.E., and Carroll, K.S. (2013). Cysteine-mediated redox signaling: chemistry, biology,

and tools for discovery. Chem. Rev. *113*, 4633–4679.

Paulsen, C.E., Truong, T.H., Garcia, F.J., Homann, A., Gupta, V., Leonard, S.E., and Carroll, K.S. (2011). Peroxide-dependent sulfenylation of the EGFR catalytic site enhances kinase activity. Nat. Chem. Biol. *8*, 57–64.

Pol, A., Renkema, G.H., Tangerman, A., Winkel, E.G., Engelke, U.F., de Brouwer, A.P.M., Lloyd, K.C., Araiza, R.S., van den Heuvel, L., Omran, H., et al. (2018). Mutations in SELENBP1, encoding a novel human methanethiol oxidase, cause extraoral halitosis. Nat. Genet. *50*, 120–129.

Poole, L.B., Karplus, P.A., and Claiborne, A. (2004). Protein sulfenic acids in redox signaling. Annu. Rev. Pharmacol. Toxicol. *44*, 325–347.

Redman, L.M., Smith, S.R., Burton, J.H., Martin, C.K., Il'yasova, D., and Ravussin, E. (2018). Metabolic Slowing and Reduced Oxidative Damage with Sustained Caloric Restriction Support the Rate of Living and Oxidative Damage Theories of Aging. Cell Metab. *27*, 805-815.e4.

Reisz, J.A., Bechtold, E., King, S.B., Poole, L.B., and Furdui, C.M. (2013). Thiol-blocking electrophiles interfere with labeling and detection of protein sulfenic acids. FEBS J. *280*, 6150–6161.

Sbodio, J.I., Snyder, S.H., and Paul, B.D. (2016). Transcriptional control of amino acid homeostasis is disrupted in Huntington's disease. Proc. Natl. Acad. Sci. *113*, 8843–8848.

Sbodio, J.I., Snyder, S.H., and Paul, B.D. (2018). Golgi stress response reprograms cysteine metabolism to confer cytoprotection in Huntington's disease. Proc. Natl. Acad. Sci. U S A *115*, 780–785.

Seo, Y.H., and Carroll, K.S. (2009). Profiling protein thiol oxidation in tumor cells using sulfenic acid-specific antibodies. Proc. Natl. Acad. Sci. U. S. A. *106*, 16163–16168.

Shibuya, N., Koike, S., Tanaka, M., Ishigami-Yuasa, M., Kimura, Y., Ogasawara, Y., Fukui, K., Nagahara, N., and Kimura, H. (2013). A novel pathway for the production of hydrogen sulfide from D-cysteine in mammalian cells. Nat. Commun. *4*, 1366.

Snijder, P.M., Baratashvili, M., Grzeschik, N.A., Leuvenink, H.G.D., Kuijpers, L., Huitema, S., Schaap, O., Giepmans, B.N.G., Kuipers, J., Miljkovic, J.L., et al. (2015). Overexpression of cystathionine γ-lyase suppresses detrimental effects of spinocerebellar ataxia type 3. Mol. Med. *21*, 758.

Stiernagle, T. (2006). Maintenance of C. elegans. WormBook 1–11.

Sulston, J., and Hodgkin, J. (1988). Methods, The Nematode Caenorhabditis elegans. In Cold Spring Harbor Monograph Archive, W. Wood, ed. pp. 587–606.

Sundaresan, M., Yu, Z.-X., Ferrans, V.J., Irani, K., and Finkel, T. (1995). Requirement for Generation of H(2)O(2) for Platelet-Derived Growth Factor Signal Tran sduction. Science (80-.). *270*, 296–299.

Szabó, C. (2007). Hydrogen sulphide and its therapeutic potential. Nat. Rev. Drug Discov. *6*, 917–935.

Szabó, C., Ischiropoulos, H., and Radi, R. (2007). Peroxynitrite: Biochemistry, pathophysiology and development of therapeutics. Nat. Rev. Drug Discov. *6*, 662–680.

Szczesny, B., Módis, K., Yanagi, K., Coletta, C., Le Trionnaire, S., Perry, A., Wood, M.E., Whiteman, M., and Szabo, C. (2014). AP39, a novel mitochondria-targeted hydrogen sulfide donor, stimulates cellular bioenergetics, exerts cytoprotective effects and protects against the loss of mitochondrial DNA integrity in oxidatively stressed endothelial cells in vitro. Nitric Oxide *41*, 120–130.

Tandon, S., and Horowitz, P.M. (1989). Reversible folding of rhodanese. Presence of intermediate(s) at equilibrium. J. Biol. Chem. *264*, 9859–9866.

Le Trionnaire, S., Perry, A., Szczesny, B., Szabo, C., Winyard, P.G., Whatmore, J.L., Wood, M.E., and Whiteman, M. (2014). The synthesis and functional evaluation of a mitochondria-targeted hydrogen sulfide donor, (10-oxo-10-(4-(3-thioxo-3H-1,2-dithiol-5-yl)phenoxy)decyl)triphenylphosphonium bromide (AP39). Med. Chem. Commun. *5*, 728–736.

Valentine, W.N., Toohey, J.I., Paglia, D.E., Nakatani, M., and Brockway, R.A. (1987). Modification of erythrocyte enzyme activities by persulfides and methanethiol: possible regulatory role. Proc. Natl. Acad. Sci. U. S. A. *84*, 1394–1398.

Vandiver, M.S., Paul, B.D., Xu, R., Karuppagounder, S., Rao, F., Snowman, A.M., Seok Ko, H., Il Lee, Y., Dawson, V.L., Dawson, T.M., et al. (2013). Sulfhydration Mediates Neuroprotective Actions of Parkin. Nat. Commun. *4*, 1626.

Vitvitsky, V., Kabil, O., and Banerjee, R. (2012). High Turnover Rates for Hydrogen Sulfide Allow for Rapid Regulation of Its Tissue Concentrations. Antioxid. Redox Signal. *17*, 22–31.

Wallace, J.L., and Wang, R. (2015). Hydrogen sulfide-based therapeutics: exploiting a unique but ubiquitous gasotransmitter. Nat. Rev. Drug Discov. *14*, 329–345.

Wang, R. (2012). Physiological Implications of Hydrogen Sulfide: A Whiff Exploration That Blossomed. Physiol. Rev. *92*, 791–896.

Wedmann, R., Bertlein, S., Macinkovic, I., Böltz, S., Miljkovic, J.L., Muñoz, L.E., Herrmann, M., and Filipovic, M.R. (2014). Working with "H2S": Facts and apparent artifacts. Nitric Oxide *41*, 85–96.

Wedmann, R., Onderka, C., Wei, S., Szijártó, I.A., Miljkovic, J.L., Mitrovic, A., Lange, M., Savitsky, S., Yadav, P.K., Torregrossa, R., et al. (2016). Improved tag-switch method reveals that thioredoxin acts as depersulfidase and controls the intracellular levels of protein persulfidation. Chem. Sci. *7*, 3414–3426.

Wood, Z.A., Poole, L.B., and Karplus, P.A. (2003). Peroxiredoxin evolution and the regulation of hydrogen peroxide signaling. Science (80-.). *300*, 650–653.

Yadav, P.K., Yamada, K., Chiku, T., Koutmos, M., and Banerjee, R. (2013). Structure and Kinetic Analysis of H2S Production by Human Mercaptopyruvate Sulfurtransferase. J. Biol. Chem. *288*, 20002–20013.

Yang, G., Wu, L., Jiang, B., Yang, W., Qi, J., Cao, K., Meng, Q., Mustafa, A.K., Mu, W., Zhang, S., et al. (2008). H2S as a Physiologic Vasorelaxant: Hypertension in Mice with Deletion of Cystathionine -Lyase. Science (80-.). *322*, 587–590.

Yang, G., Zhao, K., Ju, Y., Mani, S., Cao, Q., Puukila, S., Khaper, N., Wu, L., and Wang, R. (2013). Hydrogen sulfide protects against cellular senescence via S-sulfhydration of Keap1 and activation of Nrf2. Antioxid. Redox Signal. *18*, 1906–1919.

Yang, H.Y., Kwon, J., Choi, H.I., Park, S.H., Yang, U., Park, H.R., Ren, L., Chung, K.J., Kim, Y.U., Park, B.J., et al. (2012). In-depth analysis of cysteine oxidation by the RBC proteome: Advantage of peroxiredoxin II knockout mice. Proteomics *12*, 101–112.

Yang, J., Gupta, V., Carroll, K.S., and Liebler, D.C. (2014). Site-specific mapping and quantification of protein S-sulphenylation in cells. Nat. Commun. *5*, 4776.

Zaccarin, M., Falda, M., Roveri, A., Bosello-Travain, V., Bordin, L., Maiorino, M., Ursini, F., and Toppo, S. (2014). Quantitative label-free redox proteomics of reversible cysteine oxidation in red blood cell membranes. Free Radic. Biol. Med. *71*, 90–98.

Zhang, D., Macinkovic, I., Devarie-Baez, N.O., Pan, J., Park, C.-M., Carroll, K.S., Filipovic, M.R., and Xian, M. (2014). Detection of Protein S-Sulfhydration by a Tag-Switch Technique. Angew. Chemie Int. Ed. *53*, 575–581.

Zhang, J., Xin, L., Shan, B., Chen, W., Xie, M., Yuen, D., Zhang, W., Zhang, Z., Lajoie, G.A., and Ma, B. (2012). PEAKS DB: *De Novo* Sequencing Assisted Database Search for Sensitive and Accurate Peptide Identification. Mol. Cell. Proteomics *11*, M111.010587.

Acknowledgments: The authors would like to thank Dr Michel Toledano for careful reading of the manuscript and helpful discussions, and Bertrand Daignan-Fornier for his help with yeast experiments. **Funding:** This work was supported by the ATIP-Avenir grant, by the French State in the frame of the 'Investments for the future' Programme IdEx Bordeaux (ANR-10-IDEX-03-02) and by FRM. MW acknowledges support from MRC, UK (MR/M022706/1) and The Brian Ridge Scholarship (to RT). MM and VM were supported by the Ministry of Education, Science and Technology Development of the Republic of Serbia (173009). GS and JBK acknowledge support by the DFG, Germany (CRC1218). **Competing interests:** MW and the University of Exeter have patents on the therapeutic and agricultural use of mitochondria-targeted, and other, hydrogen sulfide delivery molecules. All other authors declare no competing interests.

Authors contribution: JZ and EK contributed equally to this study and performed most of the experiments. MRF conceived the study. JK, BA, SS-R, DT, JLjM, BB, DP, MM, BP and MRF also performed experiments. YG, KC, RT, MW, MB, VM, II-B, GS, JEG, BGZ, BP and SHS provided tools and intellectual input, and helped with data analysis. SM and JM provided DR mouse livers and helped with data analysis. MRF wrote the manuscript with the help from all co-authors.

Supplementary Materials:

Figures S1-S6

Tables S1

External Databases S1-S5

STAR METHODS
KEY RESOURCES TABLE

REAGENT or RESOURCE	SOURCE	IDENTIFIER
Antibodies		
Anti-β-actin, mouse monoclonal	Santa Cruz Biotechnology	Cat# sc-47778
Anti-β-tubulin, mouse monoclonal	Sigma Aldrich	Cat# T0198
Anti-GAPDH, mouse monoclonal	Sigma Aldrich	Cat# G8795
Anti-HSP70, mouse monoclonal	Abcam	Cat# Ab5439
Anti-KEAP1 P586, rabbit polyclonal	Cell Signalling	Cat# 4678
Anti-eNOS, rabbit monoclonal	Cell Signalling	Cat# 32027
Anti-Parkin, mouse monoclonal	Santa Cruz Biotechnology	Cat# sc-136989
Anti-SOD-2, mouse monoclonal	Santa Cruz Biotechnology	Cat# sc-137254
Anti-TST, rabbit polyclonal	GeneTex	Cat# GTX114858
Anti-SQRDL, rabbit polyclonal	Sigma Aldrich	Cat# HPA017079
Anti-PTEN, mouse monoclonal	Santa Cruz Biotechnology	Cat# sc-7974
Anti-PTP1B, mouse monoclonal	Santa Cruz Biotechnology	Cat# sc-133259
Anti-SH-PTP2, mouse monoclonal	Santa Cruz Biotechnology	Cat# sc-7384
Anti-EGFR, rabbit polyclonal	Santa Cruz Biotechnology	Cat# sc-03-G
Anti-CBS, mouse monoclonal	Santa Cruz Biotechnology	Cat# sc-133154
Anti-CBS, rabbit polyclonal	Santa Cruz Biotechnology	Cat# sc-67154
Anti-MPST, rabbit polyclonal	Sigma Aldrich	Cat# HPA001240
Anti-CTH, rabbit	From Prof. Snyder's lab (Johns Hopkins University School of Medicine)	(Paul et al., 2014)
Anti-CTH, mouse monoclonal	Santa Cruz Biotechnology	Cat# sc-365382
Anti- p-ERK, mouse monoclonal	Santa Cruz Biotechnology	Cat# sc-7383
Anti ERK 1, mouse monoclonal	Santa Cruz Biotechnology	Cat# sc-271269
Anti-DJ-1, mouse monoclonal	Santa Cruz Biotechnology	Cat# sc-55572
Anti-DJ-1 AC, mouse monoclonal	Santa Cruz Biotechnology	Cat# sc-55572 AC
Anti DJ-1 (Oxidized At C106)	BioRad	Cat# HCA024
Anti-Biotin-Peroxidase, mouse monoclonal	Sigma Aldrich	Cat# A0185
Anti-Dimedone, rabbit polyclonal	From Dr. Carroll's lab (The Scripps Research Institute)	(Seo and Carroll, 2009)
Mouse IgGκ BP-HRP	Santa Cruz Biotechnology	Cat# sc-516102
Mouse anti-rabbit IgG-HRP	Santa Cruz Biotechnology	Cat# sc-2357
Swine anti-rabbit IgG-HRP, polyclonal	Dako, Denmark	Cat# P0399
Donkey anti-mouse IgG-HRP, polyclonal	Abcam, Cambridge, UK	Cat# ab6820
Streptavidin Protein, DyLight 488	Thermo Fisher Scientific	Cat# 21832
Cy®5-Streptavidin	Sigma Aldrich	Cat# GEPA45001
EGF Pathway Phospho Antibody Array	Full Moon Biosystems	Cat# PEG214
Bacterial and Virus Strains		
OP50-1	Caenorhabditis Genetic Center	N/A
HB101	Caenorhabditis Genetic Center	N/A
E.coli MG1655 (pTrc99a)	From the laboratory of Gonzales-Zorn, Spain	N/A
E.coli MG1655 (pSB74)	From the laboratory of Gonzales-Zorn, Spain	N/A
E. coli BL21 DE3 Rosetta	Novagen	Cat# 70954-3
Biological Samples		
Kidneys from C57BL/6 WT and $CSE^{-/-}$ mice	From Professor Maik Gollasch (Charité Medical Faculty)	(Markó et al., 2016)

D. melanogaster: y^1w^{1118}	From Professor Ody Sibon (University of Groningen)	(Snijder et al., 2015)
D. melanogaster: Eip55E	From Professor Ody Sibon (University of Groningen)	(Snijder et al., 2015)
Chemicals, Peptides and Recombinant Proteins		
Chelex-100	Sigma Aldrich	Cat# C7901
Sodium Sulfide	Sigma Aldrich	Cat# 407410
GYY4137	(Alexander et al., 2015)	N/A
AP39	(Szczesny et al., 2014)	N/A
D-cystine	Sigma Aldrich	Cat# 30095
DL-propargylglycine	Sigma Aldrich	Cat# P7888
O-(Carboxymethyl)hydroxylamine hemihydrochloride	Sigma Aldrich	Cat# C13408
Hydrogen Peroxide	Sigma Aldrich	Cat# 216763
Monensin sodium salt	Sigma Aldrich	Cat# M5273-1G
Erastin	Sigma Aldrich	Cat# E7781
S-sulfocysteine (SSC)	Sigma Aldrich	Cat# C2196
Cystine	Sigma Aldrich	Cat# 30200
Imidazole	Carl Roth Gmbh	Cat# 3899.4
Isopropyl β-D-1-thiogalactopyranoside	Inalco Pharmaceuticals	Cat# 1758-1400
Dithiothreitol (DTT)	GE Healthcare	Cat# 17-1318-02
4-Chloro-7-nitrobenzofurazan (NBF-Cl)	Sigma Aldrich	Cat# 163260
Dimedone	Sigma Aldrich	Cat# D153303
DCP-Bio1	Kerafast	Cat# EE0028
DAz-2	Cayman Chemicals	Cat# 13382
BioDiaAlk	(Akter et al., 2018)	N/A
DiaAlk	(Akter et al., 2018)	N/A
Cyanine5 alkyne	Lumiprobe	Cat# FP-OO5590
Copper(II)-TBTA	Lumiprobe	Cat# 21050
L-Ascorbic acid	Sigma Aldrich	Cat# 795437
Nmc-penicillamine	(Artaud and Galardon, 2014)	N/A
EGF human recombinant	PromoKine	Cat# 60170
VEGF-165, human, recombinant	PromoCell	Cat# C-64422
Insulin human	Sigma Aldrich	Cat# I0908
Paraformaldehyde	Sigma Aldrich	Cat# P6148
Sodium thiosulfate	PROLABO	Cat# 27 910.291
Paraquat hydrochloride hydrate	Sigma Aldrich	Cat# 36541
Sodium (meta)arsenite	Sigma Aldrich	Cat# S7400
2-deoxy-D-glucose (DOG)	Sigma Aldrich	Cat# D8375
Thiazolyl Blue Tetrazolium Bromide (MTT)	Sigma Aldrich	Cat# M5655
Protease Inhibitor	Sigma Aldrich	Cat# P8340
His-Pur Ni-NTA Superflow Agarose	ThermoScientific	Cat# 25216
Streptavidin Magnetic Beads	Sigma Aldrich	Cat# 11 641 778 001
NeutrAvidin Agarose Resin	ThermoScientific	Cat# 29201
High Capacity NeutrAvidin Agarose Resin	ThermoScientific	Cat# 29202
Trypsin from porcine pancreas	Sigma Aldrich	Cat# T6567
Chymotrypsin Sequencing Grade	Sigma Aldrich	Cat# 000000011418467001
Human Serum Albumin	Sigma Aldrich	Cat# A1887
GAPDH	Sigma Aldrich	Cat# G2267
Rhodanese from bovine liver	Sigma Aldrich	Cat# R1756
MnSOD	Creative BioMart	Cat# SOD2-1039H
Cytochrome c	Sigma Aldrich	Cat# 30398

Xanthine	Sigma Aldrich	Cat# X0626
Xanthine Oxidase	Sigma Aldrich	Cat# X1875
Thioredoxin Reductase (TrxR) from rat liver	Sigma Aldrich	Cat# T9698
TRP14 (From human fibroblast cDNA)	For this paper	N/A
*hs*Trx C32S	For this paper	N/A
*hs*Trx C35S	For this paper	N/A
*hs*Trx1	For this paper	N/A
NADPH	Sigma Aldrich	Cat# N5130
DAPI	Euromedex	Cat# 1050-A
MeRho-Az	From Michael D. Pluth's lab (Dept. of Chemistry and Biochemistry, Eugene, OR)	N/A
Propidium Iodide	Sigma Aldrich	Cat# P4864
Histowax®	Histolab Product AB, Sweden	Cat# 00405
Normal swine serum	Dako, Denmark	Cat# X0901
Normal donkey serum	Abcam, Cambridge, UK	Cat# X0903
Diaminobenzidine tetrahydrochloride (DAB)	Dako North America, Inc. Carpinteria, CA, USA	Cat# K3468
DPX medium	Sigma-Aldrich	Cat# 06522
Experimental Models: Cell Lines		
Human: HeLa	ECACC	Cat# 93021013
Human: HUVEC	PromoCell	Cat# C-12203
Human: SH-SY5Y	ECACC	Cat# 94030304
Human: Fibroblasts	Coriell Institute	AG08790 and AG14245
Mouse: MEF WT	From Prof. Snyder's lab (Johns Hopkins University School of Medicine)	(Sbodio et al., 2016)
Mouse: MEF $CSE^{-/-}$	From Prof. Snyder's lab (Johns Hopkins University School of Medicine)	(Sbodio et al., 2016)
Mouse: Striatal progenitor cells ST$Hdh^{Q7/Q7}$	M. MacDonald (Massachusetts General Hospital, Boston, MA)	N/A
Mouse: Striatal progenitor cells ST$Hdh^{Q111/Q111}$	M. MacDonald (Massachusetts General Hospital, Boston, MA)	N/A
Experimental Models: *C.elegans* mutants		
Wild-type Bristol N2	Caenorhabditis Genetic Center	N/A
cth-1(ok3319)V	Caenorhabditis Genetic Center	VC2569
mpst-3(tm4387)V	MITANI Lab, National Bio-Resource Project of the MEXT, Japan	FX04387
eat-2(tm5786)II	MITANI Lab, National Bio-Resource Project of the MEXT, Japan	FX19451
eat-2(tm5786)II;cth-1(ok3319)V	This paper	N/A
eat-2(tm5786)II;mpst-3(tm4387)V	This paper	N/A
Experimental Models: Strains/Organisms		
S. cerevisiae: BY4742 (WT)	Euroscarf	N/A
S. cerevisiae: *Δcys4*	Euroscarf	ACCNO Y16696
S. cerevisiae: *Δcys3*	Euroscarf	ACCNO Y16865
S. cerevisiae: *Δtum1*	Euroscarf	ACCNO Y12507
Male Wistar Rat	Institute for Biological Research "Siniša Stanković", Belgrade, Serbia	N/A

Male C57BL/6J mice	NIA Aging Colony Resource at Charles River Laboratories (CRL)	N/A
C57BL/6 mice	Department of Pharmacology and Molecular Sciences, Johns Hopkins University School of Medicine, Baltimore, MD	N/A
Oligonucleotides		
5'-GAAGGAGATATACCATGGTGAAGC-3' (fwd)	Sigma Aldrich	*hs*Trx in pET28a
5'-CGGATCTCAGTGGTGGTG-3' (rev)	Sigma Aldrich	*hs*Trx in pET28a
5'-CACGTGGTCTGGGCCTTG-3' (fwd)	Sigma Aldrich	*hs*Trx C32S mutagenesis
5'-CAAGGCCCAGACCACGTG-3' (rev)	Sigma Aldrich	*hs*Trx C32S mutagenesis
5'-GTGTGGGCCTTCCAAAATGATCAAG-3' (fwd)	Sigma Aldrich	*hs*Trx C35S mutagenesis
5'-CTTGATCATTTTGGAAGGCCCACAC-3' (rev)	Sigma Aldrich	*hs*Trx C35S mutagenesis
5'-ACCATCACGGATCCATGGCCCGCTATGAGGAGG-3' (fwd)	Sigma Aldrich	*hs*TRP14 in pQE-80L
5'-CCGGGGTACCGTTAATCTTCAGAGAACAACATTTCCACCAG-3' (rev)	Sigma Aldrich	*hs*TRP14 in pQE-80L
Recombinant DNA		
Plasmid: pET-28a(+)	Novagen	Cat# 69864-3
Plasmid: pQE-80L	Qiagen	N/A
Software and Algorithms		
ImageJ	NIH	https://imagej.nih.gov/ij/download.html
GraphPad Prism 5.0	GraphPad Software	https://www.graphpad.com
PEAKS Studio	Bioinformatics Solutions Inc.	http://www.bioinfor.com/
OriginPro 8	OriginLab	https://www.originlab.com/
RTCA Software Version 2.0	ACEA Biosciences, Inc.	https://www.aceabio.com/products/rtca-dp/
CFLow Plus Version 1.0.202.1	BD Biosciences	http://www.bdbiosciences.com

CONTACT FOR REAGENT AND RESOURCE SHARING

Further information and requests for resources and reagents should be directed to, and will be fulfilled by the Lead Contact, Milos Filipovic (milos.filipovic@ibgc.cnrs.fr)

EXPERIMENTAL MODEL AND SUBJECT DETAILS

Cell Lines

HeLa cells and Neuroblastoma cells (SH-SY5Y) were both obtained from ECACC. HeLa cells were cultured in Dulbecco's modified Eagle's media (DMEM, high glucose) supplemented with 2 mM L-glutamine, 1% penicillin-streptomycin and 10% fetal bovine serum at 37 °C and 5% CO_2. SH-SY5Y (ECACC) cells were cultured in Ham's F12 : DMEM (1 : 1) media, supplemented with 2 mM glutamine, 1% penicillin-streptomycin and 10% fetal bovine serum at 37 °C and 5% CO_2. C-pooled human umbilical vein endothelial cells (HUVEC) were obtained from PromoCell, Germany and cultured in Endothelial Cell Growth Medium I Kit (PromoCell, Germany) at 37 °C and 5% CO_2. Mouse Embryonic Fibroblasts (MEF) were generated from $CSE^{+/+}$ and $CSE^{-/-}$ mice and immortalized using SV40T antigen (Sbodio et al., 2016). MEF cells were cultured in DMEM (high glucose), supplemented with 2 mM L-glutamine, 1% penicillin-streptomycin and 10% fetal bovine serum at 37 °C and 5% CO_2. The striatal progenitor cell line ST*Hdh*$^{Q7/Q7}$, expressing wild-type huntingtin, and ST*Hdh*$^{Q111/Q111}$, expressing mutant huntingtin, harboring 111 glutamine repeats (referred to as Q7 and Q111 cells, respectively), were from M. MacDonald (Massachusetts General Hospital, Boston, MA). The cells were maintained in DMEM (low glucose, no pyruvate) supplemented with

2 mM L-glutamine, 1% penicillin-streptomycin and 10% fetal bovine serum at 33 °C and 5% CO_2. Human Fibroblasts cell lines AG08790 (31 years old) and AG14245 (48 years old - a culture initiated from a biopsy taken 17 years earlier from this same donor is AG08790) were obtained from Coriell Institute for Medical Research. Fibroblasts were cultured in DMEM (high glucose) supplemented with 2 mM L-glutamine and 10% fetal bovine serum at 37 °C and 5% CO_2.

C. elegans

The following strains were used in this study: Wild-type Bristol N2, *cth-1(ok3319)V*, *mpst-3(tm4387)V*, *eat-2(tm5786)II*, *eat-2(tm5786)II;cth-1(ok3319)V*, *eat-2(tm5786)II;mpst-3(tm4387)V*. The original isolate VC2569 *cth-1(ok3319)V* was provided by the Caenorhabditis Genetic Center whereas the original isolates FX04387 *mpst-3(tm4387)V* and FX19451 *eat-2(tm5786)II* were provided by the MITANI Lab through the National Bio-Resource Project of the MEXT, Japan. All mutant strains were outcrossed at least 4 times before use. Double-mutant strains were constructed by using standard techniques (Brenner, 1974; Sulston and Hodgkin, 1988) and the presence of both mutations were checked by PCR. Worms were grown at 20 °C on standard nematode growth medium (NGM) plates, unless otherwise indicated, using standard *C. elegans* techniques (Stiernagle, 2006) with sufficient food (*E. coli* OP50-1) for at least two generations prior to use.

S. cerevisiae

Yeast cells were grown in liquid YPD media (1% yeast extract, 1% bactopeptone, and 2% glucose).

Wistar rats

Male Wistar rats used in the experiment were bred and housed at the Institute for Biological Research "Siniša Stanković", Belgrade, Serbia, under constant laboratory conditions (22±2˚C, 12–12 hr light-dark cycle). Food and water were available *ad libitum*. The animals were decapitated at the ages of 1, 3, 6, 12 and 24 month(s). All animal procedures were in compliance with the EEC Directive (86/609/EEC) on the protection of animals used for experimental and other scientific purposes and were approved by the Ethical Committee for the Use of Laboratory Animals of the Institute for Biological Research "Siniša Stanković", University of Belgrade.

Male C57BL/6J mice

All experiments were performed with the approval of the Harvard Medical Area Institutional Animal Care and Use Committee (IACUC). Male C57BL/6J mice were obtained from the NIA Aging Colony Resource at Charles River Laboratories (CRL) at 6 months (young) and 19 months (old) of age. Mice were allowed to acclimatize to the facility for one month to ensure weight stabilization after shipment, so at sacrifice were 7mo old (young) and 20 months (old). Initiation of caloric restriction (CR) was performed as previously described (Turturro, A., et al., 1999) (starting at 14 weeks of age, CR is initiated in a step-down fashion, where it its increased to 25% restriction at 15 weeks, and the full 40% restriction imitated at 16 weeks where it is maintained throughout the life of the animal. Ad libitum (AL) animals were fed NIH-31 diet, while CR animals are fed NIH-31 fortified diet (Turturro, A., et al., 1999). Other details about the husbandry conditions at CRL can be found here: https://www.nia.nih.gov/research/dab/aged-rodent-colonies-handbook/barrier-environmental-information.

Mice were single housed for the duration of their life in standard mouse cages. Upon arrival at Harvard, mice were housed in the barrier facility at HSPH in microisolator cages with corncob bedding, a nestlet and one shepherd shack. Mice receive free access to water, and either AL NIH-31, or fortified NIH-31 (1 pellet per day for the CR mice). CR mice were fed daily between the hours of 7:00-8:00am by feeding the ration of food onto the floor of the cage. Any remaining food was removed the next day prior to giving the new food ration. Mice were housed in a room on a 12/12 hr light/dark cycle (7am-7pm) with temperature between 20–23 °C with 30%–70% relative humidity. Cages were changed weekly using full sterile technique and performed in Class II laminar flow change stations with spot changes as required.

Mice from Bindu

METHOD DETAILS

All chemicals were purchased from Sigma Aldrich, unless otherwise mentioned. All buffers were prepared with nanopure water and treated with Chelex-100 resins to remove traces of metal ions. Na_2S solutions were prepared and handled as recommended (Wedmann et al., 2014). Nmc-penicillamine was synthesized, as previously described (Artaud and Galardon, 2014). Morpholin-4-ium 4 methoxyphenyl(morpholino) phosphinodithioate (GYY4137) and

(10-oxo-10-(4-(3-thioxo-*3H*-1,2-dithiol-5-yl)phenoxy)decyl)triphenylphosphonium bromide (AP39) were synthesized in house according to (Alexander et al., 2015; Le Trionnaire et al., 2014).

Preparation of Specific oxPTM of Proteins

Preparation of HSA-SH, HSA-SOH and HSA-SSH

Different oxPTM of HSA were prepared and their concentrations quantified as previously reported (Cuevasanta et al., 2015).

Preparation of GAPDH persulfide

GAPDH persulfide was prepared as previously described for HSA derivatives (Cuevasanta et al., 2015).

Preparation of TST and TST persulfide

Bovine TST (Sigma Aldrich) (already largely present as a persulfide) was used to prepare the fully persulfidated enzyme, by incubating with a 10-fold excess of sodium thiosulfate in 10 mM Tris buffer (pH 8) at 37 °C for 30 min and then cleaning with mini biospin column from Bio-Rad. The reduced enzyme was prepared by incubating with a 10-fold excess of DTT at 37 °C for 30 min and then cleaned on a mini biospin column.

Dimedone Switch Method to Purified Proteins

Proteins were incubated with 5 or 10 mM NBF-Cl, in PBS containing 2% SDS for 30 min at 37 °C, precipitated by methanol/chloroform precipitation ($CHCl_3$/H_2O/MeOH (1/4/4, v/v/v) 2 times and subsequently washed with MeOH 2-3 times). Pellets were resuspended in 50 mM PBS (40mM Na_2HPO_4, 10 mM NaH_2PO_4 and 130 mM NaCl, pH 7.4) containing 2% SDS, incubated with either 50 μM dimedone or DCP-Bio1 for 1 hr at 37 °C, precipitated with $CHCl_3$/H_2O/MeOH (1/4/4, v/v/v) twice, and re-suspended in Laemmli buffer for SDS-PAGE. For some experiments, the DCP-Bio1-labeled samples were redissolved in 50 mM PBS only, incubated with neutravidin beads (Thermo Fischer Scientific) for 2 hr at room temperature with continuous mixing. Beads were then washed with 10 volumes of PBS (containing 0.01% Tween-20) and bound proteins were eluted by boiling the beads in a minimum volume of Laemmli buffer for SDS-PAGE for 5 min and gels were recorded on a Typhoon Fla 9500 at 473 nm and 635 nm.

ESI-TOF MS of the dimedone switch reaction with LMW persulfides

Mass spectrometry was performed on maXis 5G, Bruker Daltonic (Bremen, Germany), an ESI-TOF MS capable of resolution of at least 40,000 FWHM. Detection was in positive-ion mode. 100 μM nmc-penicillamine persulfide was mixed with 100 μM NBF-Cl in ammonium bicarbonate buffer, (pH 7.4, 23 °C) and the reaction monitored for 15 min. 500 μM dimedone was then added and the reaction monitored for an additional 15 min.

MS of Protein Persulfide Models Labeled with DCP-Bio1

Protein persulfides switch labeled with DCP-Bio1 as previously described and resolved by SDS-PAGE, and protein bands excised and digested with either trypsin or chymotrypsin following previously described protocol (Crouzet et al., 2017). Trypsin digested peptides were analyzed by LC-MS/MS on a Thermo Scientific Q Exactive Orbitrap mass spectrometer in conjunction with a Proxeon Easy-nLC II HPLC (Thermo Fisher Scientific) and Proxeon nanospray source at Bordeaux Proteomic Platform. The digested peptides were loaded a 100 micron x 25 mm Magic C_{18} 100Å 5U reverse phase trap where they were desalted online before being separated with a 75 micron x 150 mm Magic C18 200Å 3U reverse phase column. Peptides were eluted using a 120 min gradient with a flow rate of 300 nL/min. An MS survey scan was obtained for the m/z range of 350-1600; MS/MS spectra were acquired using a top 12 method, where the top 12 ions in the MS spectra were subjected to High Energy Collisional Dissociation (HCD). An isolation mass window of 2 m/z was used for the precursor ion selection, and normalized collision energy of 27% was used for fragmentation. Five second duration was used for the dynamic exclusion. Peptide identification was performed using PEAKS Studio (BSI, Canada) (Zhang et al., 2012). The search settings were: precursor Δm tolerance = 10 ppm, fragment Δm tolerance = 0.2 Da, missed cleavages = 2, modifications of lysine: NBF (163.0012), modifications of cysteine: NBF (163.0012), DCP-Bio1 (394.1557), or hydrolyzed DCP-Bio1 (168.0786).

Proteomic Analysis of Persulfidated Proteins in Red Blood Cell Lysates

9 mL of peripheral whole blood from participants of this study, who provided informed consent in accordance with the Declaration of Helsinki, was collected in citrate and processed immediately following previously described protocol (Pasini et al., 2006) with modification that the lysis buffer contained 5 mM NBF-Cl. After 30 min of incubation with lysis buffer at 4 °C, additional NBF-Cl was added (to final concentration of 15 mM NBF-Cl) with SDS (to final concentration of 2%) and incubated for 30 min. Methanol/chloroform precipitation was performed and the protein pellet obtained was redissolved in 50 mM PBS supplemented with 0.1% SDS. Endogenously biotinylated proteins were precleared by incubating with Pierce™ NeutrAvidin™ Agarose (ThermoFisher) at room temperature for 2 hr with agitation. The resins were subsequently removed on a Pierce™ Disposable Column (ThermoFisher) and

the solution obtained was precipitated by methanol/chloroform. The resulting protein pellet was redissolved in 50 mM PBS supplemented with 2% SDS and was incubated with 50 µM DCP-Bio1 at 37 °C for 1.5 hr. Solution was precipitated with methanol/chloroform and redissolved in 50 mM PBS supplemented with 0.1% SDS. The protein solution was incubated with Pierce™ High Capacity NeutrAvidin™ Agarose (ThermoFisher) at 4 °C overnight with agitation. Samples were then brought to room temperature and loaded on a column. The resins were washed with 8 column volumes of 50 mM PBS supplemented with 0.001% Tween, 2 column volumes of 50 mM PBS and finally with 1 column volume of H_2O. After washing, the resins were collected from the column and incubated with 2.25 M ammonium hydroxide at room temperature, overnight with agitation. The sample was then neutralized with formic acid and protein concentration was determined. 1 equivalent of enzyme digestion buffer was added (for trypsin digestion: 100 mM ammonium bicarbonate buffer (Sigma); for chymotrypsin digestion: 100 mM Tris and 10 mM $CaCl_2$, pH 7.8). Digestion was performed at an enzyme-to-substrate ratio of 1:50 (wt:wt) and incubated at 37 °C overnight with agitation. Enzyme was added again to solution at an enzyme-to-substrate ratio of 1:20 (wt:wt) and re-incubated at 37 °C for 5 hr with agitation. The resulting peptide sample was then quenched by bringing to pH 3, with conc. HCl, and analyzed at Bordeaux Proteomic Platform. Trypsin digested peptides were analyzed by LC-MS/MS on a Thermo Scientific Q Exactive Orbitrap mass spectrometer in conjunction with a Proxeon Easy-nLC II HPLC (Thermo Fisher Scientific) and Proxeon nanospray source. Samples were separated on 300-µm ID x 5-mm C_{18} PepMapTM precolumn and 75 µm ID x 25 cm nanoViper C_{18}, 2 µm, 100 Å – Acclaim® PepMap RSLC column using 4-40% gradient of B (A: H_2O/MeCN/HCOOH, 95/05/0.1, B: H_2O/MeCN/HCOOH, 20/80/0.1). Peptides were eluted using a 120 min gradient with a flow rate of 300 nL/min. An MS survey scan was obtained for the m/z range of 350-1600; MS/MS spectra were acquired using a top 12 method, where the top 12 ions in the MS spectra were subjected to High Energy Collisional Dissociation (HCD). An isolation mass window of 2 m/z was used for the precursor ion selection, and normalized collision energy of 27% was used for fragmentation. Five second duration was used for the dynamic exclusion. Peptide identification was performed using PEAKS Studio (BSI, Canada). The search settings were: precursor Δm tolerance = 10 ppm, fragment Δm tolerance = 0.2 Da, missed cleavages = 2, -10log$P$>50, modifications of lysine: NBF (163.0012), modifications of cysteine: NBF (163.0012), DCP-Bio1 (394.1557), or hydrolyzed DCP-Bio1 (168.0786).

In Gel Detection of Persulfidation (Dimedone Switch Method)

Preparation of DAz-2:Cy-5 Click Mix

1 mM DAz-2 (Cayman Chemical), 1 mM Cyanine5 alkyne (Lumiprobe), 2 mM copper(II)-TBTA complex (Lumiprobe) and 4 mM ascorbic acid made *in situ*, was added in 15 mM PBS buffer with 30% acetonitrile. The solution was mixed at room temperature overnight and quenched with 20 mM ethylenediaminetetraacetic acid (EDTA).

Persulfide Detection in Cell Lysates

Two 100 mm dishes of 80-90% confluent HeLa cells were lysed in cold HEN lysis buffer (50 mM Hepes, 1 mM EDTA, 0.1 mM Neocuproine, 1% IGEPAL and 2% SDS, adjusted to pH 7.4) supplemented with 1% protease inhibitor (Sigma) in the control dish and with an additional 5 mM 4-chloro-7-nitrobenzofurazan (NBF-Cl) in the second dish. Both dishes were gently scrapped, lysates were collected, homogenized with a syringe and needle and immediately placed for incubation at 37 °C for 30 min, protected from light. A methanol/chloroform precipitation was performed and protein pellets obtained were washed with cold methanol, dried, protected from light and redissolved in 50 mM Hepes (Euromedex, adjusted pH 7.4) supplemented with SDS (final conc. 2%). When fully dissolved, protein concentration was determined using DC Assay (BioRad) and adjusted to 2-3 mg/ml. Each protein sample was separated into two tubes; to one of the control sample tubes and one NBF-Cl lysed sample tubes, 25 µM of DAz-2:Cy-5 click mix prepared without DAz-2, as described above was added. Additionally, in the remaining control and NBF-Cl lysed sample tubes, 25 µM of DAz-2:Cy-5 click mix prepared as described above was added. All four tubes were placed for incubation at 37 °C for 30 min, protected from light. Following incubation, methanol/chloroform precipitation was performed as described above and the protein concentration was determined and adjusted to 2-2.5 mg/ml. 1 equivalent of Laemmli (4X) buffer (BioRad) supplemented with 10% β-mercaptoethanol was added to 3 equivalents of sample and boiled at 95°C for 5 min protected from light. Samples were resolved by SDS-PAGE and gels were fixed in fixation buffer for 30 min, protected from light. The gel was recorded, at 635 nm for the Cy5 signal and 473 nm for NBF-Cl signal, on the Typhoon FLA 9500 (GE Healthcare).

The H_2S donor treatments were performed with 200 µM Na_2S for 45 min, 200 µM GYY4137 for 2 hr, 200 nM AP39 for 2 hr and 2 mM D-Cysteine for 1 hr, all at 37 °C and 5% CO_2. Erastin treatments were preformed with 1 µM and 10 µM Erastin for 18.5 hr. Monensin treatments were performed by treating cells with 1 µM for 18 hr, both at 37 °C and 5% CO_2. Cells were lysed and processed as previously described.

Persulfide Detection in Escherichia coli Lysates

The laboratory strain *E. coli* MG1655 was transformed with the pSB74 plasmid that contains the *phsABC* operon of *S. Enterica* serovar Typhimurium for H_2S production. As a negative control, *E. coli* was transformed with an empty vector (pTrc99a). Both strains were streaked on TSA plates supplemented with ampicillin 50 mg/ml, and incubated overnight at 37 °C. The next day, one colony of each strain was inoculated into TSB medium supplemented with 50 mg/ml of ampicillin and grown at 37 °C with agitation (100 rpm), as a starter inoculum. 10 µl of each of these overnight-grown cultures were transferred into 10 ml of fresh TSB medium supplemented with the appropriate antibiotic. Both strains were treated with 20 mM sodium thiosulfate for 4 hr at 37 °C with agitation (120 rpm). After the incubation time, samples were harvested by centrifugation at 5000 rpm for 4 min, washed with ice-cold PBS and resuspended in HEN lysis buffer supplemented with 1% protease inhibitor and 25 mM NBF-Cl. Cells were disrupted on ice by sonication, 20 seconds at 190 MHz 2 times with a 2 min pause, and incubated at 37 °C for 1 hr, protected from light. Samples were then precipitated and dissolved as previously described and incubated with 50 µM DAz-2:Cy5 preclick mix, for 1 hr at 37 °C protected from light.

Persulfide Detection in Saccharomyces cerevisiae Lysates

For persulfide detection 200 µL yeast cells of WT, *Δcys3*, *Δcys4* and *Δtum1* strains were mixed with 1 mL HEN lysis buffer supplemented with 1% protease inhibitor for yeast and 20 mM NBF-Cl. Mixture was added dropwise into liquid nitrogen and grinded using a mortar and pestle, together with glass beads, reaching a fine powder consistency. Samples were transferred in 2 ml tubes and centrifuged on 1500 *x g* for 15 min at 4 °C. Supernatants were collected and incubated at 37 °C for 1 hr, protected from light. After precipitation, protein pellets were processed as previously described with 50 µM DAz-2:Cy5 preclick mix for 45 min at 37 °C.

Persulfide Detection in Caenorhabditis elegans Lysates

Synchronous populations of embryos were obtained by lysing gravid hermaphrodites in alkaline bleach as described by Emmons et al. (1979). Once washed free of the alkaline bleach by centrifugation, the embryos were inoculated on standard NGM agar plates, ~4000 embryos/plate. At Day-1 adult stage worms of different strains (N2, *cth-1*, *mpst-3*, *eat-2*, *eat-2;cth-1*, *eat-2;mpst-3*) were collected from the NGM plates, 4 plates/strain, into 15 ml falcons using M9 buffer and washed three times. Worm pellets were frozen in liquid nitrogen and 500 µl of glass beads was added in every tube. Samples were put in the bead beater (FastPrep-24, MP Biomedicals, California, USA) for 35 seconds at speed 6.5 m/s, followed by an additional cycle at the same speed for 20 seconds. HEN lysis buffer supplemented with 1% protease inhibitor and 20mM NBF-Cl was added to each tube, and centrifuged for 15 min at 13000 rpm at 4°C. Supernatants were collected and incubated at 37 °C for 45 min. Protein pellets were processed and labeled with 25 µM DAz-2:Cy5 preclick mix, as previously described.

Synchronous populations of embryos were obtained as described above, and inoculated on standard NGM agar or NGM agar plates supplemented with 1 mM sodium thiosulfate seeded with *E. coli* OP50-1. The plates were then incubated at 20°C until worms reached Day-1 adult stage. Worms were collected from the plates and processed, as previously described.

Persulfide Detection in Drosophila melanogaster Lysates

As wild-type control, the y^1w^{1118} *Drosophila* line was used. *Eip55E* (*Drosophila CSE*)-overexpressing lines were a kind gift from Professor Ody Sibon (University of Groningen). 3-4 whole flies were grinded in dounce homogenizer with 50 µL of HEN lysis buffer supplemented with 1% protease inhibitor and 20 mM NBF-Cl on ice. Homogenates were centrifuged at 30 000 x *g* for 20 min and the supernatant was incubated for 30 min at 37 °C, protected from light. Next, persulfide labeling was performed as previously described.

Persulfide Detection in Mouse Kidney Lysates

$CSE^{+/+}$ and $CSE^{-/-}$ C57BL/6 mice were generated and previously characterized (Markó et al., 2016). $CSE^{+/-}$ males and females were bred to obtain $CSE^{+/+}$ and $CSE^{-/-}$ littermates. Mice were allowed free access to standard chow and water. The mice were kept in a 12:12-h light-dark cycle. The kidneys from these mice were kind gift from Professor Maik Gollasch (Charité Medical Faculty). 5-10 mg of kidney tissue was homogenized with 500 µL of HEN lysis buffer supplemented with 1% protease inhibitor and 20 mM NBF-Cl on ice in dounce homogenizer. Homogenates were centrifuged at 30 000 x *g* for 20 min and the supernatant was incubated for 30 min at 37 °C, protected from light. Next, persulfide labeling was performed as previously described.

Persulfide Detection in Rat Tissue Lysates

Immediately after decapitation, the brain, heart and liver were quickly removed and snap frozen in liquid nitrogen. The organs were shredded and homogenized in HEN lysis buffer supplemented with 1% protease inhibitor and 20 mM NBF-Cl using a dispersion system (Ultra-Turax T25, Janke & Kunkel, IKA-Labortechnik, Germany) at 8000 rpm

on ice. After 1 hr incubation at 37 °C protected from light, samples were precipitated and processed as previously described with 50 μM DAz-2:Cy5 click mix for 45 min at 37 °C.

Persulfide Detection in Liver of Aging Mice following dietary restriction (AL and CR)

On the day of the experiment, mice were brought to the procedure room (6.30 am) and placed in clean cages. Food for AL mice was transferred to the hopper, and CR mice were fed per usual at 7am with one pellet per mouse on the floor of the cage. They were allowed to eat for 2 hr and then starting at 9am, mice were anesthetized with isoflurane (2-5% in oxygen) and a cardiac puncture was performed to withdraw blood. Cervical dislocation was performed to ensure euthanasia and tissues were excised and snap frozen in liquid nitrogen. From the time of cervical dislocation to excision and snap freezing of the liver, this period did not exceed 30 seconds (mice were not fasted for this experiment). 20 mg of liver was cut into small pieces with a scalpel placed in 1 ml of HEN buffer supplemented with 1% protease inhibitor and 20 mM NBF-Cl, which were then homogenized using a dispersion system on ice and processed as previously above.

Persulfide Detection in Skeletal Muscle of Mice following a Glucose Tolerance Test

A glucose tolerance test (GTT) was performed on 2- old and 12- month old mice which were fasted for 16 hr prior to being injected i.p. with D-glucose (2 g/kg body weight). Blood glucose level was recorded by tail vein bleeding immediately before and at indicated time points (15 min and 60 min) after injection using an Ascensia Contour blood glucose meter and test strips. At the indicated time points, the mice were euthanized by cervical decapitation and the skeletal muscle was isolated and snap frozen in liquid nitrogen. 20 mg of frozen muscle was cut in to small pieces with a scalpel and placed in 2 ml of HEN buffer supplemented with 1% protease inhibitor and 20 mM NBF-Cl. The suspension was then homogenized using a dispersion system on ice and processed for persulfidation labelleing as described above.

Persulfide Detection in Human Erythrocyte Lysates

Erythrocyte lysates were prepared in two ways, to obtain membranes and cytosol. Packed erythrocytes were lysed with 5 volumes of 10 mM phosphate buffer containing 5 mM NBF-Cl for 30 min at 4 °C with frequent vortexing. After 20 min centrifugation (30,000 *x g*) supernatant was separated from cell membrane pellet. SDS (for a final conc. of 2%) and 10 mM NBF-Cl (final concentrations) were added to the supernatant and incubated for an additional 60 min at 4 °C. Membrane pellets were washed 3 times with PBS containing 5 mM NBF-Cl, and then resuspended in PBS containing 5 mM NBF-Cl and SDS (final conc. 2%) and incubated for 30 min at 37 °C. Both membrane and cytosol proteins were precipitated as previously described, and persulfides labeled with 50 μM DAz-2:Cy5 click mix for 45 min at 37 °C.

Persulfidation Detection by Confocal Microscopy and Epifluorescence Deconvolution Microscopy

$CSE^{+/+}$ and $CSE^{-/-}$ MEF cells were grown in μ-dishes (35 mm, Ref. 81158) obtained from Ibidi® (Martinsried, Germany) following manufacturer's instructions. The treatments with 2 mM D-cysteine and 200 μM Na_2S (H_2S) were performed over 1 hr at 37 °C. After treatments, the cells were washed twice with warm sterile PBS, and incubated with 1 mM NBF-Cl in PBS for 30 min at 37 °C. Fixation was carried out by incubation with ice-cold methanol at -20 °C for 20 min and subsequent permeabilization with ice-cold acetone at -20 °C for 5 min. The dishes were washed with PBS and incubated with 1 mM NBF-Cl in PBS for 1 hr at 37 °C. Cells were washed with PBS overnight, and incubated with 10 μM DAz-2:Cy-5 click mix in PBS for 1 hr at 37 °C. For the negative control cells were incubated with 10 μM DAz-2:Cy-5 click mix prepared without DAz-2. After overnight washing with PBS, cells were washed with methanol 3 x 10 min, followed by an additional washing with PBS. DAPI staining was performed according to the manufacturer's recommendation. Images were obtained using a Confocal Leica TCS SP5 microscope equipped with an Argon laser (458, 476, 488, 514 nm), a diode laser (405 nm) and Helium-Neon laser (633 nm). A x40 oil objective lens was used. For examination of co-localization of immunofluorescence, single optical sections at the same focus plane were taken separately and the three corresponding channels were merged into a 8-bit RGB tiff-file using ImageJ. *Z*-stack images were taken on Olympus IX81 inverted fluorescence microscope using x 100 oil objective lens, used for image deconvolution.

Antibody Array-like Approach for Detection of Persufidation

Each antibody was added into the appropriate wells of a 96 well plate with 3D-NHS Surface (PolyAn, Berlin) at a final volume of 50 μl in PBS buffer (150 mM Na_2HPO_4 / $NaHPO_4$ and 50 mM NaCl, pH 8.5). Additionally, in the negative control wells 50 μl of 5% BSA in TBST (137 mM NaCl, 20 mM Trizma base, 0.1% Tween) and 0.002% NaN_3 was added. The plate was covered and incubated at 4 °C overnight with agitation. The solutions were discarded and the wells were washed 5 times with 15 mM PBS Tween using a multi-channel and inverting the clean plate against paper towels for complete removal of liquid. All wells were then blocked with 50 mM ethanolamine in 100 mM Tris

at pH 9 for 2 hr at room temperature with agitation. The blocking solution was discarded and wells were re-blocked with 5% BSA in TBS Tween for a further 1 hr at room temperature with agitation. Wells were washed again as described above. Following complete removal of liquid, 100 µl of treated samples were added to appropriate wells and incubated at 4 °C, overnight with agitation. After washing, the plate was recorded on Typhoon FL9500 at 473 nm and 635 nm.

For experiments where $CSE^{+/+}$, $CSE^{-/-}$ and $CSE^{+/+}$ treated with D-cysteine MEF cells, lysates were obtained and labeled for persulfides, as previously explained. The following antibodies were used: 1. β-actin (0.04 mg/ml, sc-47778, Santa Cruz Biotechnology); 2. β-tubulin (0.04 mg/ml, T0198, Sigma Aldrich); 3. GAPDH (0.04 mg/ml, G8795, Sigma Aldrich); 4. HSP70 (0.04 mg/ml, ab5439, Abcam); 5. KEAP1 P586 (0.0062 mg/ml, 4678, Cell Signalling); 6. eNOS (0.0025 mg/ml, 32027, Cell Signalling); 7. Parkin (0.04 mg/ml, sc-136989, Santa Cruz Biotechnology); 8. SOD-2 (0.04 mg/ml, sc-137254, Santa Cruz Biotechnology); 9. Anti-TST (0.04 mg/ml, GTX114858, GeneTex); 10. Anti-SQR (0.04 mg/ml, HPA017079, Sigma Aldrich).

For experiments with lysates of HeLa cells treated in a time-dependent manner with EGF and labeled for persulfides as previously described. The following antibodies were used: PTEN (1:1000, sc-7974, Santa Cruz Biotechnology,); 2. PTP1B (1:1000, sc-133259, Santa Cruz Biotechnology); 3. SH-PTP2 (0.04 mg/ml, sc-7384, Santa Cruz Biotechnology); 4. EGFR (0.04 mg/ml, sc-03-G, Santa Cruz Biotechnology).

MnSOD Persulfidation and Activity Experiments

Human recombinant MnSOD was purchased from Creative BioMart. SOD activity was measured using cytochrome c assay, as described previously. Peroxynitrite was prepared following well established protocol (Filipovic et al., 2012) and tyrosine nitration assessed using characteristic spectral properties: an increase in the absorbance at 430 nm was attributed to nitrotyrosine formation due to the characteristic shift (from 430 to 357 nm) observed with decreasing pH (Filipovic et al., 2012).

Detection of Protein Sulfenylation

Following respective treatments, cells were lysed in cold HEN lysis buffer supplemented with 1% protease inhibitor and 100 µM DCP-Bio1. Cells were gently scrapped, lysate was collected, homogenized with a syringe and needle and immediately placed for incubation at 37 °C for 1 hr. A methanol/chloroform precipitation was performed and protein pellet obtained was redissolved in 50 mM Hepes with SDS (final conc. 2%). Protein pellets were prepared for SDS-PAGE, as previously explained. After resolving samples on gel, protein transfer was performed, followed by blocking in 5% dry-milk in PBS Tween and incubated with Streptavidin Protein DyLight 488 in 50 mM PBS (1:10000, 21832, ThermoFisher) for 1 hr protected from light. Nitrocellulose membrane was recorded at 473 nm, using a Typhoon FLA 9500 (GE Healthcare).

Detection of Protein Sulfinylation

Following respective treatments, cells were lysed in cold HEN lysis buffer supplemented with 1% protease inhibitor and 5 mM NBF-Cl or 20 mM NEM. Cells were gently scrapped, lysate was collected, homogenized with a syringe and needle and immediately placed for incubation at 37 °C for 30 min or 1 hr respectively. A methanol/chloroform precipitation was performed and protein pellet obtained was redissolved in 50 mM Hepes with 2% SDS. Protein concentration was determined and adjusted to 2.5 mg/ml. Samples were treated with 1 mM BioDiaAlk at room temperature for 1 hr, protected from light. Reaction was quenched by the addition of 1 mM DTT incubated overnight at 4 °C or preformed a methanol/chloroform precipitation. Sample were then mixed with 4X Laemmli (1:4) and incubated for 20 min at 55 °C. After resolving samples on gel, protein transfer was performed, followed by blocking in 5% dry-milk in PBS Tween and incubated with Streptavidin Cy5 (1:4000, 21832, ThermoFisher) for 1 hr protected from light. Nitrocellulose membrane was recorded at 635 nm, using a Typhoon FLA 9500 (GE Healthcare).

Receptor Tyrosine Kinase Activation of Cells

Activation Conditions

EGF (PromoKine) treatments in HeLa and MEF cells, and insulin treatments in SH-SY5Y cells, were performed with cells cultured in 100 mm cell culture dishes at a 80-90% confluency. VEGF (PromoCell) treatments were performed with HUVECs cultured in T25 flasks (Greiner) at a 70-80% confluency. For pretreatments, media was replaced with complete media supplemented with 100 µM GYY4137 or inhibitor mix (PG and AOAA, 1 mM of each), incubated at 37 °C and 5% CO_2 for 30 min and then washed with warm sterile PBS. Subsequently, media was replaced with complete media (as described above) for control and media supplemented with respective treatments (100 or 200 ng/ml EGF; 100 nM or 200 nM insulin; 40 ng/ml VEGF). Following treatments, cells were washed with cold PBS twice and lysed for persulfide or sulfenic acid labeling, as previously explained.

Real-time activity of EGFR in HeLa cells

Cells were seeded at $1x10^4$ cell/well in an equilibrated E-Plate VIEW 16 PET and grown overnight at at 37 °C with 5% CO_2. Next, cells were incubated in serum-free complete medium for four hr prior to experiments and pretreated with 100 µM of GYY4137 or inhibitor mix (PG and AOAA, 1 mM of each), as indicated. Basal receptor tyrosine kinase activity in cells was recorded for 20 min and upon the addition of 150 ng/ml EGF, cells were further recorded in 2 hr with the integration time of 1 minute using xCELLigence RTCA DP system (ACEA Biosciences, Can Diego, USA).

Detection of Persulfidation of EGFR Pathways (EGF pathway phosphorylation antibody array)

The persulfidation of the proteins associated to the EGFR pathways were assessed using an EGF pathway phospho antibody array comprising of 214 antibodies related to the EGF pathway (Full Moon Biosystems, CA) performed in duplcates. The glass strips (barcode: 4000026018, 4000026019, 4000026022 and 4000026023) were equilibrated to r.t. 1 hr and dried for 45 mins. They were then blocked with 5% BSA in TBS Tween by rocking at 55 rpm at r.t. for 45 mins. The slides were then washed extensively with TBS Tween (twice), TBS (twice) and then with H_2O (five times). Lysates of HeLa cells untreated and treated with 100 ng of EGF for 30 mins and labeled for persulfides, as previously explained, were prepared and dissolved in 50 mM Hepes in 2% SDS and further diluted 60 times with 1% BSA in TBS up to 6 ml. The glass strips were then submerged in the samples and incubated by rocking at 55 rpm for 2 hr. The slides were then washed as done previously, left to dry and recorded at 473 nm and 635 nm, using a Typhoon FLA 9500 (GE Healthcare). Persulfide levels of each dot for each type of antibody (in pentaplicates on glass strip) were averaged and the intensity of their cy5 (635 nm) signal adjusted to the 473 nm signal of the internal standards, GAPDH and beta-actin.

Immunoblotting

Untreated or specifically treated cells were washed twice with cold PBS and harvested in RIPA lysis buffer (50 mM Tris-HCl, 150 mM NaCl, 2 mM EDTA, 1% IGEPAL and 2% SDS, adjusted to pH 7.4) supplemented with 1% protease inhibitor. Cells were scrapped, lysates were collected, homogenized with syringe and needle, and centrifuged at 30,000 x *g* for 5 min at 4 °C. Clear lysate was transferred to a new tube. Protein concentration of lysate was determined using the DC assay (BioRad).

Protein samples were resolved by SDS-PAGE and transferred to a nitrocellulose blotting membrane (GE Healthcare). Primary antibodies used: CBS (1:1000, sc-133154, Santa Cruz Biotechnology), MPST (1:4000, HPA001240, Sigma Aldrich), CTH (MEF cells, 1:4000), CTH (HeLa cells, 1:1000, sc-374249, Santa Cruz Biotechnology), p-ERK (1:1000, sc-7383, Santa Cruz Biotechnology), total-ERK (1:1000, sc-271269, Santa Cruz Biotechnology), DJ-1 (1:250, sc-55572, Santa Cruz Biotechnology), DJ-1 Oxidized At C106 (1:1000, HCA024, BioRad) and β-tubulin (1:5000, T0198, Sigma Aldrich). Species-specific horseradish-conjugated secondary antibodies (1:5000, Santa Cruz Biotechnology) were used for antigen detection and visualized using Clarity™ Western ECL Substrate (BioRad).

Immunoprecipitation and detection of DJ-1 Persulfidation, Sulfinylation and Sulfenylation Following H_2O_2 Treatment

MEF cells ($CSE^{+/+}$ and $CSE^{-/-}$) were treated with 100 µM H_2O_2 for 15 or 30 min. For the detection of persulfides NBF-Cl was used and switched with DCP-Bio1, for sulfenic acid labeling DCP-Bio1 was used and for sulfinic acid labeling NEM was used and then labeled with BioDiaAlk, as previously described. Proteins were then precipitated and resuspended in 50 mM Hepes with 0.01% SDS at 1 mg/ml. Samples were incubated overnight at 4 °C with anti-DJ-1 agarose coupled antibody (Santa Cruz Biotechnology, sc-55572 AC). After incubation agarose resins were collected by centrifugation (2,000 x g) and washed with 10 mM TBS supplemented with 0.001% Tween (three times) and with 10 mM TBS (twice). DJ-1 protein was eluted from the resins for 10 min at 95 °C in 10 mM TBS with 3.5% SDS. This was then mixed with 4X Laemmli (1:4) supplemented with 10% β-mercaptoethanol and incubated overnight at 55 °C. Elution fractions were collected by centrifugation (30,000 x*g*) and resolved by SDS-PAGE. Protein transfer was performed, followed by blocking in 1% BSA in TBS Tween. Monoclonal anti-Biotin-Peroxidase-conjugated antibody (1:1000, Sigma) was used for detection and visualized using Clarity™ Western ECL Substrate (BioRad).

Trx-catalyzed reduction of S-sulfocysteine (SSC)

Cloning and Mutagenesis of Human TRP14 and Trx1

Genetic sequence of human TRP14 was obtained by generating cDNA from mRNA isolated from human fibroblasts. The target sequence was amplified by PCR using forward primer 5'-ACCATCACGGATCC**ATG**GCCCGCTATGAGGAGG-3' containing a BamHI restriction site (underlined) and a start codon (boldface type), in combination with reverse primer 5'-

CCGGGGTACCG**TTA**ATCTTCAGAGAACAACATTTCCACCAG-3' 3'containing a KpnI restriction site (underlined) and a stop codon (boldface type). The sequence of the target band was verified by commercial sequencing (GATC Biotech). The PCR product was ligated into a pQE80-L expression vector (Qiagen). Human Thioredoxin 1 (Trx1) was expressed in *E. coli* using pET28a expression vector. Mutagenesis of the C32S & C35S variants were conducted using PCR-mediated site-directed mutagenesis, and the Trx1-pET28a expression plasmid was used as a scaffold.

Expression and Purification of Human TRP14 and Trx1

E. coli BL21 (DE3) Rosetta cells were transformed with the respective expression plasmid and cultured at 37 °C, 140 rpm in LB medium supplemented with the necessary antibiotics and grown until OD_{600} reached 0.5. Protein expression was induced using isopropyl-β-D-thiogalactopyranosid (IPTG) at a final concentration of 250 µM. The expression temperature and rotation was changed to 30 °C, 120 rpm for TRP14 and 18 °C, 120 rpm for Trx1 variants; expression was conducted for ~16 hr. Cells were harvested and lysed in lysis buffer (50 mM potassium phosphate, pH 7.4, 250 mM NaCl, 10 mM imidazole) supplemented with complete EDTA-free protease inhibitor (Roche). Cells were lysed using egg white lysozyme (VWR) and homogenized in an Emulsiflex. Residual nucleic acids were disrupted using a sonication rod at 25% amplitude, 10 seconds. The cell lysate was centrifuged at 48000 x *g* for 45 min, and His-tagged proteins were isolated using His-Pur Ni-NTA Superflow Agarose (ThermoFischer) in accordance with the manufacturer's protocol. Elution was performed using lysis buffer supplemented with 250 mM imidazole. Elution fractions were analyzed using SDS-PAGE and subsequent Coomassie Brilliant Blue staining, and fractions containing increased amounts of target protein were further purified using anion exchange chromatography (Source 15Q, GE Healthcare; low salt buffer: 50 mM sodium phosphate, pH 7.4; high salt buffer: 50 mM sodium phosphate, pH 7.4, 1 M NaCl). Elution was performed in a gradient over five column volumes. Elution fractions were again analyzed using SDS-PAGE and Coomassie Brilliant Blue staining. Relevant fractions were buffer exchanged into storage buffer (50 mM sodium phosphate, pH 7.4, 150 mM NaCl, 100 µM DTT), flash-frozen in liquid nitrogen and stored at -80 °C. Proteins were again buffer exchanged after thawing into the relevant experimental buffer.

Coupled Assay of Trx1 / TRP14 and TrxR with Cystine / SSC

Activities of hTrx and TRP14 with cystine and SSC were recorded measuring NADPH oxidation on a Tecan Infinite M200 plate reader, set to record absorption at 340 nm. 3 µM hTrx1 or TRP14, 30 nM TrxR from rat liver (Sigma Aldrich) and 250 µM NADPH were used in all measurements. Concentration of cystine or SSC were set at 1 mM. Absorption at 340 nm were recorded in 10 seconds intervals over 900 seconds. The initial rate of A_{340} decrease was fitted linearly, and consumption of NAPDH over time was determined using an NADPH extinction coefficient ε_{340} of 6020 M^{-1} cm^{-1}.

Kinetics of Direct Reaction of Human Trx with SSC

Kinetics of the reaction of hTrx with cysteine persulfide was monitored on FP-8200 spectrofluorometer (Carry Eclipse, Agilent) using an excitation wavelength of 280 nm and a maximal emission of 345 nm. Concentration of the enzyme was kept at 4 µM while substrate concentrations ranged between 25 µM and 100 µM. Given pseudo first-order conditions, observed rate constants k_{obs} were obtained by fitting the decrease in emission at 345 nm at a given SSC concentration using a first order exponential decay fit in Origin® analysis software.

Ultra High Resolution ESI-TOF Mass Spectrometry of Reaction Between Trx and SSC

Human recombinant Trx, Trx C35S and Trx C32S (10 µM) were incubated with 10 µM SSC in 20 mM ammonium carbonate buffer pH 7.8 for 5 min and recorded on maXis 5G (Bruker Daltonics) ESI-TOF MS capable of resolution of at least 40,000 FWHM, following previously described protocol (Wedmann et al., 2016).

MEF cells Stress Assays

MEF cells ($CSE^{+/+}$ and $CSE^{-/-}$) were plated in 96-well plates at 5 x 10^4 cells/well. Cells were treated with H_2O_2 (concentration range 0.2-2 mM) for 24 hr and the cell survival was assessed by an MTT assay as previously described (Liu et al., 2015).

***C. elegans* Stress Assays**

Worms were initially synchronised by picking approximately 100 young adult worms per strain onto NGM-plates, and allowed to lay eggs over 4 hr at 20 °C. The young adults were then removed, and the remaining embryos were washed off and collected from the NGM-plates using M9 buffer and transferred to a 15 ml polypropylene tube. The worm suspension was centrifuged (850 x *g*, 1 min) and washed with M9 buffer 3 times. The resulting pellet of embryos was re-suspended in 12 ml of M9 buffer, and incubated with agitation (100 rpm) for 24 hr at 20 °C. The synchronised L1 worms were collected, centrifuged (850 x *g*, 1 min) and re-suspended in S-basal buffer. The number and

synchronicity of L1 worms was determined and the worms were transferred to an Erlenmeyer, diluted in the respective amount of HB101 in S-Basal buffer for a conc. of 60 worms/10 mg of HB101/ml of S-basal buffer. They were then incubated with agitation (115 rpm) for 48 hr at 20 °C. The worms were then collected, centrifuged (400 rpm, 1 min), washed with M9 buffer 3 times and re-suspended in M9 buffer.

For experiments with the pretreatment of worms, synchronised young adults (as described above) were transferred in an Erlenmeyer with 12 ml of M9 buffer and 500 µM GYY4137 or 100 nM AP39 was added. Worms were then incubated for 3 hr at 20 °C with agitation (115 rpm). Worms were centrifuged (400 rpm, 1 min) and re-suspended in M9 buffer. To assess the effect of CTH on stress resistance, 60 mM paraquat dichloride hydrate or 5 mM sodium (meta) arsenite dissolved in M9 buffer was added to the synchronised young adult worm suspension and plated on a 96 well plate with approximately 5 - 10 worms per well. Viability was monitored by counting dead worms over 5 - 6 hr, whilst incubating the plate at 20 °C, with agitation (110 rpm).

Yeast stress Assays and H2S production

Spot assays were carried out by spotting 5 µl of early exponential phase cultures (OD_{600}=0.5) sequentially diluted (approximately 3.5×10^4 to 3.5 cells) on plates with YPD media supplemented with different concentrations of H_2O_2 (0, 1 mM, 2 mM and 5 mM). Growth was recorded after incubation of 24 and 48 hr, at 30 °C. Survival assays were done by preparing overnight cultures in YPD media (cell in stationary phase), from which the experimental cultures were set, by diluting to OD_{600}=2 in a 5 ml final volume, with or without respective concentrations of H_2O_2 (0, 10 mM and 20 mM). The cultures were subsequently grown in culture tubes for 27 hr at 30 °C with agitation (180 rpm). Yeast cells were then washed once in PBS and collected by centrifugation (5000 x g, 3 min). Cells were then resuspended in PBS supplemented with 2 µM propidium iodide, at 1×10^6 cells/ml and incubated for 5 min in the dark. Analysis was performed by flow cytometry using 150,000 cells per condition, on a BD Accuri™ C6 and results were analysed using the CFlow Plus Software. For the quantification of H_2S levels, overnight cultures were washed with PBS and diluted as described above. Cell suspensions were incubated with 20 µM MeRho-Az sensor for 45 mins, at 30 °C and analysed by flow cytometry.

***C. elegans* Lifespans**

For the lifespan experiments a synchronous population of worms was obtained by transferring 5-6 young adults on medium plates and allowing them to lay eggs over 3 hr at 20 °C. Lifespan measurements were conducted at 20 °C, worms were transferred daily during the reproductive period. Death was scored by failure of the animal to move in response to gentle prodding with a platinum wire. For lifespan analysis with 1 mM sodium thiosulfate treatment or 5 mM 2-deoxy-D-glucose (DOG), new plates containing treatments in NGM agar were prepared every second day. Lifespan measurements were repeated at least twice unless otherwise stated.

Immunohistochemistry on Rat Brains

Brains were fixed in 4% paraformaldehyde for 24 hr, dehydrated in a series of increasing concentrations of ethanol (30%–100%), enlightened in xylene and embedded in Histowax® (Histolab Product AB, Göteborg, Sweden). Sagittal plane of each brain was sectioned at 5 µm thickness on a rotary microtome (RM 2125RT Leica Microsystems, Wetzlar, Germany). Sections were placed on Superfrost Ultra Plus® manufactured slides and used for immunohistochemical staining. In brief, after tissue deparaffinization, brain sections were exposed to heat-induced antigen retrieval to demask target antigens. Slides were placed in a container and covered with 0.01 mol/l sodium citrate buffer pH 6.0, and then heated at 750 W in microwave oven for 3 x 7 min. Next, sections were incubated with 0.3% H_2O_2 in MeOH for 15 min to block endogenous peroxidase. Slides were washed in PBS (pH 7.4) and reduction of non-specific background staining was achieved by incubation with normal swine (1:10, Dakopatts) and donkey serum (1:10, Abcam) for 45 min at room temperature. Afterward, sections were incubated with rabbit-anti-human: CBS (1:200, sc-67154, Santa Cruz Biotechnology), MPST (1:500, HPA001240, Sigma Aldrich), and with mouse-anti-human CTH/CSE antibody (1:200, sc-365382, Santa Cruz Biotechnology), overnight at 4 °C. For the negative control, the primary antibody was substituted with PBS. After washing 5 min in PBS, brain tissue sections were incubated with swine-anti-rabbit and donkey-anti-mouse IgG-horseradish peroxidase (HRP; 1:100; Dakopatts and Abcam) for 1 hr at room temperature. Slides were washed in PBS and visualization was performed using Dako liquid diaminobenzidinetetrahydrochloride (DAB) substrate chromogen system (Dako North America Inc.) at concentrations suggested by the manufacturer. Hematoxylin was used as counterstain and slides were mounted in DPX medium (Sigma-Aldrich).

QUANTIFICATION AND STATISTICAL ANALYSIS

The experiments were performed at least in triplicates. Key methodological experiments were verified by at least three different researchers in three different labs. Protein expression levels, persulfidation, sulfenylation and sulfinylation levels were compared with an unpaired t test with *$p < 0.05$ and **$p < 0.01$. Lifespan data were analyzed using

Kaplan-Meier survival analysis to detect statistical differences. Plotting of the data were performed using GraphPad Prism 5.0, Origin 8 and Microsoft Excel.

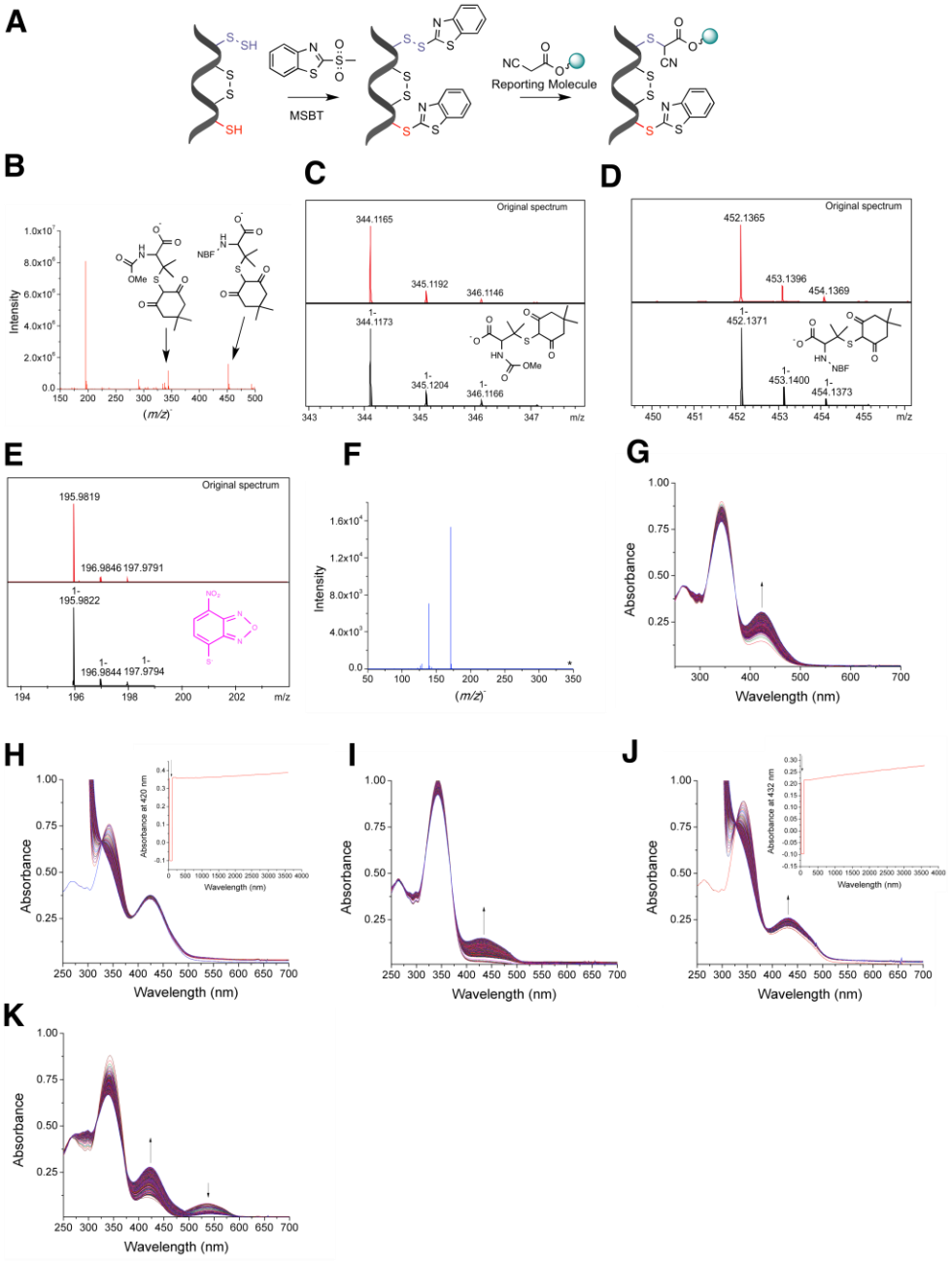

Figure S1. Testing dimedone switch method on low molecular weight and protein persulfides. Related to Figure 1.

(**A**) Original tag switch strategy for persulfide labeling.

(**B**) ESI-TOF-MS spectrum of the reaction mixture containing 100 μM nmc-penicillamine persulfide, 100 μM NBF-Cl, and 500 μM dimedone (ammonium carbonate buffer, pH 7.4, 23 °C). 100 μM nmc-penicillamine persulfide and 100 μM NBF-Cl were mixed for 10 min and after the completion of the reaction dimedone was added and the reaction was monitored by ESI-TOF-MS. (**C**-**E**) Speciation of the observed (red) peaks and simulation of the isotopic distribution for each species (black).

(**F**) MS/MS spectrum of *m/z* 344 peak. Asterisk marks the position of *m/z* 344 peak that decomposed to fragments which correspond to species shown in **Figure 1C**.
(**G**) UV-vis spectral changes upon addition of 100 μM NBF-Cl to 23 μM HSA-SH (50 mM phosphate buffer, pH 7.4 with 1% SDS, at 37 °C).
(**H**) UV-vis spectral changes caused by subsequent addition of 100 μM dimedone to a reaction mixture from (**G**). Inset: Kinetic trace at 420 nm.
(**I**) UV-vis spectral changes upon addition of 100 μM NBF-Cl to 23 μM HSA-SOH (50 mM phosphate buffer, pH 7.4 with 1% SDS, at 37 °C).
(J) UV-vis spectral changes caused by subsequent addition of 100 μM dimedone to a reaction mixture from (**I**). Inset: Kinetic trace at 420 nm.
(**K**) UV-vis spectral changes upon addition of 100 μM NBF-Cl to 23 μM HSA-SOH (50 mM phosphate buffer, pH 7.4 with 1% SDS, at 37 °C).

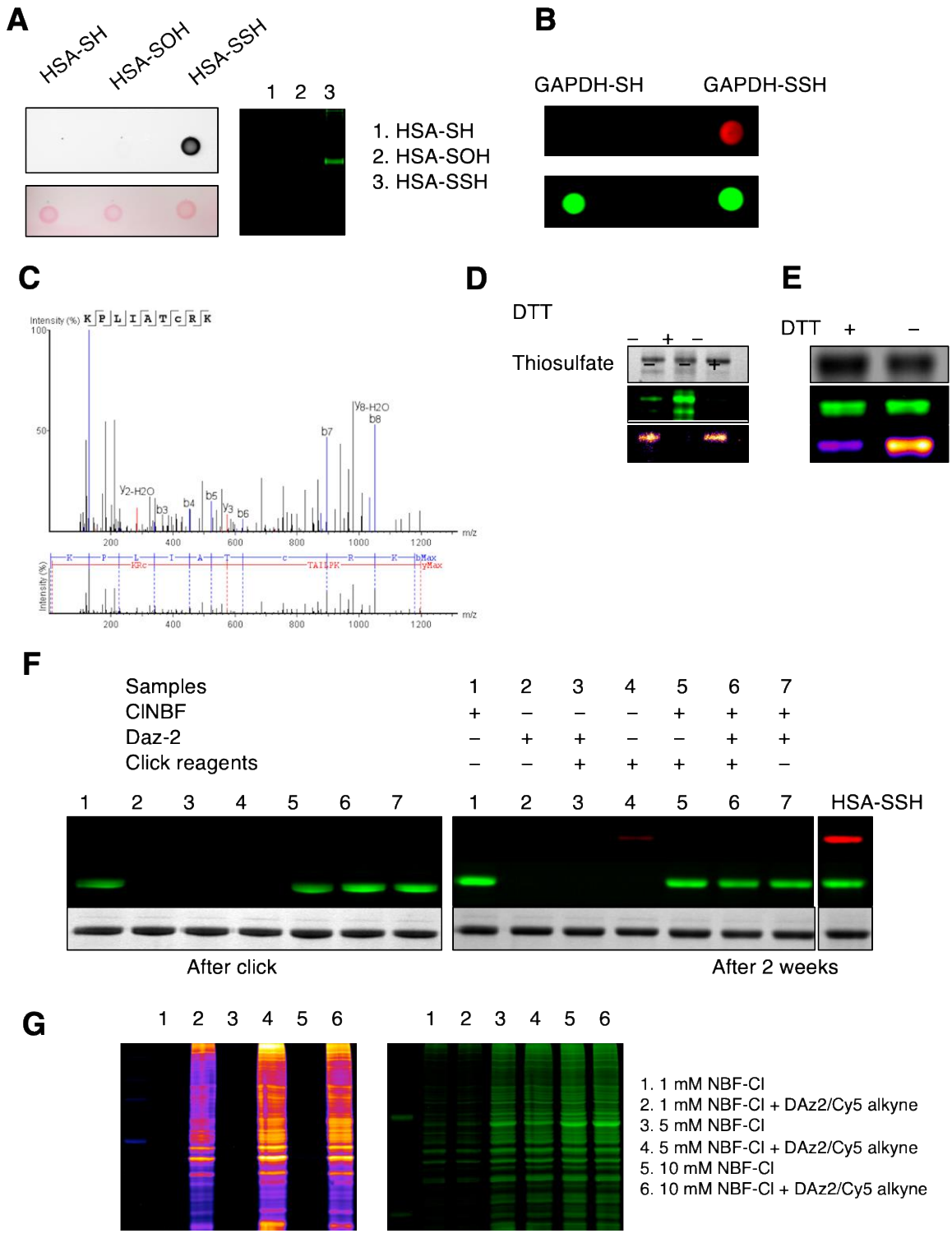

Figure S2. Probing the selectivity and conditions for persulfide labeling by dimedone switch method. Related to Figure 2.

(**A**) Human serum albumin (HSA), sulfenylated HSA and HSA persulfide were treated with 5 mM NBF-Cl (50 mM phosphate buffer, pH 7.4 with 1% SDS, at 37 °C), proteins precipitated and cleaned from NBF-Cl and then incubated with 100 μM DCP-Bio1 for 30 min at 37 °C. Following the precipitation and washing from the excess of DCP-Bio1, proteins were resuspended in 50 mM phosphate buffer, pH 7.4 and spotted on nitrocellulose membrane. Detection of dimedone-labeled adduct was done with streptavidin-Cy5. In addition, the same samples were incubated with

streptavidin magnetic beads and after careful washing, the bound protein was eluted by boiling with Laemmli buffer 5 min at 95 °C. Eluted proteins were separated by electrophoresis and in-gel fluorescence of NBF-protein adduct detected by Typhoon 9500.
(**B**) Detection of GAPDH-persulfide switch labeled with DCP-Bio1. Proteins were spotted on nitrocellulose membrane and biotinylation detected with streptavidin-Cy5. Green fluorescence (NBF-protein adduct) serves as a measure of protein load.
(**C**) MS/MS of peptide fragment obtained by trypsin digestion of bovine rhodanese (TST) shows labeling of C248 with hydrolyzed DCP-Bio1. Full MS data are given in Data S1-2.
(**D**) Commercially available TST was either incubated with thiosulfate or DTT to form fully persulfidated or reduced form, respectively. 20 μM enzyme was mixed with 50 μM NBF-Cl and persulfide visualized by using Daz-2/Cy5 CuAAC. While both untreated and thiosulfate treated showed Cy5 signal, the green fluorescence signal was significantly reduced in fully persulfidated enzyme, despite the same load. On the other hand, green fluorescence signal was much stronger in fully reduced enzyme, suggesting that at low NBF-Cl/protein ratio, switch caused by dimedone-based probe could affect the intensity of green fluorescence.
(**E**) When 1 mM NBF-Cl was used to initially react with 20 μM of TST, in an experiment similar to that shown in (**D**), the Cy5 signal was reduced when DTT treated TST was used, whilst the green fluorescence signal remained stable, suggesting that it can be used as a measure of the total protein load. It is worth mentioning that it is known that DTT is unable to fully reduce TST. (Tandon and Horowitz, 1989)
(**F**) The reaction of human serum albumin with click reagents in all possible combinations (left) show no nonselective labeling. The same samples run 2 weeks after being kept at -20 °C. Small unselective labeling can be observed in sample treated with Cy5-alkyne, Cu(II)-TBTA and ascorbate (probably due to the direct coupling of alkynes for thiols), but the signal was still negligible when compared to the signal obtained for labelled HSA-SSH.
(**G**) In-gel detection of protein persulfidation levels in HeLa cells, labeled with Daz-2/Cy5-alkyne CuAAC, after using different concentrations of NBF-Cl. Green fluorescence corresponds to NBF-protein adducts.

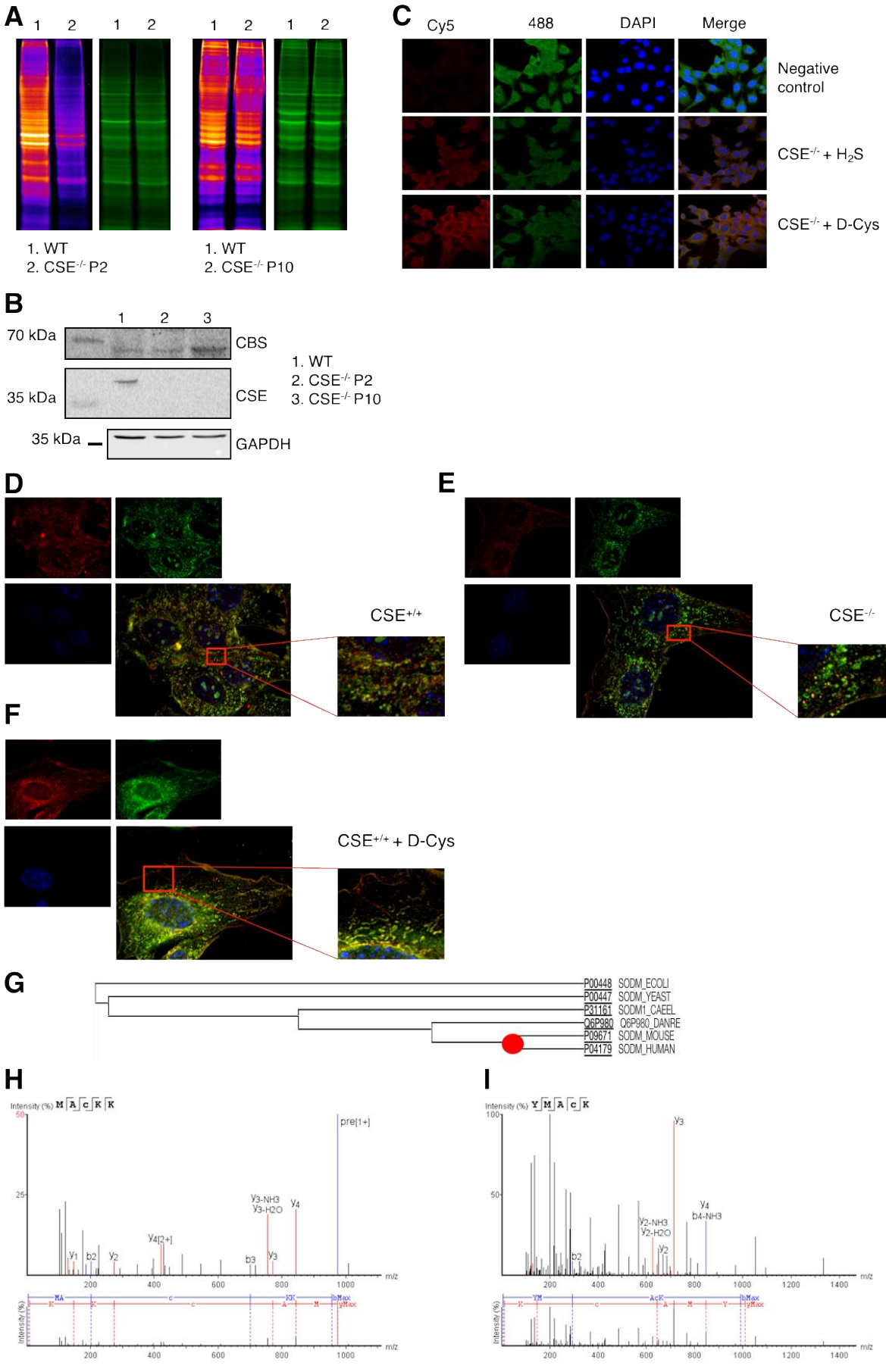
A
1 2 1 2
1 2 1 2
1. WT
2. CSE-/- P2
1. WT
2. CSE-/- P10
C
Cy5
488
DAPI
Merge
Negative control
CSE-/- + H2S
CSE-/- + D-Cys
B
1 2 3
70 kDa
CBS
35 kDa
CSE
35 kDa
GAPDH
1. WT
2. CSE-/- P2
3. CSE-/- P10
D
CSE+/+
E
CSE-/-
F
CSE+/+ + D-Cys
G
P00448 SODM_ECOLI
P00447 SODM_YEAST
P31161 SODM1_CAEEL
Q6P980 Q6P980_DANRE
P09671 SODM_MOUSE
P04179 SODM_HUMAN
H
Intensity (%) M A c K K
pre[1+]
y3-NH3
y3-H2O
y4
y4[2+]
y1
b2
y2
b3
y3
m/z
I
Intensity (%) Y M A c K
y3
y2-NH3
y2-H2O
y4
b4-NH3
b2
y2
m/z

Figure S3. Broad applicability of dimedone switch method. Related to Figure 3.

(**A**-**B**) Protein persulfidation levels and corresponding CSE and CBS expression levels in wild type and $CSE^{-/-}$ cells of passage (P) 2 and 10.

(**C**) *In situ* labeling of intracellular protein persulfidation detected by confocal microscopy. Related to the **Figure 3K**.

(**D**-**F**) High-resolution images of protein persulfidation in $CSE^{+/+}$, $CSE^{-/-}$ and $CSE^{+/+}$ MEF cells treated with 2 mM D-cysteine for 1 hr, obtained by wide-field fluorescence deconvolution.

(**G**) Protein evolution phylogenic tree showing the common origin of cysteine containing MnSOD.

(**H**) MS/MS spectra of peptide obtained by trypsin digestion of MnSOD containing C193 labeled with hydrolyzed DCP-Bio1.

(**I**) MS/MS spectra of peptide obtained by chymotrypsin digestion of MnSOD containing C193 labeled with DCP-Bio1.

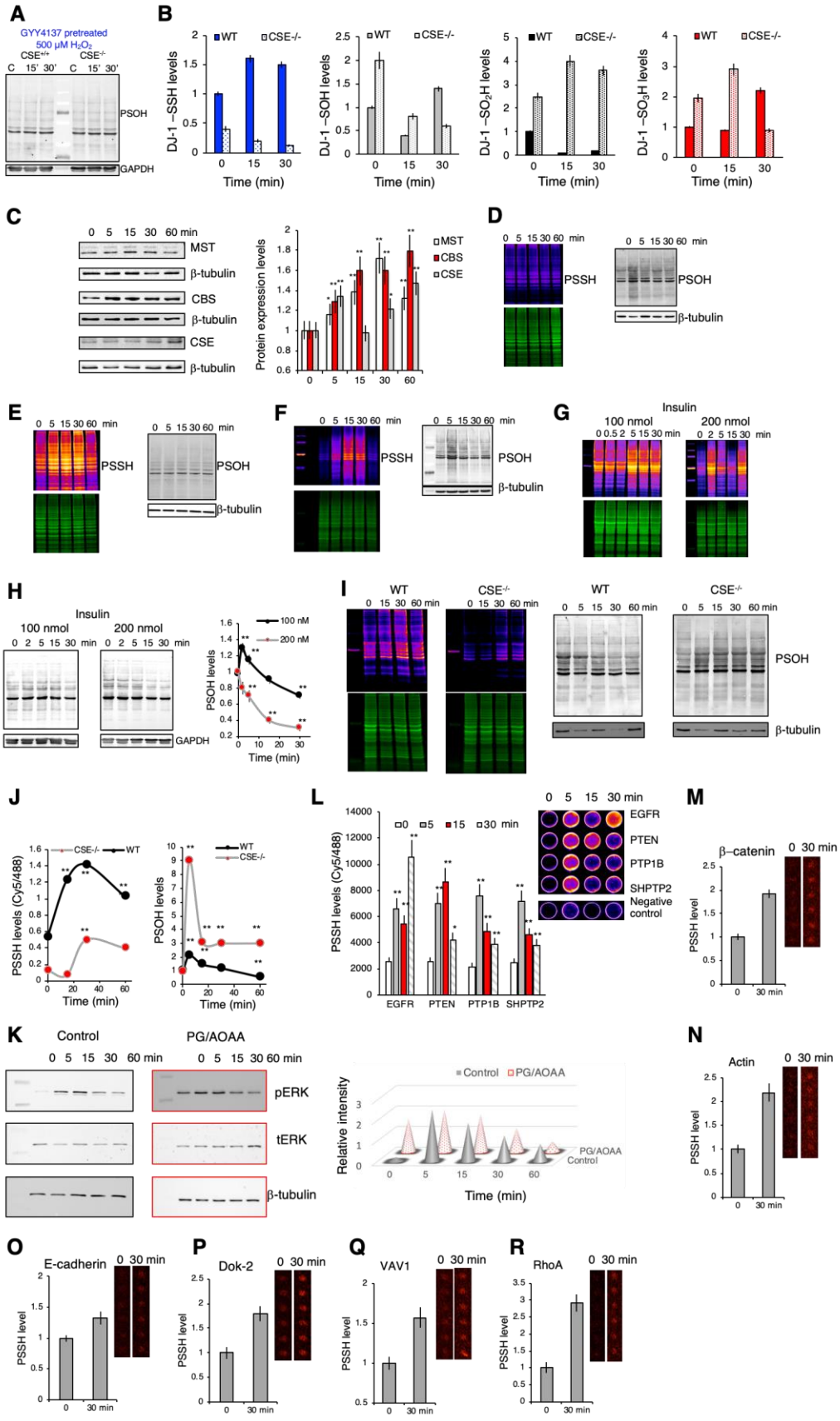

Figure S4. Protein persulfidation is an integral part of cellular response to H_2O_2 and RTK activation. Related to Figures 4 and 5.

(A) Representative blot showing the effect of GYY4137 (200 µM) on H_2O_2 (500 µM)-induced sulfenylation in $CSE^{+/+}$ and $CSE^{-/-}$ MEF cells. Sulfenylation was visualized by streptavidin-488 and normalized against GAPDH. n=3
(B) Evaluation of DJ-1 immunoprecipitation experiments shown in **Figure 4E.** Values represent mean ± SD. n=4.
(**C**) Expression levels of H_2S producing enzymes, MST, CBS and CSE in HeLa cells after treatment with EGF for the indicated amount of time. Densitometric analysis of data from 3 independent experiments was normalized against β-tubulin. Values represent mean ± SD.
(D) Representative images showing protein persulfidation and sulfenylation, used for **Figure 5C**. HeLa cells were pretreated with 200 µM GYY4137 and then exposed to 100 ng/ml EGF for the indicated amount of time. Persulfidation was detected in-gel by measuring Cy5/488 signal ration. Sulfenylation was visualized by streptavidin-488 and normalized against β-tubulin.
(**E**) Representative images showing protein persulfidation and sulfenylation, used for **Figure 5D**. HeLa cells were pretreated with 2 mM mixture of AOAA and PG (1:1, 30 min) and then exposed to 100 ng/ml EGF for the indicated amount of time. Persulfidation was detected in-gel by measuring Cy5/488 signal ration. Sulfenylation was visualized by streptavidin-488 and normalized against β-tubulin.
(**F**) Representative images showing protein persulfidation and sulfenylation, used for **Figure 5E**. HUVEC were treated with 40 ng/ml VEGF for the indicated amount of time. Persulfidation was detected in-gel by measuring Cy5/488 signal ratio. Sulfenylation was visualized by streptavidin-488 and normalized against β-tubulin.
(**G**) Representative images showing protein persulfidation used for **Figure 5F**. SH-SY5Y cells were treated with either 100 nM or 200 nM insulin.
(**H**) Sulfenylation changes in SH-SY5Y cells treated with either 100 nM or 200 nM insulin. n = 3.
(**I-J**) Changes in persulfidation and sulfenylation dynamics in $CSE^{+/+}$ and $CSE^{-/-}$ MEF cells after treatment with 100 ng/ml of EGF. Representative images (**I**) and quantification of the change (**J**). Values are given as mean ± SD from n = 3.
(**K**) Inhibition of H_2S production by the pretreatment of HeLa cells with 2 mM mixture of AOAA and PG (1:1) for 30 min and subsequent treatment with EGF causes changes in phosphorylation levels of pERK. Expression levels of pERK were normalized against total ERK expression in the same immunoblot, while total ERK was normalized against β-tubulin. Densitometric analysis of the data from three independent experiments is shown as mean ± SD.
(**L**) Antibody microarray-like approach was used to address persulfidation status of EGFR, PTEN, PTP1B and SHPTP2 from HeLa cells treated with 100 ng/mL EGF for the indicated amount of time. Original readouts obtained by Typhoon FLA 9500 are pseudo-coloured in ImageJ to visually enhance the changes in the signal. Quantification of the data from two independent experiments.
(**M-R**) Persulfidation levels of ß-catenin (**M**), actin (**N**), E-cadherin (**O**), Dok-2 (**P**), VAV1 (**Q**), RhoA (**R**) in HeLa cells treated or not with 100 ng/ml EGF for 30 min, measured using EGFR pathway microarray glass slips. Related to **Figure 5K**. Each antibody is spotted in pentaplicates. Values are given as mean ± SD from two independent experiments.

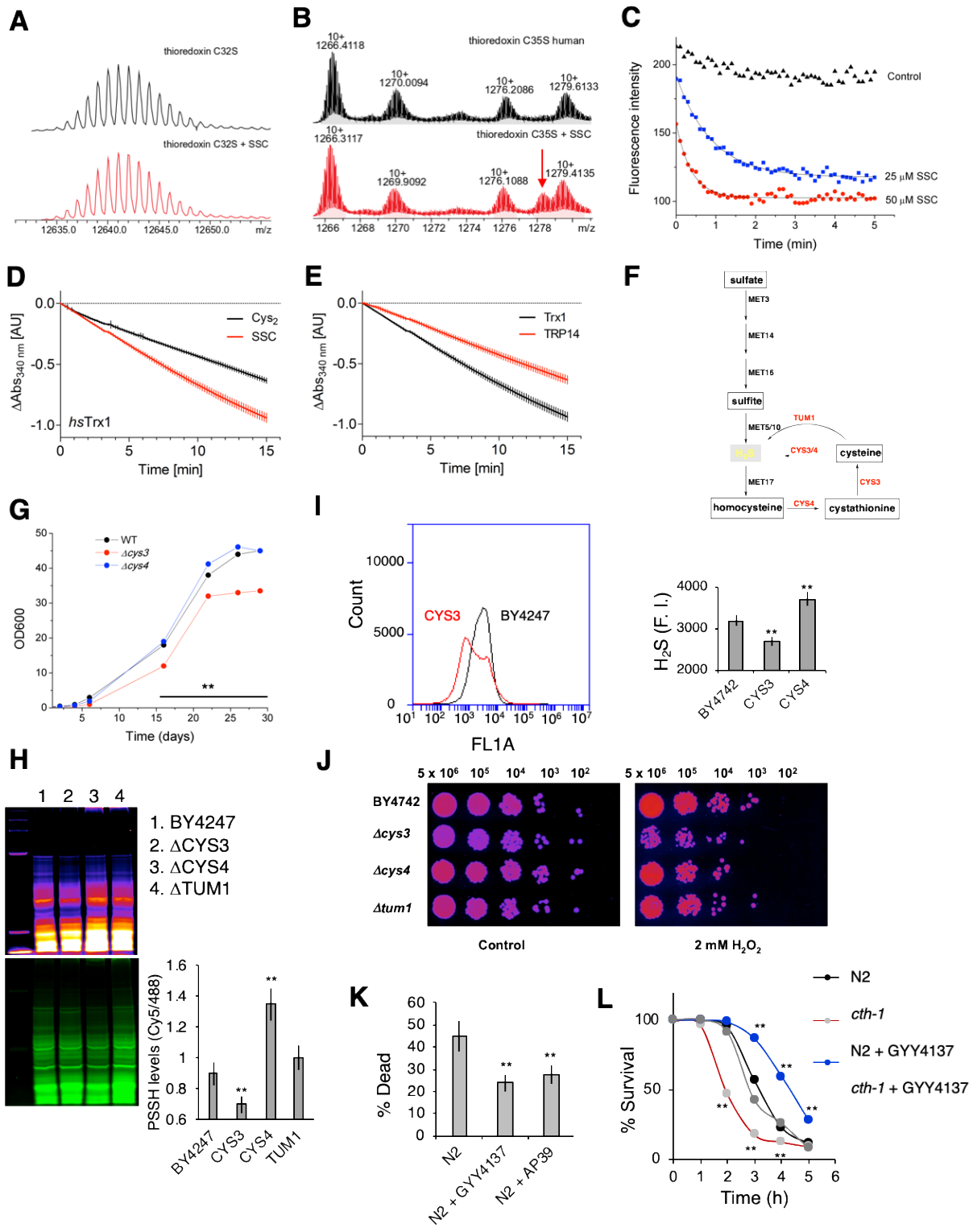

Figure S5. Trx-catalyzed reduction of S-sulfocysteine (SSC) and protection against ROS-induced death. Related to Figure 6

(**A**) Deconvoluted mass spectra of 10 µM C32S Trx before (black) and after the reaction with 10 µM SSC showing no difference.

(**B**) ESI-TOF-mass spectra of 10 µM C35S Trx before (black) and after the reaction with 10 µM SSC (red). The arrow indicates the peak that is absent in the control spectrum.

(**C**) Kinetics of human Trx (4 μM) oxidation with 25 μM (blue line) and 50 μM SSC (red line), followed by tryptophan fluorescence (λ_{ex} 280 nm) changes. Spontaneous oxidation of Trx alone is shown in black.
(**D**-**E**) Activities of human Trx (**D**) with cystine and SSC and TRP14 with SSC (**E**) were recorded measuring NADPH oxidation on a Tecan Infinite M200 plate reader, set to record absorption at 340 nm. 3 μM human Trx1 or TRP14, 30 nM TrxR from rat liver and 250 μM NADPH were used in all measurements. Concentration of cystine or SSC were set at 1 mM. Absorption at 340 nm was recorded. The initial rate of A_{340} decrease was fitted linearly, and consumption of NAPDH over time was determined using an NADPH extinction coefficient ε_{340} of 6020 M^{-1} cm^{-1}.
(**F**) Metabolic pathways for H_2S biosynthesis in *S. cerevisae.*
(**G**) Growth curves for wild type, *Δcys3*, *Δcys4* and *Δtum1* mutants of *S.cerevisiae*.
(**H**) Persulfidation level in wild type, *Δcys3*, *Δcys4* and *Δtum1* mutants of *S. cerevisiae.*
(**I**) Drop dilution assay for evaluating the sensitivity of *Δcys3*, *Δcys4* and *Δtum1* mutants to 2 mM H_2O_2.
(**J**) Flow cytometric analysis of H_2S levels (green fluorescence, FL1A) in different mutants of *S. cerevisiae.*
(**K**) The effect of short-term (3 hr) preexposure to GYY4137 (500 μM) or AP39 (100 nM) on survival rate of *C. elegans* treated with 60 mM paraquat for 5 hr.
(**L**) The effect of short-term (3 hr) pre-exposure to GYY4137 (500 μM) on survival rate of N2 and *cth-1 C. elegans* mutants exposed to sodium arsenite. N>50 worms.

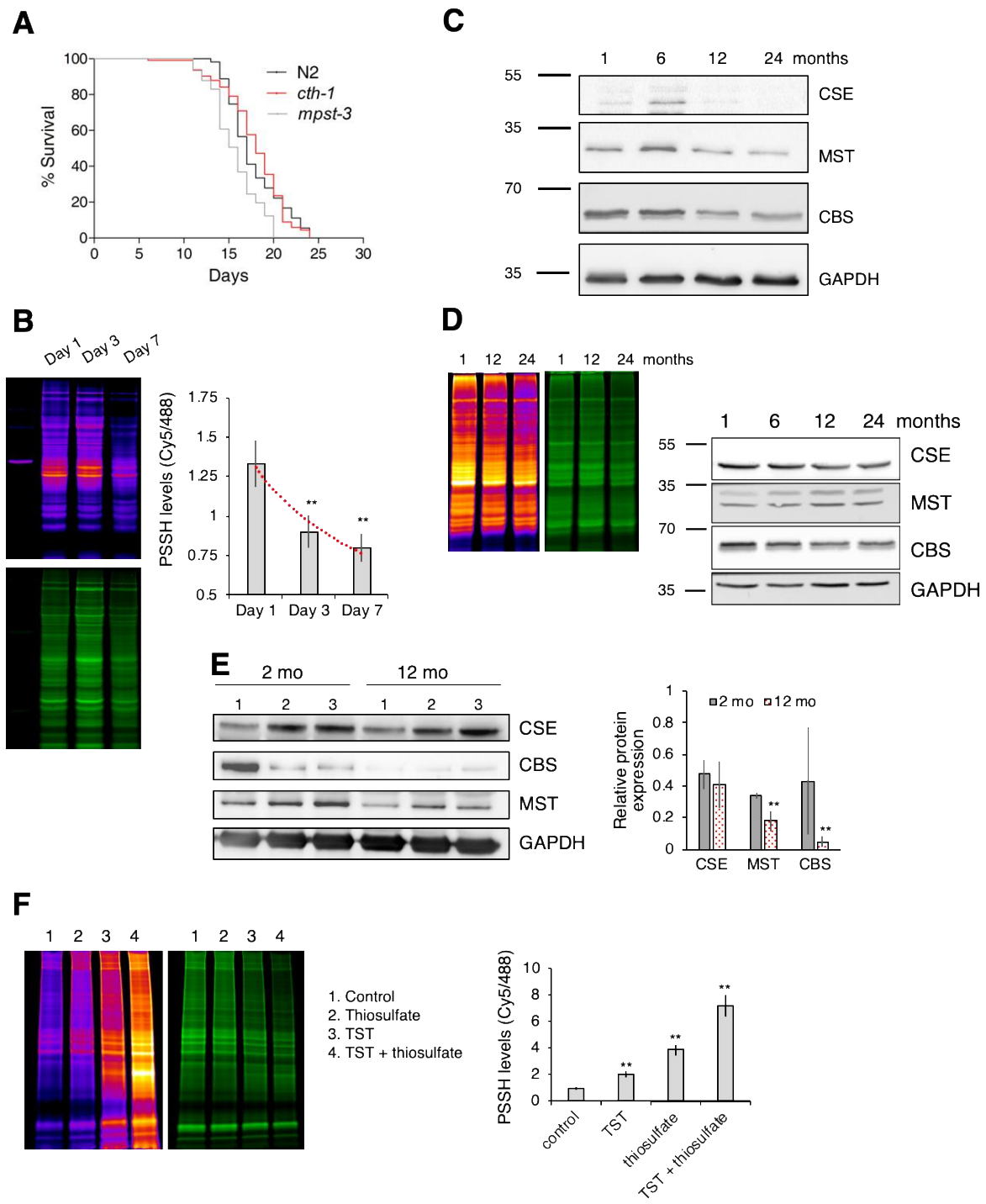

Figure S6. P-SSH levels correlate with aging. Related to Figure 7.

(**A**) Lifespan analysis of N2, *cth-1* and *mpst-3* mutant strains. n > 110 per each line.
(**B**) Persulfidation levels in N2 *C. elegans* at different days of adulthood. Intensity of persulfidation is expressed as Cy5/488 ratio Values represent mean ± SD from three different experiments.
(**C**) Expression levels of CSE, CBS and MPST in brain extracts from 1, 6, 12 and 24 months old rats. GAPDH is used as a loading control. Representative blots form n=3.
(**D**) Persulfidation levels, CSE, CBS and MPST expression levels in liver extracts from 1, 6, 12 and 24 months old rats. GAPDH is used as a loading control. Representative images from n=3.

(**E**) Expression levels of CSE, CBS and MPST in muscle extracts from 2 and 12 months old mice. GAPDH is used as a loading control. n=3.
(**F**)Thiosulfate and thiosulfate sulfur transferase (TST) increase protein persulfidation in HeLa cell lysates.

Table S1. List of proteins found to be endogenously persulfidated in human red blood cells.* Related to Figure 2.

Nº	Protein name (UniProtKB database)	UniProtKB	-10logP	Peptides	Coverage %	MW (Da)	Ref.
1	Carbonic anhydrase 1	P00915	308.61	54	73	*28,870*	(Delobel et al., 2016)
2	Spectrin alpha chain, erythrocytic 1	P02549	266.65	101	43	*280,014*	(Zaccarin et al., 2014)
3	Spectrin beta chain, erythrocytic	P11277	248.03	61	30	*246,468*	(Zaccarin et al., 2014)
4	Ankyrin 1	P16157	218.79	32	21	*206,265*	(Yang et al., 2012; Zaccarin et al., 2014)
5	Catalase	P04040	218.65	35	45	*59,756*	(Delobel et al., 2016; Yang et al., 2012)
6	Flavin reductase	P30043	197.55	17	64	*22,119*	(Delobel et al., 2016)
7	Band 3 anion transport protein	P02730	197.26	23	26	*101,792*	(Zaccarin et al., 2014)
8	Carbonic anhydrase 2	P00918	192.22	25	65	*29,246*	(Delobel et al., 2016)
9	Peroxiredoxin 2	P32119	187.35	26	59	*21,892*	(Delobel et al., 2016; Zaccarin et al., 2014)
10	Bisphosphoglycerate mutase	P07738	135.16	14	51	*30,005*	(Delobel et al., 2016)
11	Glyceraldehyde-3-phosphate dehydrogenase	P04406	131.26	9	39	*36,053*	(Valentine et al., 1987; Zaccarin et al., 2014)
12	Protein/nucleic acid deglycase DJ-1	Q99497	129.49	8	50	*19,891*	(Delobel et al., 2016)
13	Peroxiredoxin 1	Q06830	123.63	10	45	*22,110*	(Delobel et al., 2016)
14	Protein DDI1 homolog 1	Q8WTU0	121.85	6	22	*44,124*	
15	Fructose-bisphosphate aldolase A	P04075	116.71	9	20	*39,420*	(Valentine et al., 1987)
16	Purine nucleoside phosphorylase	P00491	114.54	7	30	*32,118*	(Delobel et al., 2016)
17	Methanethiol oxidase	Q13228	112.56	7	17	*52,391*	
18	Protein 4.1	P11171	112.26	7	10	*97,017*	(Yang et al., 2012; Zaccarin et al., 2014)
19	Transitional endoplasmic reticulum ATPase	P55072	164.3	16	21	*89,322*	(Yang et al., 2012)
20	Peroxiredoxin 6	P30041	153	11	52	*25,035*	(Delobel et al., 2016)
21	Stress-induced-phosphoprotein 1	P31948	140.13	11	19	*62,639*	(Delobel et al., 2016)
22	Triosephosphate isomerase	P60174	125.54	6	31	*30,791*	(Delobel et al., 2016)
23	Phosphoglycerate kinase 1	P00558	120.79	8	19	*44,615*	(Valentine et al., 1987)

24	Heat shock cognate 71 kDa protein	P11142	119.28	10	20	*70,898*	(Delobel et al., 2016; Yang et al., 2012)
25	Tropomyosin alpha-3 chain	P06753	112.7	6	25	*32,950*	
26	L-lactate dehydrogenase B chain	P07195	111.71	10	25	*36,638*	(Delobel et al., 2016)
27	Alpha enolase	P06733	107.69	7	21	*47,169*	(Delobel et al., 2016; Valentine et al., 1987; Yang et al., 2012)
28	T-complex protein 1 subunit theta	P50990	106.44	7	16	*59,621*	
29	Low molecular weight phosphotyrosine protein phosphatase	P24666	103.76	5	38	*18,042*	
30	Alpha adducin	P35611	99.94	7	11	*80,955*	(Yang et al., 2012)
31	Erythrocyte band 7 integral membrane protein	P27105	98.78	7	29	*31,731*	(Zaccarin et al., 2014)
32	Eukaryotic translation initiation factor 5 alpha	P55010	95.91	4	31	*49,223*	
33	Heat shock protein HSP 90-alpha	P07900	94.83	7	13	*84,660*	
34	Peroxiredoxin 4	Q13162	93.27	6	11	*30,540*	
35	Adenylate kinase isoenzyme 1	P00568	91.30	5	23	*21,635*	(Valentine et al., 1987)
36	Ubiquitin-like modifier-activating enzyme 1	Q5JRR6	89.97	4	5	*56,852*	(Yang et al., 2012)
37	Ubiquitin carboxyl-terminal hydrolase 14	P54578	87.61	4	13	*56,069*	(Yang et al., 2012)
38	β adducin	P35612	87.23	3	5	*80,854*	
39	Hsc70 interacting protein	P50502	85.19	4	12	*41,332*	
40	Proteasome subunit alpha type-5	P28066	82.21	3	18	*26,411*	
41	Thioredoxin	P10599	79.82	4	31	*11,737*	
42	Rab GDP dissociation inhibitor β	P50395	79.5	4	10	*50,663*	(Delobel et al., 2016)
43	Glutathione S-transferase A1	P08263	78.34	3	13	*25,631*	(Delobel et al., 2016)
44	Erythrocyte membrane protein band 4.2	P16452	75.97	4	8	*77,009*	(Zaccarin et al., 2014)
45	Rho GDP dissociation inhibitor 1	P52565	75.91	3	16	*23,207*	
46	Dematin	Q08495	75.59	4	12	*45,514*	
47	Ankyrin 3	Q12955	75.45	5	1	*480,410*	(Zaccarin et al., 2014)
48	3-mercaptopyruvate sulfur transferase	P25325	68.09	4	9	*33,178*	
49	Carbonic anhydrase 3	P07451	69.76	3	14	*29,557*	(Delobel et al., 2016)
50	Ubiquitin conjugating enzyme E2	P51668	72.33	3	30	*16,602*	
51	Serine/threonine protein kinase OSR1	O95747	68.46	4	8	*58,022*	

52	Copper chaperone for superoxide dismutase	O14618	67.22	3	10	*29,041*	
53	Transaldolase	P37837	66.97	4	9	*37,540*	(Delobel et al., 2016)
54	Protein S100-A6	P06703	80.68	5	43	*10,180*	
55	Malate dehydrogenase	P40925	60.29	3	13	*36,426*	(Delobel et al., 2016)
56	Glutamate--cysteine ligase catalytic subunit	P48506	59.76	2	10	*72,766*	
57	Proteasome subunit alpha type-1	P25786	59.18	2	10	*29,556*	
58	14-3-3 protein beta/alpha	P31946	50.89	2	8	*28,082*	

***** The table consists of proteins identified by at least 2 reliable peptides and -10logP>50, obtained by trypsin and/or chymotrypsin digestion.